ENERGY CONSERVATION

ORNL/Sub/81-7762/6 & 01

# Measurements of Heat-Transfer Coefficients of Nonazeotropic Refrigerant Mixtures Condensing Inside Horizontal Tubes

D. DeGrush
W. F. Stoecker

Prepared by
UNIVERSITY OF ILLINOIS AT URBANA-CHAMPAIGN
Department of Mechanical and Industrial Engineering
1206 West Green Street
Urbana, Illinois 61801

under
Subcontract 7762-X01

for

OAK RIDGE NATIONAL LABORATORY
operated by
MARTIN MARIETTA ENERGY SYSTEMS, INC.
for the

U.S. DEPARTMENT OF ENERGY

OFFICE OF BUILDINGS
AND COMMUNITY SYSTEMS

Printed in the United States of America. Available from
National Technical Information Service
U.S. Department of Commerce
5285 Port Royal Road, Springfield, Virginia 22161
NTIS price codes—Printed Copy: Microfiche A01

This report was prepared as an account of work sponsored by an agency of the United States Government. Neither the United States Government nor any agency thereof, nor any of their employees, makes any warranty, express or implied, or assumes any legal liability or responsibility for the accuracy, completeness, or usefulness of any information, apparatus, product, or process disclosed, or represents that its use would not infringe privately owned rights. Reference herein to any specific commercial product, process, or service by trade name, trademark, manufacturer, or otherwise, does not necessarily constitute or imply its endorsement, recommendation, or favoring by the United States Government or any agency thereof. The views and opinions of authors expressed herein do not necessarily state or reflect those of the United States Government or any agency thereof.

ORNL/Sub/81-7762/6 & 01

# MEASUREMENTS OF HEAT-TRANSFER COEFFICIENTS OF NONAZEOTROPIC REFRIGERANT MIXTURES CONDENSING INSIDE HORIZONTAL TUBES

D. DeGrush
W. F. Stoecker

Date of Issue--November 1987

Prepared by

UNIVERSITY OF ILLINOIS AT URBANA-CHAMPAIGN
Department of Mechanical and Industrial Engineering
1206 West Green Street
Urbana, Illinois 61801

under
Subcontract 7762-X01

for

OAK RIDGE NATIONAL LABORATORY
Oak Ridge, Tennessee 37831
operated by
MARTIN MARIETTA ENERGY SYSTEMS, INC.
for the
U.S. DEPARTMENT OF ENERGY
under Contract DE-AC05-84OR21400

TABLE OF CONTENTS

Page

LIST OF FIGURES....iv

NOMENCLATURE....ix

ABSTRACT....xi

1. INTRODUCTION....1
   1.1 Interest in Refrigerant Mixtures....1
   1.2 Previous Findings....1
   1.3 Study of Condensing Coefficients....6

2. EXPERIMENTAL FACILITY....9
   2.1 Introduction....9
   2.2 The Test Facility....9
   2.3 Components of the System....12
   2.4 The Transparent Condenser....13
   2.5 System Modifications....13
      2.5.1 Relocation of Charging Port....13
      2.5.2 Addition of Sample Removal Port on Condenser....16
   2.6 Procedure Modifications....16
      2.6.1 Sample Removal Modifications....16
      2.6.2 Photography Modifications....21

3. NONEQUILIBRIUM PHENOMENA IN THE CONDENSER....23
   3.1 Purpose of Tests....23
   3.2 Test Conditions....23
   3.3 Test Results: Experimental Data....24
      3.3.1 Introduction....24
      3.3.2 Temperature Profiles....24
      3.3.3 Flow Regimes During Condensation....32
      3.3.4 Temperature Gradient/Fluctuations....33
      3.3.5 Refrigerant Concentration Measurements....35

4. COPPER CONDENSER TEST FACILITY....39
   4.1 Introduction....39
   4.2 Overall Condenser Layout....39
   4.3 Copper Condenser Instrumentation....41
   4.4 Thermocouples....41
      4.4.1 Refrigerant Thermocouples....42
      4.4.2 Refrigerant-Tube Temperature Measurement....42
      4.4.3 Temperature Measurement of Cooling Water....45
   4.5 Pressure Measurements....45
   4.6 Calculations During and Following Tests....45

5. COPPER CONDENSER TEST RESULTS....50
   5.1 Test Objectives....50
   5.2 Test Conditions....50
   5.3 Test Reproducibility....52
   5.4 Refrigerant Temperature Profiles Along Condenser....53
   5.5 Condensing Coefficients Along Condenser....56
      5.5.1 Condensing Coefficient Profiles....56

5.5.2 Effect of Concentration on Condensing Coefficients.....60
5.5.3 Effect of Increasing Heat-Transfer Rate in Condenser.....60
5.6 Experimental Error.....70
5.7 Reasons for Reduction in Heat-Transfer Coefficient.....76

6. CONDENSING COEFFICIENT CORRELATIONS.....79
6.1 Introduction.....79
6.2 Individual Correlations.....80
6.2.1 Akers and Rosson Correlation.....80
6.2.2 Azer Correlation.....84
6.2.3 Traviss Correlation.....88
6.2.4 Chato and Shah Correlations.....91
6.2.5 Tandon Correlation.....95
6.2.6 Cavallini and Zecchin Correlation.....97
6.3 Summary of Results.....99
6.4 Effect of Slip.....100
6.5 Entrance Effects in the Condenser.....103

7. SUMMARY AND CONCLUSIONS.....108
7.1 Introduction.....108
7.2 Condensing Coefficient Results.....108
7.2.1 Local Coefficients.....108
7.2.2 Influence of Mixture Concentration on Condensing Coefficients.....109
7.2.3 Effect of Heat Flux in Condenser.....109
7.3 Condensing Coefficient Correlations.....110
7.4 Nonequilibrium Phenomena.....111
7.5 Conclusions.....111

REFERENCES.....113

APPENDIX REFRIGERANT AND COOLING WATER TEMPERATURES ALONG WITH LOCAL HEAT-TRANSFER COEFFICIENTS.....115

# LIST OF FIGURES

Page

Figure

1.1. Refrigeration process using a single refrigerant.....2

1.2. Refrigeration process using a nonazeotropic refrigerant mixture.....2

1.3. Individual film heat-transfer coefficients for boiling and condensing propane/n-butane mixture. From G. G. Haselden and L. Klimek [2].....4

1.4. Condensing heat-transfer coefficients in the high-temperature condenser (HTC) and low-temperature condenser (LTC). From Kornota and Stoecker [10].....5

1.5. Calculated heat-transfer coefficient profiles along the condenser for R-21/R-22 mixtures. The refrigerant conditions entering the condenser are (a) saturated, and (b) superheated. From Burr and Haselden [1].....7

2.1. Schematic diagram of heat-transfer system.....10

2.2. Photograph of control and instrumentation panel to heat-transfer studies system.....11

2.3. Diagram showing location of instrumentation for system with transparent condenser.....14

2.4. Transparent condenser numbering system for brass test sections and photography locations.....15

2.5. Modified refrigerant sample-removal canister.....18

2.6. Secondary canister used in refrigerant mixture composition analysis.....19

2.7. Schematic diagram of secondary canister.....20

3.1. Thermocouple and sample-removal locations for test series 4.....23

3.2. Refrigerant temperature profiles along condenser for R-114 concentrations in R-12/R-114 mixtures used in test series 4.....26

3.3. Photograph location 1, 1.0 m downstream; annular flow, little liquid.....28

3.4. Photograph location 2, 2.6 m downstream annular flow.....28

3.5. Photograph location 3, 4.0 m downstream; annular flow....28

3.6. Photograph location 4, 5.9 m downstream; annular flow....29

3.7. Photograph location 5, 7.5 m downstream; annular to wavy flow transition.....29

3.8. Photograph location 6, 9.0 downstream; annular to wavy flow transition.....29

3.9. Photograph location 7, 12.0 m downstream; wavy flow.....30

3.10. Photograph location 8, 13.6 m downstream; wavy flow.....30

3.11. Photograph location 9, 15.3 m downstream; wavy flow.....30

3.12. Photograph location 10, 17.1 m downstream; wavy flow.....31

3.13. Photograph location 11, 18.7 m downstream; slug flow.....31

3.14. Photograph location 12, 20.1 m downstream; slug flow.....31

3.15. Temperature fluctuations at the tube bottom at test section 10 for test 23.....34

3.16. Temperature fluctuations 9.22 mm (2/3 diameter) from the tube bottom at test section 10 for test 26.....34

3.17. Experimental composition results compared to condensation occurring at a uniform rate over entire length of the condenser under equilibrium conditions.....36

4.1. Schematic diagram of copper condenser.....40

4.2. Refrigerant-side instrumentation.....43

4.3. Refrigerant temperature measurement.....44

4.4. Determination of tube temperature $T_{p_i}$ at location i (i = 1,6).....44

4.5. Water-side instrumentation.....46

4.6. Temperature measurement of the condenser cooling water...47

4.7. Calculation of local heat-transfer coefficients $h_i$ at test location i (i = 1,6).....49

5.1. Test reproducibility: temperature profiles in R-12/R-114 mixtures.....54

5.2. Test reproducibility: condensing coefficients in R-12/R-114 mixtures.....55

5.3. Temperature profiles for the various R-12/R-114 mass concentrations from test series A.....57

5.4. Typical refrigerant temperature profile along condenser.....58

5.5. Condensing coefficient profile for pure R-12 (test series A).....59

5.6. Condensing coefficient profile for pure R-114 (test series A).....59

5.7. Condensing coefficient profile for 30% R-114 (test series A).....61

5.8. Condensing coefficient profile for 50% R-114 (test series A).....61

5.9. Condensing coefficient profile for 70% R-114 (test series A).....62

5.10. Variation in condensing coefficients with concentration at 2.4 and 4.6 m downstream (test series A).....63

5.11. Variation in condensing coefficients with concentration at 7.1, 12.3, 14.6, and 17.1 m downstream (test series A).....64

5.12. Condensing coefficient profile for pure R-12 (test series B).....66

5.13. Condensing coefficient profile for pure R-114 (test series B).....66

5.14. Condensing coefficient profile for 30% R-114 (test series B).....67

5.15. Condensing coefficient profile for 50% R-114 (test series B).....67

5.16. Condensing coefficient profile for 70% R-114 (test series B).....68

5.17. Increase in condensing coefficient with increasing heat flux at 4.6 m downstream from condenser entrance (test location 2).....69

5.18. Uniform increase in condensing coefficients with increasing heat flux for 70% R-114.....71

5.19. Variation in condensing coefficients with concentration at 2.4, 4.6, and 7.1 m downstream (test series B).....72

5.20. Variation in condensing coefficients with concentration at 12.3, 14.6, and 17.1 m downstream (test series B).....73

5.21. Vapor concentrations existing and condensing at one position in a condenser tube.....78

6.1. Akers and Rosson correlation [18] applied to R-12/R-114 mixture tests of series A.....82

6.2. Akers and Rosson correlation [18] applied to R-12 and R-114 tests of series A.....82

6.3. Akers and Rosson correlation [18] applied to R-12/R-114 mixture tests of series B.....83

6.4. Akers and Rosson correlation [18] applied to R-12 and R-114 tests of series B.....83

6.5. Azer et al. correlation [20] applied to R-12/R-114 mixture tests of series A.....86

6.6. Azer et al. correlation [20] applied to R-12 and R-114 tests of series A.....86

6.7. Azer et al. correlation [20] applied to R-12/R-114 mixture tests of series B.....87

6.8. Azer et al. correlation [20] applied to R-12 and R-114 tests of series B.....87

6.9. Traviss et al. correlation [22] applied to R-12/R-114 mixture tests of series A.....89

6.10. Traviss et al. correlation [22] applied to R-12 and R-114 tests of series A.....89

6.11. Traviss et al. correlation [22] applied to R-12/R-114 mixture tests of series B.....90

6.12. Traviss et al. correlation [22] applied to R-12 and R-114 tests of series B.....90

6.13. Shah correlation [25] applied to R-12/R-114 mixture tests of series A.....93

6.14. Shah correlation [25] applied to R-12 and R-114 tests of series A.....93

6.15. Shah correlation [25] applied to R-12/R-114 mixture tests of series B.....94

6.16. Shah correlation [25] applied to R-12 and R-114 tests of series B.....94

6.17. Tandon et al. correlation [15] applied to R-12/R-114 mixture tests of series A.....96

6.18. Tandon et al. correlation [15] applied to R-12 and R-114 tests of series A.....96

6.19. Tandon et al. correlation [15] applied to R-12/R-114 mixture tests of series B.....98

6.20. Tandon et al. correlation [15] applied to R-12 and R-114 tests of series B.....98

6.21. Graphic representation of Miropolskiy et al. correlation [27] with pressures reduced by Shah [23]....105

6.22. Miropolskiy et al. correlation [27] applied at 2.4 m downstream (test location 1) in the condenser.....106

# NOMENCLATURE

$A$ = cross-sectional area of tube, $m^2$

$C_{p_\ell}$ = specific heat of liquid, J/(kg°C)

$C_{p_v}$ = specific heat of vapor, J/(kg°C)

$D$ = inner diameter of tube, m

$g$ = acceleration due to gravity, 9.81 $m/s^2$

$G$ = total mass velocity based on tube cross-sectional area, $kg/(m^2s)$

$G_e$ = equivalent mass velocity, $G_v(\rho_\ell/\rho_v)^{1/2} + G_\ell$, $kg/(m^2s)$

$G_\ell$ = saturated liquid mass velocity based on tube cross-sectional area, $kg/(m^2s)$

$G_v$ = saturated vapor mass velocity based on tube cross-sectional area, $kg/(m^2s)$

$h$ = local heat-transfer coefficient, $W/(m^2°K)$

$h_B$ = local heat-transfer coefficient evaluated at $T_B$, $W/(m^2°K)$

$i$ = enthalpy, J/kg

$i_{\ell v}$ = latent heat of vaporization, J/kg

$i_{s\ell}$ = enthalpy of saturated liquid, J/kg

$k_\ell$ = thermal conductivity of liquid, W/(m°C)

$\dot{m}$ = mass flowrate, kg/s

$p_r$ = reduced pressure, absolute pressure/critical pressure

$P_{r\ell}$ = Prandtl number of liquid, $C_{p_\ell}\ \mu_\ell/k_\ell$

$Q$ = relative enthalpy, $(i - i_{s\ell})/i_{\ell v}$

$Q_B$ = border relative enthalpy

$Re_\ell$ = liquid Reynolds number, $DG_\ell/\mu_\ell$

$Re_v$ = vapor Reynolds number, $(DG_v/\mu_\ell)(\rho_\ell/\rho_v)^{1/2}$

$Re_{\ell T}$ = Reynolds number assuming all mass flowing is liquid, $DG/\mu_\ell$

$Re_{vT}$ = Reynolds number assuming all mass flowing is vapor, $DG/\mu_v$

$Re_{\ell s}$ = superficial liquid Reynolds number, $Re_{\ell T}\ (1 - x)$

$Re_{vs}$ = superficial vapor Reynolds number, x $Re_{vT}$

T = temperature, °C

$T_B$ = border temperature, °C

TD = temperature difference between saturation temperature and tube wall temperature, °C

$T_{SAT}$ = saturation temperature, °C

$U_v$ = vapor velocity, m/s

x = vapor quality, x = 1 for saturated vapor and x = 0 for saturated liquid

$X_{tt}$ = Lockhart-Martinelli parameter,

$$(\mu_\ell/\mu_v)^{0.1} (\rho_v/\rho_\ell)^{0.5} ((1 - x)/x)^{0.9}$$

$\Delta T$ = temperature drop across condensate film, °C

$\mu_\ell$ = saturated liquid dynamic viscosity, kg/(m s)

$\mu_v$ = saturated vapor dynamic viscosity, kg/(m s)

$\rho_\ell$ = saturated liquid density, $kg/m^3$

$\rho_v$ = saturated vapor density, $kg/m^3$

## ABSTRACT

Some preliminary observations from previous system tests on a refrigeration facility using a mixture of R-12/R-114 indicated a reduction in condensing heat-transfer coefficients with the mixture in comparison to either constituent operating alone. Further exploration of this phenomenon involved a glass tube condenser constructed previously for observation of the flow regimes during the condensation process. The study, which is documented by this report, was pursued still further with a copper-tube condenser constructed only for the purpose of measuring heat-transfer coefficients and correlating them with the flow regimes previous observed.

In tests that duplicated the flow regimes of the earlier work, the previous results were confirmed in that a low heat-transfer coefficient prevails in the early stage of the condenser, for both a single refrigerant and a mixture. It is in the midrange of the condenser that the mixture experiences its greatest reduction in coefficient in comparison to either constituent. Stratified flow prevails in the midrange of the condenser, so that liquid/vapor slip, if it does occur, would be most prominent in this section. Attempts to measure liquid and vapor concentrations to establish the existence of slip were not successful. From an application standpoint, heat-transfer enhancers such as turbulence promoters should be considered for this midsection of the condenser.

Another objective of this study was to compare experimental results with some of the correlations presented in the literature. Most of the equations were developed with flow models in mind and applied to only one section of the condenser, where the agreement of our experimental data was good. Most of the correlations overpredicted the magnitude of heat-transfer coefficient in the early stage of the condenser, and agreement was achieved only when a model that incorporated the entrance effects was used. One of the uses of the correlations is to adjust them for changes in fluid properties attributable to slip. Indeed, the existence of slip alter the magnitudes predicted by all correlations.

Another series of tests was conducted with a higher heat flux than the one that duplicated the flow regime tests in the transparent condenser. The effect of higher heat flux was essentially to increase the coefficients throughout the condenser and to inhibit the amount of reduction when using a mixture, particularly in the last half of the condenser.

# 1. INTRODUCTION

## 1.1 Interest in Refrigerant Mixtures

The potential use of nonazeotropic mixtures of refrigerants in conventional vapor compression refrigeration systems has been a topic of great interest in recent years. The use of these mixtures in refrigerators, air conditioners, and heat pumps is very attractive from the standpoint of cycle efficiency when it is possible to exploit the "gliding" temperatures that occur during constant-pressure boiling and condensing. Other advantages offered by nonazeotropic refrigerant mixtures are adjustable heat-pumping capacities with a constant compressor-volume flow rate.

Figure 1.1 illustrates the temperature profiles of the working fluids in a refrigeration process when a single refrigerant is used. Note that at one end of each heat exchanger there is quite a large temperature difference between the refrigerant and the media with which it is exchanging heat. These large temperature differences result in irreversible heat transfer which in turn leads to excessive energy consumption.

Figure 1.2 shows the gliding temperatures obtained in the condenser and evaporator when a nonazeotropic refrigerant mixture is employed as a working fluid. With proper selection of the refrigerant mixture, the temperature profile of the refrigerant will closely parallel the temperature profile of at least one of the media with which the refrigerant is exchanging heat. It is apparent that the temperature differences between the refrigerant and the other media have been reduced in Fig. 1.2 compared with those in Fig. 1.1. Avoidance of the very large temperature difference at one end of the heat exchanger reduces the amount of irreversible heat transfer, resulting in less energy consumption. In an actual vapor-compression refrigeration system, the savings in energy would most likely show up as a reduction in compressor power for a given refrigerating or heat-pumping capacity.

## 1.2 Previous Findings

Many investigators have predicted savings in energy based on the thermodynamic properties of the nonazeotropic refrigerant mixtures mentioned above when using the mixtures in conventional vapor-compression refrigeration systems [1-6]. However, at this time, only a few experimenters have been able to demonstrate significant savings in energy by using refrigerant mixtures as

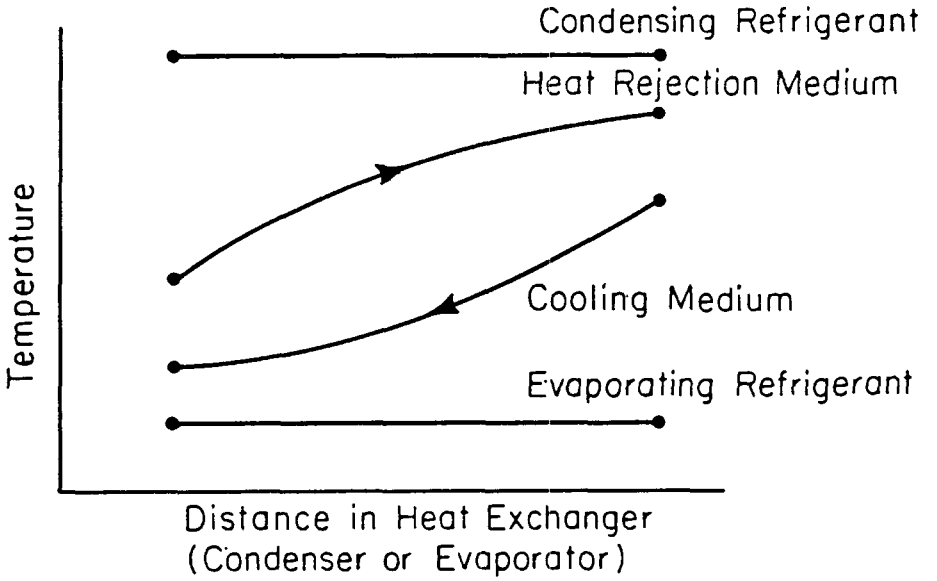


Figure 1.1. Refrigeration process using a single refrigerant.

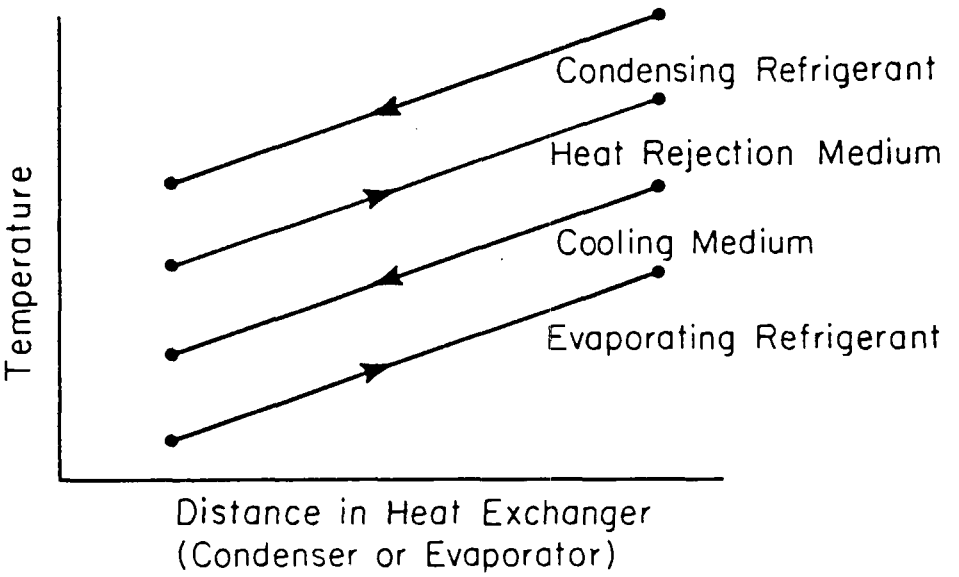


Figure 1.2. Refrigeration process using a nonazeotropic refrigerant mixture.

the working fluid [4,5]. Rojey [5] states that he obtained a 40 percent improvement in the coefficient of performance (COP) of a commercial heat pump using a mixture of refrigerants as opposed to a single refrigerant. He states that no modification of the heat-transfer surfaces was made in order to obtain these results and that the measured heat-transfer coefficients in the condenser and evaporator are nearly equal when either a nonazeotropic refrigerant mixture or a single refrigerant was used.

The experimentation done by Rojey has certainly been the exception, for many of the investigators have not been able to obtain as great a saving in energy as that theoretically predicted using nonazeotropic refrigerant mixtures. Some were able to obtain savings by increasing the heat-transfer area in the condenser and the evaporator [2,6]. Along these same lines, most of the investigators noted a reduction in local heat-transfer coefficients [7] during the condensation and evaporation processes when a mixture, as opposed to a single refrigerant, was employed as the working fluid. A widely-referenced study by Arora [8] clearly shows a reduction in the boiling heat-transfer coefficients of a mixture compared with those of a pure refrigerant. Similarly, a study by Bokhanovskiy [9] showed lower condensing coefficients for nonazeotropic refrigerant mixtures than for their single counterparts.

Figure 1.3 illustrates the reduction of local heat-transfer coefficients in the evaporator and condenser in an experimental study by Haselden and Klimek [2] using mixtures of propane and n-butane. Kornota and Stoecker [10] conducted experiments using a vapor-compression refrigeration system that had two condensers located in series. The superheated refrigerant entered the high-temperature condenser and left subcooled from the low-temperature condenser. Figure 1.4 illustrates a reduction in condensing coefficients using a nonazeotropic mixture of refrigerants R-12 and R-114.

So that the potential energy-saving benefits of nonazeotropic mixtures can be obtained, it is essential that the local heat-transfer coefficients be maintained at least as high as those of their pure counterparts. Thus the importance of reaching the local heat-transfer coefficients in refrigerant mixtures is apparent.

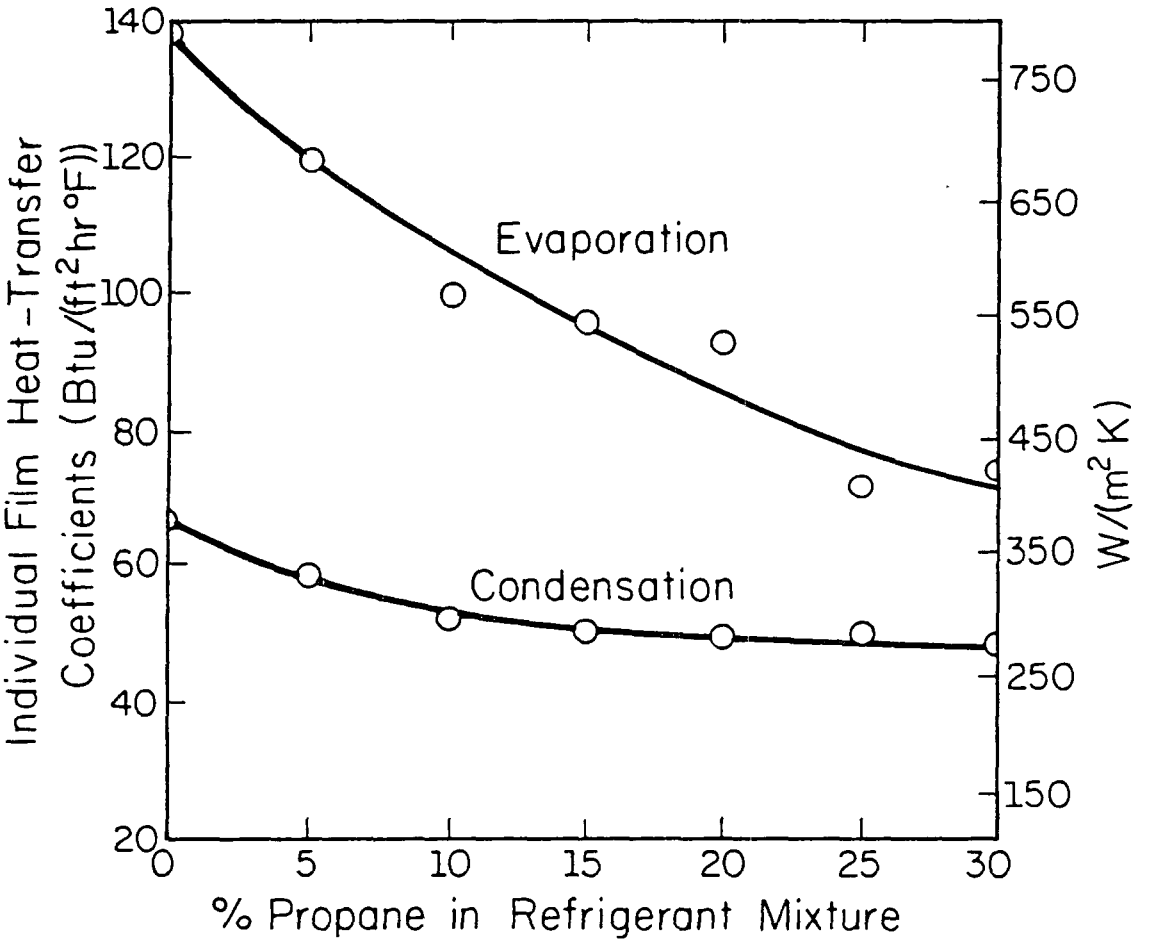


Figure 1.3. Individual film heat-transfer coefficients for boiling and condensing propane/n-butane mixture. From G. G. Haselden and L. Klimek [2].

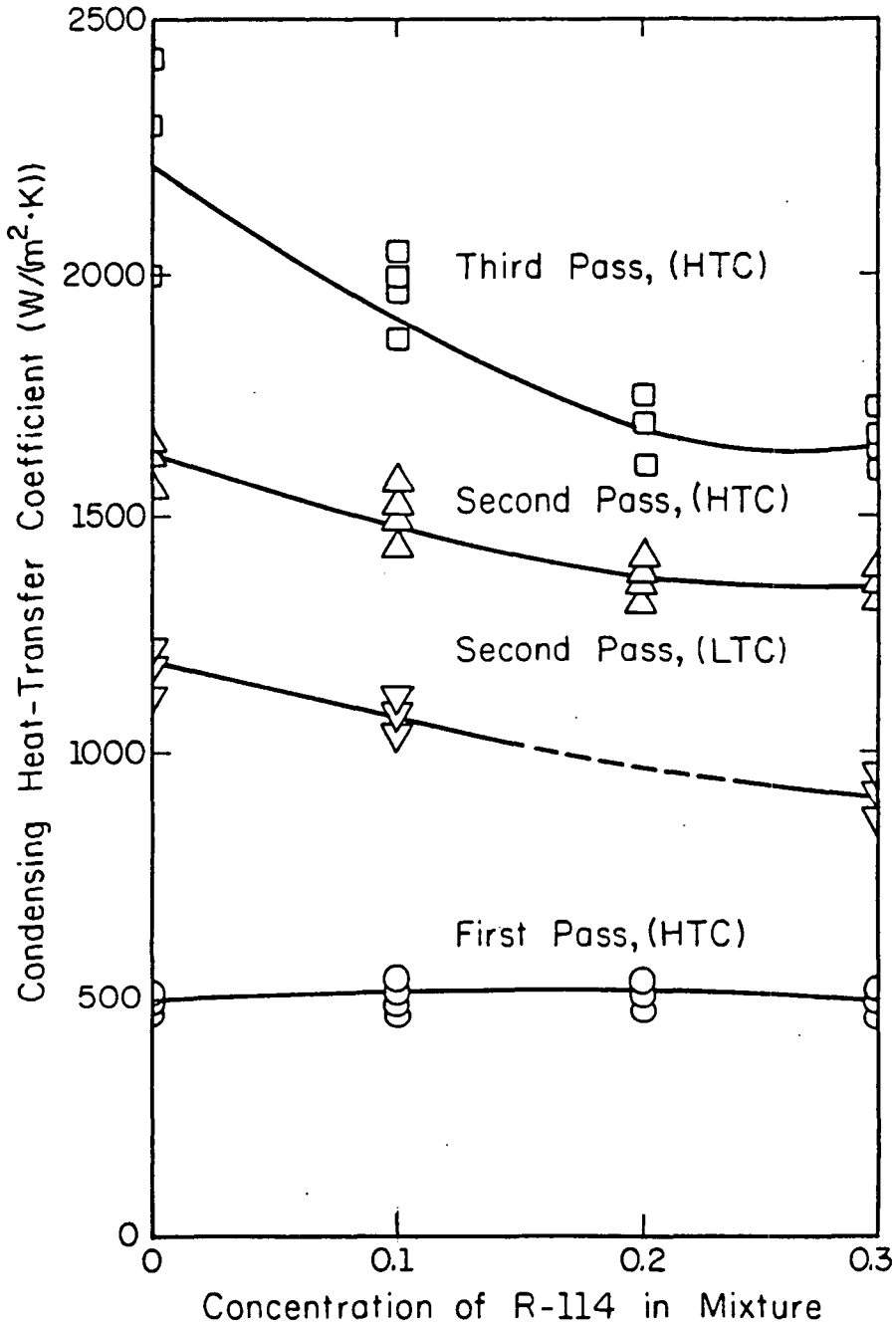


Figure 1.4. Condensing heat-transfer coefficients in the high-temperature condenser (HTC) and low-temperature condenser (LTC). From Kornota and Stoecker [10].

## 1.3 Study of Condensing Coefficients

When previous findings concerning the use of nonazeotropic refrigerant mixtures in vapor-compression machines are reviewed, it becomes obvious that some contradictory findings have been reported by different investigators. Clearly, more investigation is needed in this area to explain the differences. To this end, a two-part study focusing on the condensation of nonazeotropic refrigerant mixtures of R-12 and R-114 was undertaken.

The first part of the study, carried out at the University of Illinois [10], was entitled "Flow Regimes of Refrigerant Mixtures Condensing Inside Tubes." In this study a transparent condenser was used to visualize the various flow patterns and their location along the condenser during the condensation of R-12 and R-114 refrigerant mixtures. Also, techniques were developed for obtaining refrigerant samples from the transparent condenser during the condensation process. These samples were analyzed using a gas chromatograph to determine the composition of the condensate or the saturated vapor.

The work contained herein is the second part of the condensation study. A minor portion deals with a continuation of the sample analyses conducted with the transparent condenser. A series of tests was run with various R-12 and R-114 concentrations, and refrigerant samples were removed from the transparent condenser during each test. The samples were then analyzed with the intent of gaining quantitative knowledge on the degree of nonequilibrium that exists between the two phases in the condenser.

The major part of this present work, however, deals with the determination and study of local heat-transfer coefficients along the condenser when nonazeotropic refrigerant mixtures are condensing. Figure 1.5 shows an example of predicted heat-transfer coefficient profiles in a condenser using a nonazeotropic mixture of refrigerants. In parts a anb b of Fig. 1.5, the refrigerant is flowing from right to left through the condenser. In Fig. 1.5a, the refrigerant mixture enters the condenser saturated. In Fig. 1.5b, the refrigerant mixture enters the condenser superheated. In both parts the flat portion of the refrigerant heat-transfer coefficient profile located near the end of the condenser (left side of Fig. 1.5a and b) represents the heat transfer from the totally condensed liquid refrigerant. The figures were obtained from a study by Burr and Haselden using nonazeotropic refrigerant mixtures for various air conditioning duties [1].

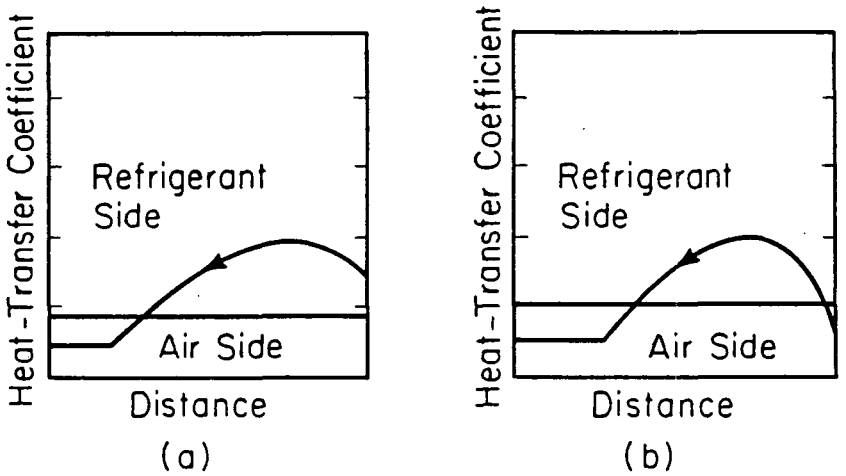


Figure 1.5. Calculated heat-transfer coefficient profiles along the condenser for R-21/R-22 mixtures. The refrigerant conditions entering the condenser are (a) saturated, and (b) superheated. From Burr and Haselden [1].

In the present study, condensing coefficient profiles were determined experimentally for various mixtures of R-12 and R-114 using a fully instrumented copper condenser constructed especially for this study. The copper condenser was constructed similar in size to the transparent condenser so that the tests run with similar conditions on both condensers would allow any trends in coefficients found from the copper condenser tests to be correlated with flow patterns observed from the transparent condenser tests.

# 2. EXPERIMENTAL FACILITY

## 2.1 Introduction

The motivation behind this study stems from work by Stoecker and McCarthy [11]. In testing a nonazeotropic mixture in a vapor-compression refrigeration system, they found local heat-transfer coefficients to decrease in the condenser as the percent of R-114 was increased in an R-114/R-12 mixture. It is understood that in order to realize the full thermodynamic advantages of using refrigerant mixtures, the magnitudes of the local heat-transfer coefficients of the mixtures must be maintained close to those of the pure components. For verification of the reduction in the local heat-transfer coefficients and study of the mechanisms behind the reduction, a test facility was constructed.

The test facility used in this work was constructed with the objective of duplicating the conditions experienced in the vapor-compression refrigeration system. The facility, which is located in the Mechanical Engineering Laboratory, Department of Mechanical and Industrial Engineering, at the University of Illinois at Urbana-Champaign, consists of both a transparent condenser and a copper condenser. The two condensers are connected in parallel although only one is in operation at any given time.

The transparent condenser allows observation of the various flow regimes and the positions along the condenser where they occur. In addition, the transparent condenser allows measurement of refrigerant temperature and pressure profiles. At selected locations along the condenser, refrigerant samples can be removed with the intent of performing composition analyses on them. The copper condenser is instrumented with thermocouples allowing the calculation of local heat-transfer coefficients at six different locations. Information on the pressure drop occurring during the condensation process can be obtained from the copper condenser.

## 2.2 The Test Facility

A schematic diagram of the test facility is shown in Fig. 2.1, and a photograph of the control panel to the test apparatus is shown in Fig. 2.2. A major portion of the system, i.e., the entire boiler loop, refrigerant pump, and subcooler, is located directly behind the control panel. The transparent condenser and the copper condenser are located above and to the right of the control panel.

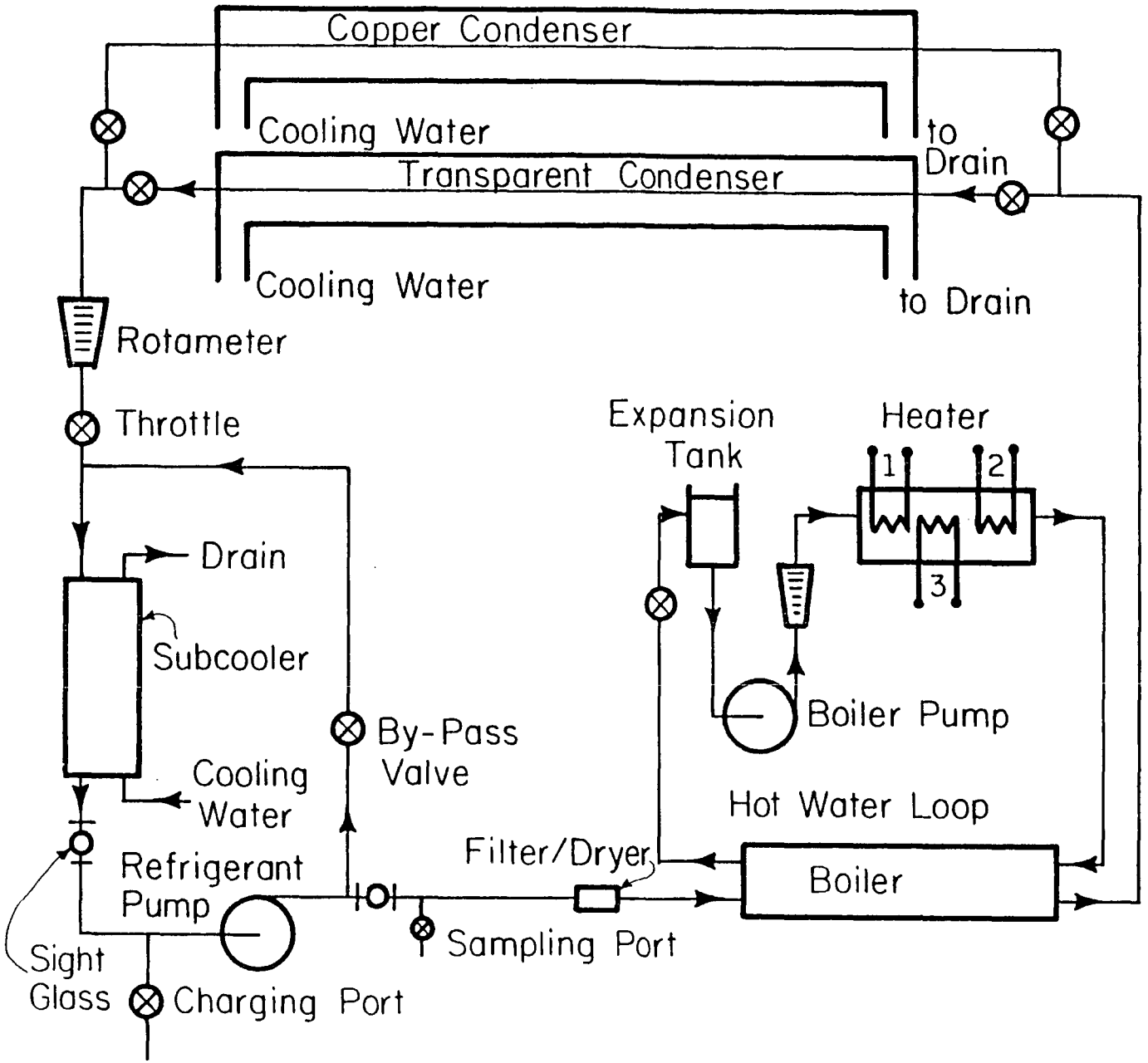


Figure 2.1. Schematic diagram of heat-transfer system.

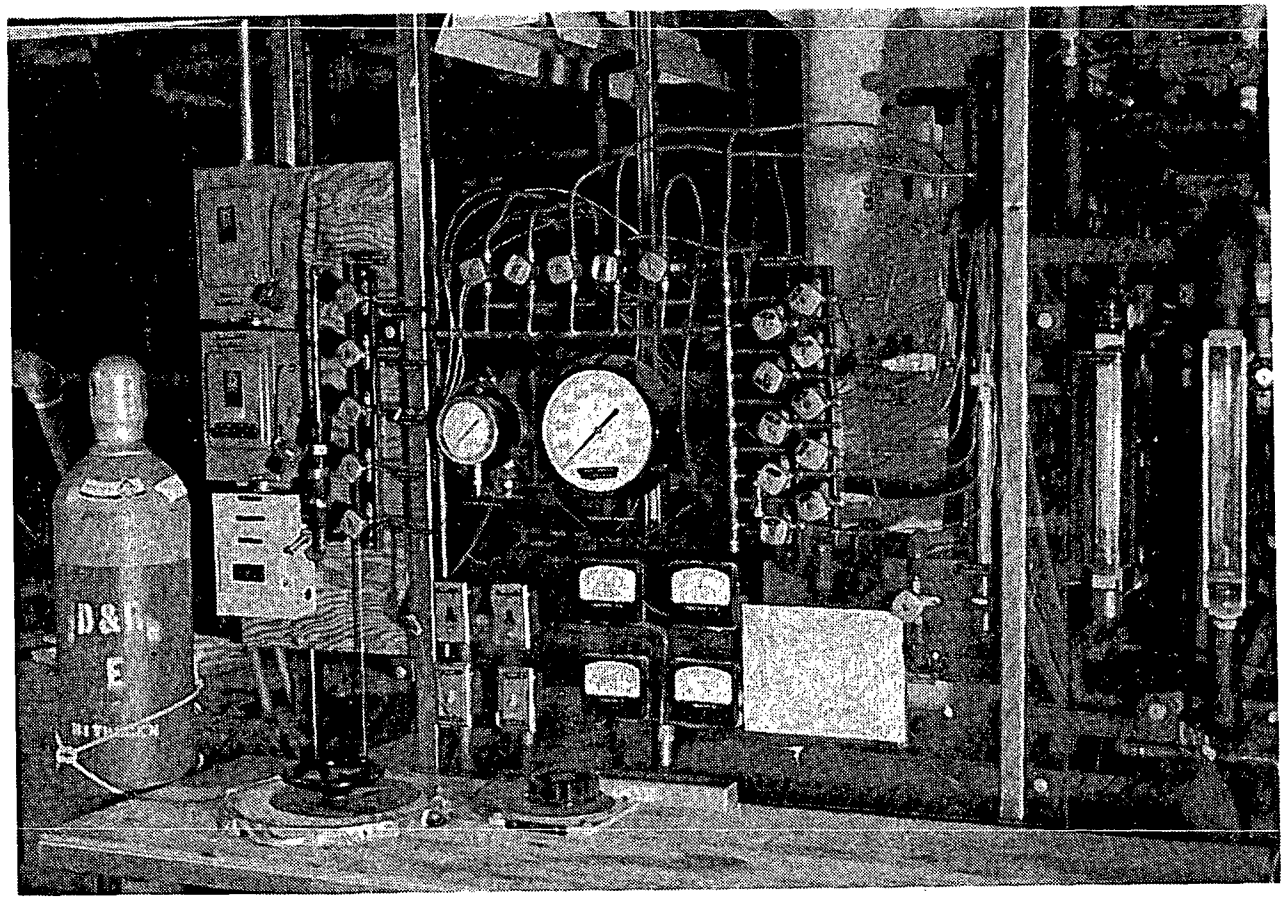

Figure 2.2. Photograph of control and instrumentation panel to heat-transfer studies system.

A large part of this facility was built by Kornota [10], but some modifications were made to the original system to meet the objectives of this current research study. The major modification was the addition of the copper condenser. The major portion of the work reported here centers around testing done with the copper condenser; thus, description of the copper condenser will be deferred until later where an entire section will be devoted to it. The remainder of this chapter deals with system and procedure modifications. Also, a brief description of the transparent condenser is given, as some of the testing was performed using this part of the system.

## 2.3 Components of the System

Unlike most compression refrigeration systems, this system uses a heavy-duty, bracket-mounted, positive-displacement pump to circulate the refrigerant. It is driven by a 3/4-hp, 1725-rpm motor. The ratio of pump speed to motor speed is 1:4.3.

Due to the requirement that liquid refrigerant be supplied to the pump, a copper, tube-in-tube heat exchanger (acting as a subcooler) is located upstream from the pump. Water from the city water supply flows in the annulus of this heat exchanger to cool the refrigerant. A sight glass is located between the subcooler and the pump for verification that the refrigerant is entirely liquid entering the pump.

The boiler and hot-water loop are downstream from the refrigerant pump. The refrigerant boiler is a copper, tube-in-tube, counterflow heat exchanger used to vaporize the liquid refrigerant before it enters the condenser. Hot water flows through the annulus of the boiler and provides the heat required to boil the refrigerant.

The hot water is circulated around an enclosed loop with a 1/4-hp centrifugal pump. The flow rate in the hot-water loop is measured with a rotameter. The heat input to the water is supplied by three 2000-W, 240-V heating elements. The power supplied to the heaters is controlled by two variable transformers. The heaters are located in a 75 mm (3-in.) galvanized pipe. The water flows through the pipe over the elements and is warmed to the desired temperature.

The liquid refrigerant flow rate leaving the condenser is measured with a rotameter. A throttle valve is located downstream from the rotameter to enable fine adjustment of the flow rate.

## 2.4 The Transparent Condenser

Figure 2.3 shows the points at which temperatures and pressure are measured on the transparent-condenser system. Figure 2.4 is a schematic diagram of the transparent condenser showing the 15.2-cm (6-in.) brass test section locations and also photography locations. The test sections are designed so that the thermocouples and the sample-removal ports can be adjusted to different vertical positions within the diameter of the refrigerant tube. The condenser is a tube-in-tube counterflow heat exchanger that has a two-pass configuration. The total length of the condenser is 20.7 m, and each of the test sections is approximately 1.5 m from the next. The refrigerant is condensed in the inner tube, which is 12.7-mm (1/2-in.) glass tubing. Cooling water flows in counterflow fashion through the annulus, the outer wall of which is made up of 6.35-cm-ID (2 1/2-in.) transparent plastic tubing. The test sections also contain pressure taps, which yield information on the pressure drop occurring along the condenser.

## 2.5 System Modifications

### 2.5.1 Relocation of Charging Port

Due to the nature of the experimental facility (i.e., low temperatures and pressures at startup), it is intentionally overcharged with refrigerant to ensure liquid to the pump. Therefore, some of the refrigerant must be released prior to the start of the test in order to achieve the desired conditions. The charging port, through which refrigerant is also released, was originally located after the expansion valve and before the subcooler. During tests when a refrigerant mixture is used, it is critical that the refrigerant be released at a location where the mixture is all vapor or all liquid so that the sample released is of the same concentration as that in the system. A special test using a gas chromatograph was conducted to measure the

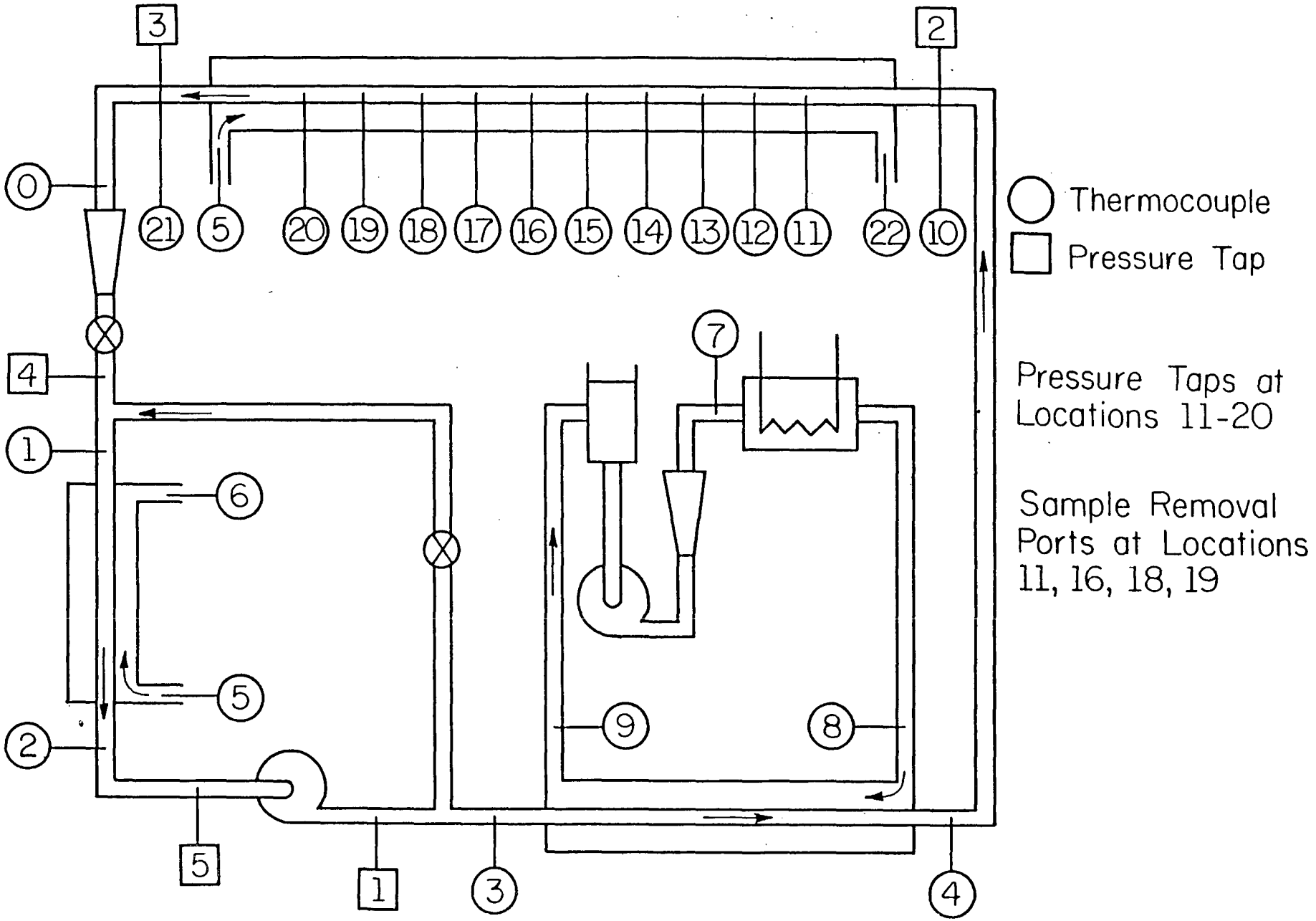


Figure 2.3. Diagram showing location of instrumentation for system with transparent condenser.

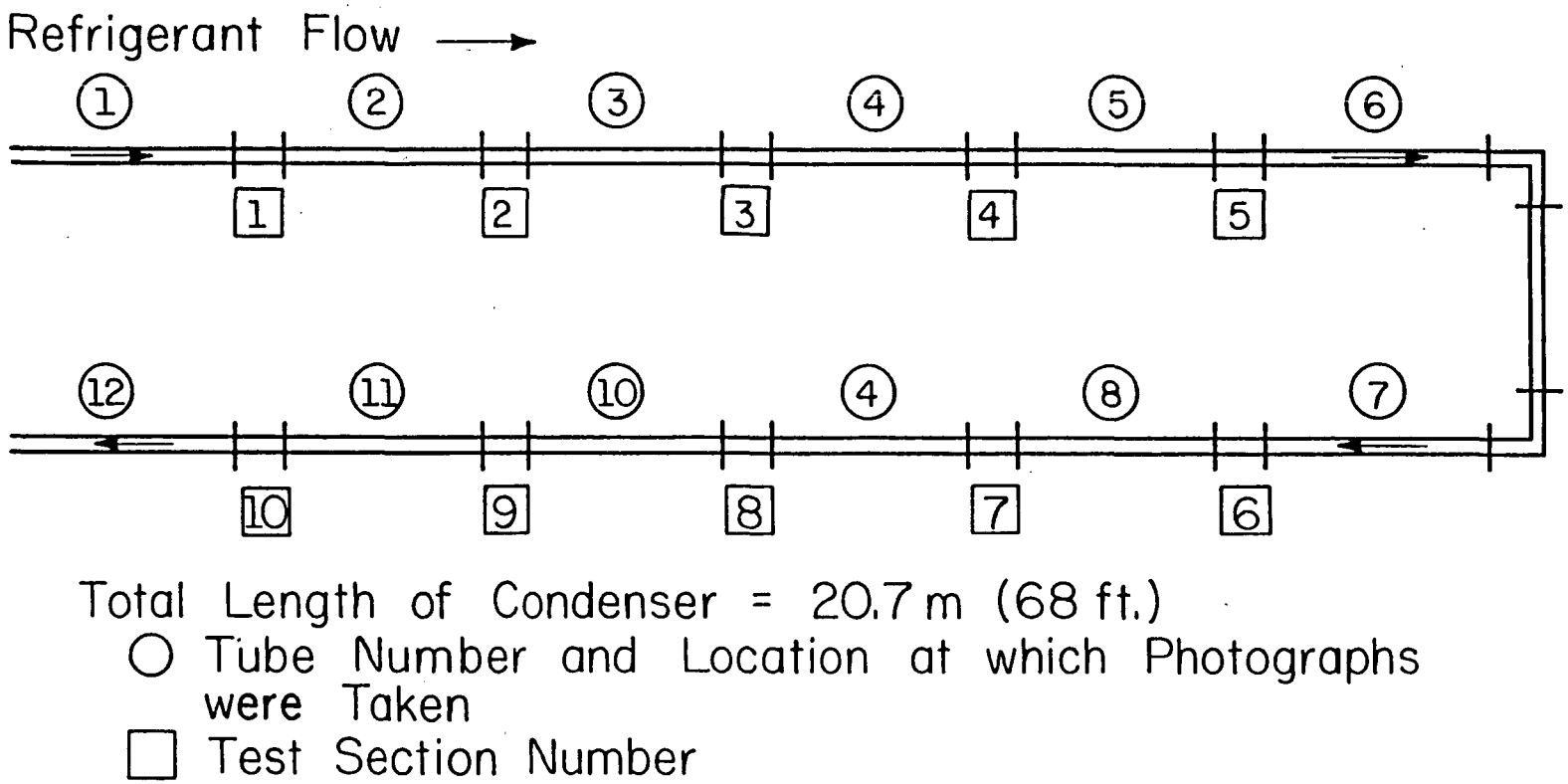


Figure 2.4. Transparent condenser numbering system for brass test sections and photography locations.

concentration of the refrigerant released at the charging port when it is located after the expansion valve. The average mass composition in the system was 50 percent R-12 and 50 percent R-114, but the composition being vented was 30 percent R-12, and 70 percent R-114 by mass. These results indicated that the composition in the system would be distorted by venting refrigerant at the original location. Therefore, a new discharge port was added to the system at test section 1.

### 2.5.2 Addition of Sample Removal Port on the Condenser

Initially, the transparent condenser was equipped with three refrigerant-sample-removal ports: at brass test sections 6, 8, and 9. All of these sample-removal locations are located downstream of the condenser mid-point. The flow regimes that exist at these locations (wavy/stratified or slug-flow) make it very difficult to remove a sample that is entirely vapor. It was desirable to have sample-removal capabilities at a location in the condenser where a vapor-only sample could be removed. Furthermore, it was noticed in previous tests that at test section 1, liquid was present when the temperature indicated that the refrigerant should be superheated. However, because this location offered the best opportunity for extracting a vapor-only sample, a sample-removal port was installed at test section 1.

## 2.6 Procedure Modifications

### 2.6.1 Sample-Removal Modifications

Upon reviewing the procedure in the previous work in which the samples were removed from the system and ultimately analyzed in the gas chromatograph, we determined that some improvements could be made. The two steps in the procedure targeted for improvement were (1) the sample extraction from the system, and (2) the removal of refrigerant from the sample-removal canister when preparing it for analysis.

When a refrigerant sample is removed from the system, it is important that a vapor-only or liquid-only sample be taken. A sample of part liquid, part vapor would give meaningless composition results because there is no way of determining the fraction of liquid in the sample. Likewise, when refrigerant is taken from the sample-removal canister and prepared for composition analysis, the sample must exist in the canister as one phase. Analysis of a

sample taken from a canister in which saturation conditions exist would give incorrect results.

In the method previously used, the refrigerant sample for the gas chromatographic analysis was removed directly from the sample-removal canister. This procedure required that the refrigerant extraction from the system be done in a very precise manner to avoid saturation conditions in the canister. Furthermore, for each test, refrigerant samples were extracted at four different locations along the condenser. Since samples were removed one at a time and not simultaneously, it was desirable to remove a minimum amount of refrigerant to avoid disturbance of the test conditions in the condenser. To this end the sample-removal canister was redesigned to remove a minimum amount of refrigerant.

The modified refrigerant-removal canister shown in Fig. 2.5 incorporates the following changes in comparison with the previously used model. It is much smaller than the original canister, which reduces the amount of refrigerant to be extracted from the system. The need for the charging hose is eliminated because a quick-connect refrigerant charging valve fits directly on a spring-loaded access valve on the system. Also, in the new procedure, the canister was evacuated, and when a sample was to be taken, the hand valve on the canister was opened momentarily to draw in a sample. The canister was then disconnected from the system.

At this point in the procedure the refrigerant could, and very likely did, exist at saturated conditions in the sample-removal canister. This problem was remedied by using a second canister as shown in Fig. 2.6. The numbering scheme used to describe the canister is depicted in Fig. 2.7. The canister containing the refrigerant sample was snapped on to the previously evacuated secondary canister through the use of the quick-connect refrigerant fitting (point 1 in Fig. 2.7). Evacuation of the canister was possible through the use of the hand valves (point 2 in Fig. 2.7). Due to the sudden increase in volume and the warning to room temperature, the refrigerant was entirely superheated vapor in the two-canister combination. The pressure gauge (point 3 on Fig. 2.7) was used to confirm this fact.

The refrigerant was then ready to be extracted from the two-canister configuration and prepared for chromatographic analysis. The gas syringe adapter (point 4 on Fig. 2.7) allowed the gas syringe to be inserted directly

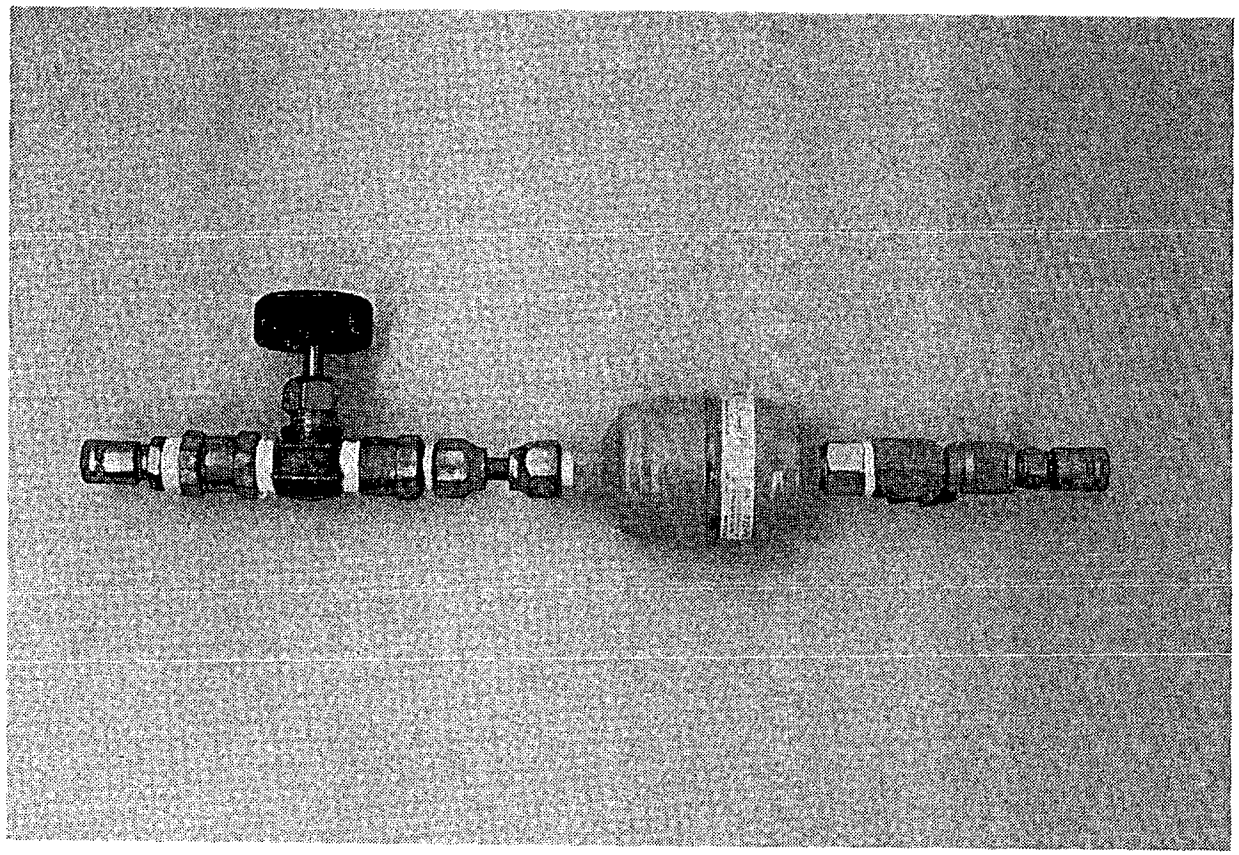

Figure 2.5. Modified refrigerant sample-removal canister.

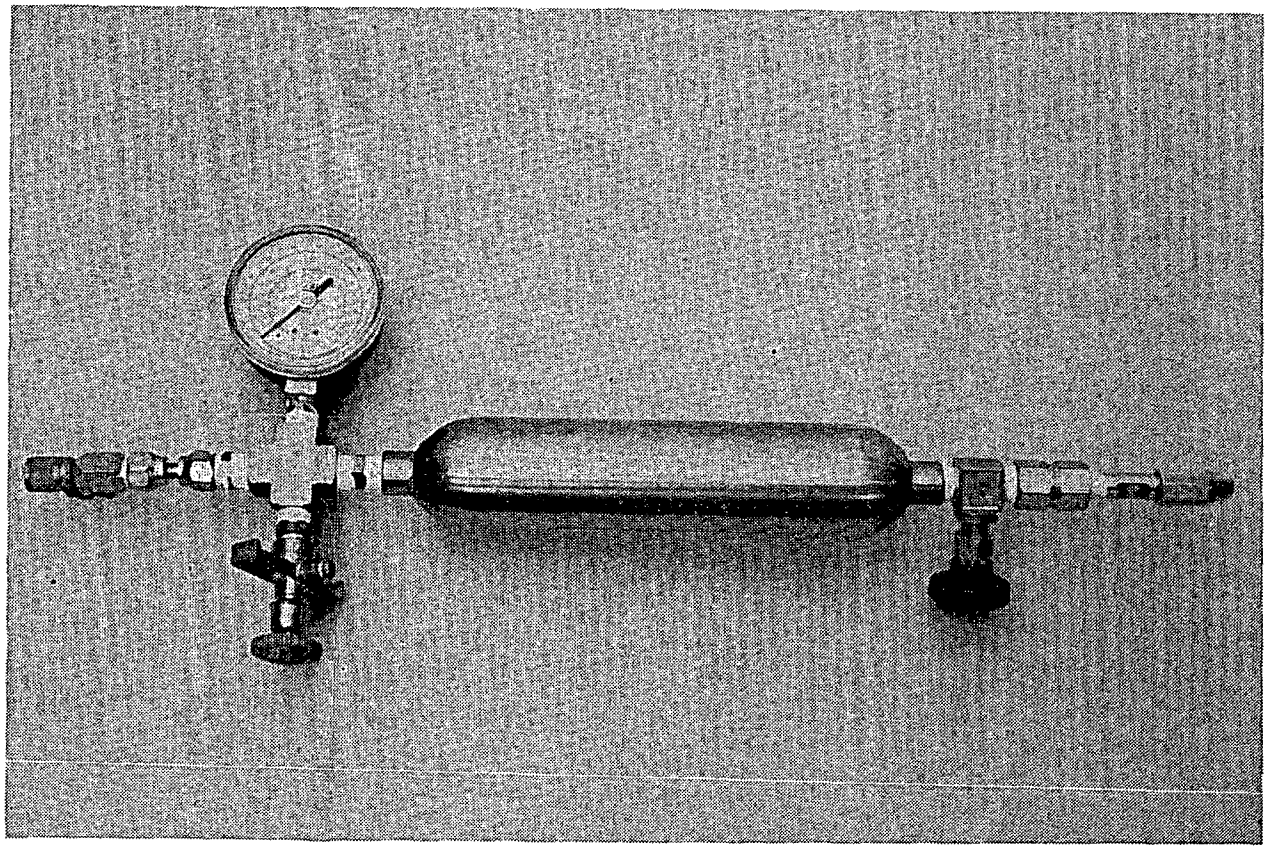

Figure 2.6. Secondary canister used in refrigerant mixture composition analysis.

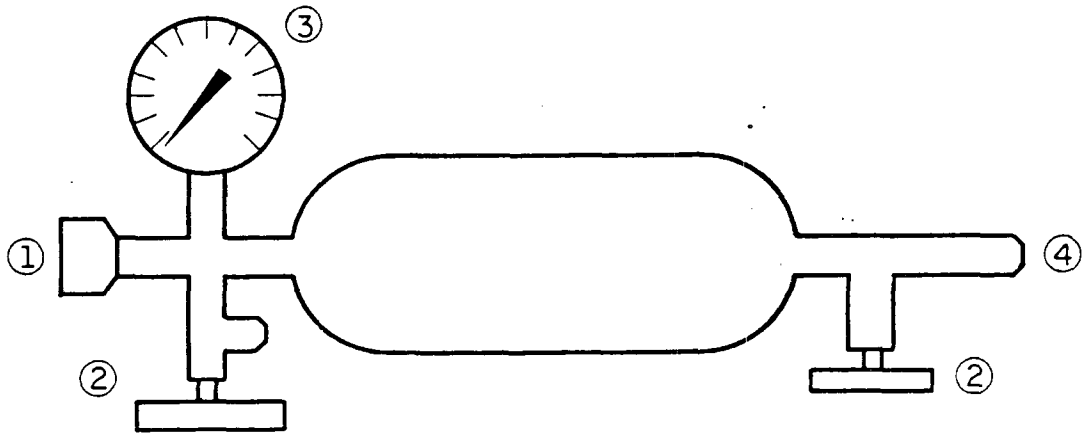


① Refrigerant Fitting (Quick-Connect)

② Hand Valve

③ Pressure Gauge

④ Gas Syringe Adapter

Figure 2.7. Schematic diagram of secondary canister.

into the canister. From this point on, sample preparation and chromatographic analysis proceeded as usual. A measured volume of refrigerant was removed from the refrigerant canister and injected into a vial containing liquid hexane. The hexane was used as a solvent in which the refrigerant could dissolve. A measured volume of the hexane-refrigerant solution was injected into the gas chromatograph. The actual concentrations of refrigerants in the mixture were determined from the graphic output of the gas chromatograph. The details of the entire procedure including the gas chromatograph settings and analysis of the chromatograph output can be found in Ref. 10.

### 2.6.2 Photography Modifications

To correlate various flow patterns with the resulting heat-transfer coefficients, we photographed the flow patterns occurring at various locations (Fig. 2.4) along the condenser. The photographs were taken with a 35-mm camera with a regular 50-mm lens. Black-and-white "Tri-X" pan film was used. The camera was supported by a tripod resting on a mobile cart. The camera was positioned normal to the condenser tubes, in the same horizontal plane, approximately 3/4 to 1 m from the condenser. The background consisted of two 100- by 350-mm black cardboard sheets separated by a 75- by 350-mm double-layered semitransparent piece of plastic sheeting. The background was placed immediately behind the condenser tube. The setup was illuminated with a tungsten-filament lamp with diffusers located approximately 1 m directly behind the background. The semitransparent plastic sheeting was aligned with the condenser tubes, allowing the diffused light from the lamp to shine through and illuminate the tubes while reducing glare.

# 3. NONEQUILIBRIUM PHENOMENA IN THE CONDENSER

## 3.1 Purpose of Tests

Tests 21 through 28 constituted a fourth series of tests run with the transparent condenser and represented a continuation of the three series of tests performed by Kornota [10]. This fourth series was conducted with the intent of identifying nonequilibrium phenomena occurring during the condensation of binary refrigerant mixtures. For these tests, the thermocouples and sample-removal ports were located at different vertical locations within the tube cross sections. Also, a sample-removal port was installed at the condenser entrance so that composition information would be available at the entrance, midpoint, and exit of the condenser. It was hoped that the data obtained from a vertical traverse of the tube diameter with the instrumentation would provide insight into nonequilibrium phenomena occurring within the condenser. If nonequilibria could be identified, it was hoped that those effects due solely to "slip" could be singled out. Slip occurs in two-phase flow when the velocity of the vapor at the liquid-vapor interface exceeds that of the liquid.

## 3.2 Test Conditions

Test series 4 consisted of three separate groups of tests. Each group of tests included a mixture test and tests of pure R-12 and of pure R-114. The thermocouple probes and sample-removal ports were located at different vertical positions within the tube for each group of tests. The three vertical elevations at which the thermocouple and sample probe were located, corresponding to the three groups of tests, were at 0 diameter (bottom of tube), 1/3 tube diameter from the bottom, and 2/3 tube diameter from the bottom. Figure 3.1 is a schematic diagram of the instrumentation locations for test series 4.

The mixture tests had an overall mass composition of approximately 70 percent R-12 and 30 percent R-114. The decision to use this particular concentration stems from experimentation by Kornota [10] where he found a major reduction in condensing coefficients occurring at approximately a 30 percent concentration of R-114. An additional reason to study the chosen mixture concentration stems from work by Arora [8] who found that the boiling heat-transfer coefficients decreased as the percent of R-114 was increased in

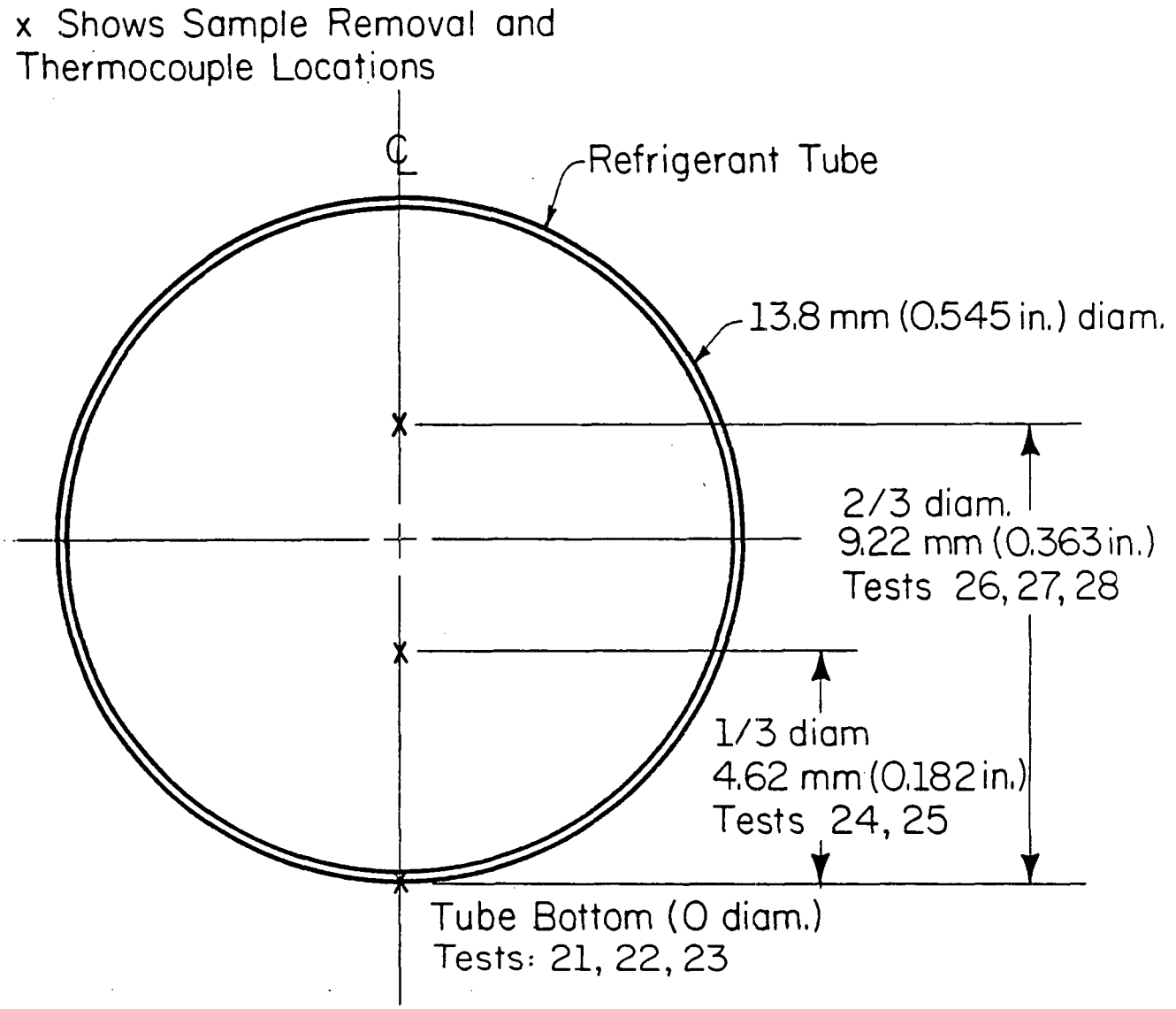


Figure 3.1. Thermocouple and sample-removal locations for test series 4.

the mixture. Arora reported that the coefficients reached a minimum at a 30 percent R-114, 70 percent R-12 mixture by mass.

The tests in the series were standardized by specifying the refrigerant inlet temperature (45.0°C). Also, the outlet temperature for each composition was chosen to ensure complete condensation of the refrigerant. With the inlet and outlet temperatures specified for each composition, a flow rate was chosen such that the overall heat-transfer rate (or average heat flux) was kept constant for each test. A summary of the test conditions for series 4 is given in Table 3.1.

## 3.3 Test Results: Experimental Data

### 3.3.1 Introduction

We hoped that collecting experimental data from different points along the vertical traverse in the condenser would yield information about the extent of nonequilibrium. Due to restrictions on movement of the instrumentation, data at only one vertical location along the tube diameter could be obtained per test. The ideal situation of making a vertical traverse of the condenser tube diameter during a test of each mixture composition was not possible because movement of the instrumentation required removal of seals on the condenser tube. To this end great care was taken to keep test conditions the same between the three groups of tests for each mixture composition.

Some minor variations existed between tests of similar composition in the different groups of tests. For example, minor pressure variations, 20 to 60 kPa, existed between tests of similar concentration in different groups mainly because of slight changes in the condenser cooling-water temperature. Therefore, comparisons will be made only where it can be assumed that these minor variations would be of no consequence. Also, due to slight differences in amounts of superheating and subcooling, comparisons between tests of different mixture compositions will be limited.

### 3.3.2 Temperature Profiles

Figure 3.2 displays representative longitudinal temperature profiles for each mixture composition used in test series 4. For test 24, the system was initially charged with a 28.6 percent mass concentration of R-114. Note that points along the abscissa are denoted by test section

Table 3.1 Summary of Actual Conditions for Test Series 4

| Group No. (Instru-mentation Location) | Test No. | % R-114 by Mass | Refrig. Flow Rate (kg/s) | Avg. Heat Flux ($kW/m^2$) | Condenser Entering/ Leaving Refrig. Temp. (°C) | Condenser Entering/ Leaving Refrig. Pressure (kPa Gauge) | Equilibrium Temperature Dew/Bubble Pts. for Mean Condenser Pressure(°C) |
|---|---|---|---|---|---|---|---|
| Group 1: | 21 | 100.0 | 0.0250 | 4.56 | 45.0/16.8 | 191/170 | 33.9/33.9 |
| 0 dia. | 22 | 0.0 | 0.0231 | 4.36 | 45.0/19.5 | 640/632 | 29.6/29.6 |
| (bottom of tube) | 23 | 29.6 | 0.0226 | 4.34 | 45.0/18.4 | 428/418 | 30.7/23.1 |
| Group 2: | 24 | 28.6 | 0.0226 | 4.33 | 45.0/18.5 | 469/459 | 33.0/25.6 |
| 1/3 dia. 4.62 mm | 25 | 100.0 | 0.0251 | 4.57 | 45.0/16.8 | 189/169 | 33.5/33.5 |
| Group 3: | 26 | 30.3 | 0.0227 | 4.36 | 45.0/18.5 | 410/399 | 29.8/22.0 |
| 2/3 dia. | 27 | 0.0 | 0.0231 | 4.36 | 45.0/19.5 | 643/630 | 29.6/29.6 |
| 9.22 mm | 28 | 100.0 | 0.0233 | 4.20 | 45.0/18.5 | 179/149 | 31.8/31.8 |

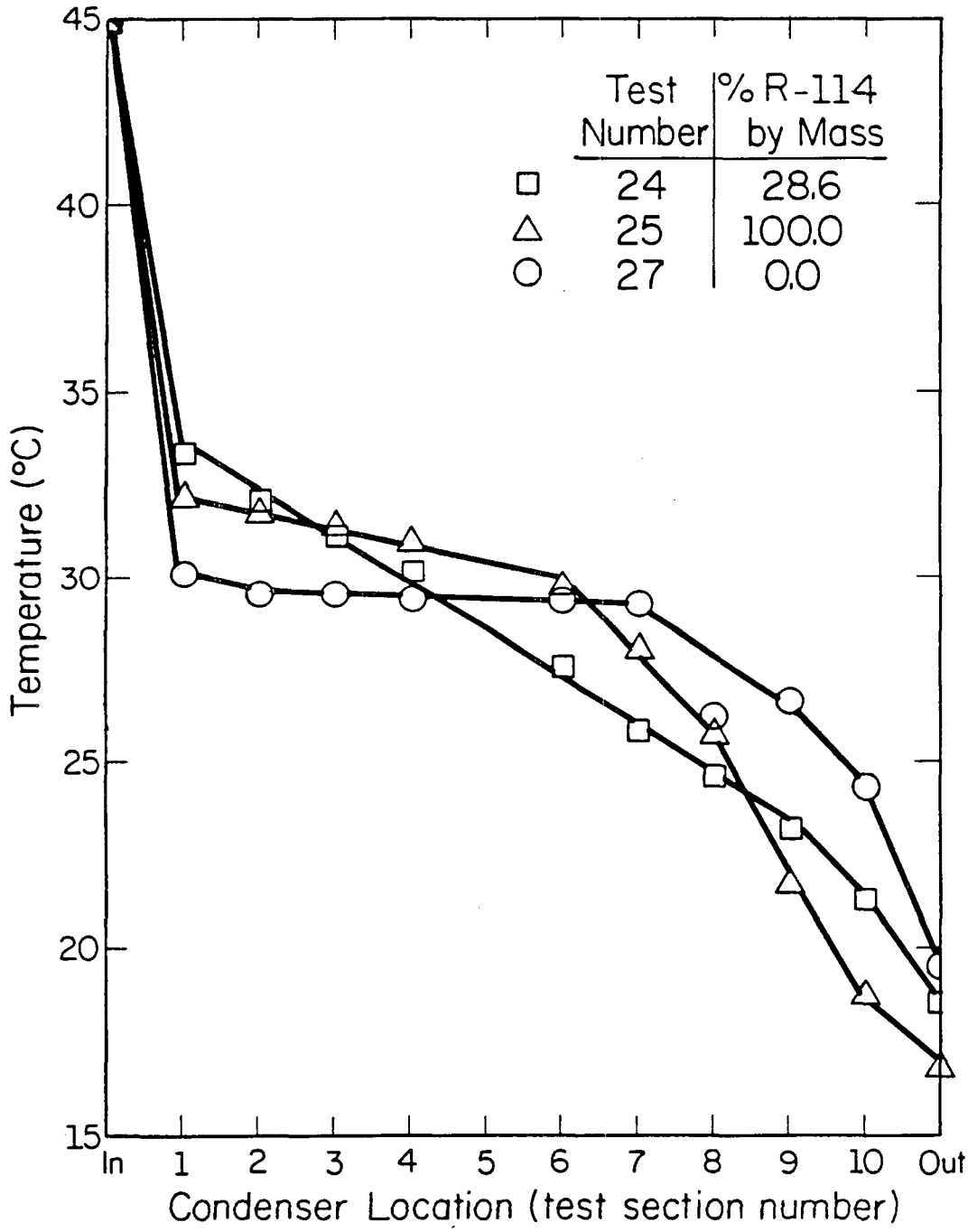


Figure 3.2. Refrigerant temperature profiles along condenser for R-114 concentrations in R-12/R-114 mixtures used in test series 4.

numbers which refer to specific locations along the condenser as shown in Fig. 2.4. The results depicted in Fig. 3.2 are similar to the results shown in the profiles obtained by Kornota. The temperature of the refrigerant mixture steadily decreased during the condensation process. The temperature of the pure R-12 was fairly constant during condensation. On the other hand, the temperature of the pure R-114 showed a slight decline during the condensing process due to the pressure drop along the condenser which was approximately twice that of the tests of pure R-12.

By examining the test data, the fluid properties, and a proposed correlation for pressure drop inside a horizontal tube, one can mathematically verify the doubling of $\Delta p$ from pure R-12 to pure R-114. The test data revealed that 77 percent of the pressure drop for pure R-12 occurred in the first half of the condenser. This number swells to 86 percent for pure R-114. Thus, a major portion of the $\Delta p$ occurs while the fluid is predominantly vapor.

The Blasius correlation [12] for pressure drop in horizontal tubes at low turbulent Reynolds numbers shows the pressure drop to be dependent on the tube geometry, fluid properties, and flow conditions.
For $4000 < Re_d < 10^5$:

$$\Delta p \cong 0.158 \frac{L}{\rho_v} \left(\frac{\dot{m}}{A}\right)^{1.75} \mu_v^{0.25} D^{-1.25} \tag{3.1}$$

For this expression, $Re_d$ is the Reynolds number based on the tube diameter, and L is the length of the tube in meters. The remainder of the terms are defined in the NOMENCLATURE.

The pipe geometry was constant for both fluids while the flow conditions were nearly equal. Thus, the differences in $\Delta p$ occurring between the R-12 and R-114 must have been caused by fluid properties. Moreover, since most of the pressure drop occurred in the first half of the condenser, concentration was focused on the vapor properties of viscosity and density (or specific volume). At a representative test temperature (300 K), the viscosities of vapor R-12 and vapor R-114 are nearly equal [13]. At the same temperature, the specific volume of vapor R-114 is 2.3 times greater than that for R-12 [13]. The pressure drop correlation from Blasius showed $\Delta p$ to be inversely proportional to density (or directly proportional to specific volume). Thus,

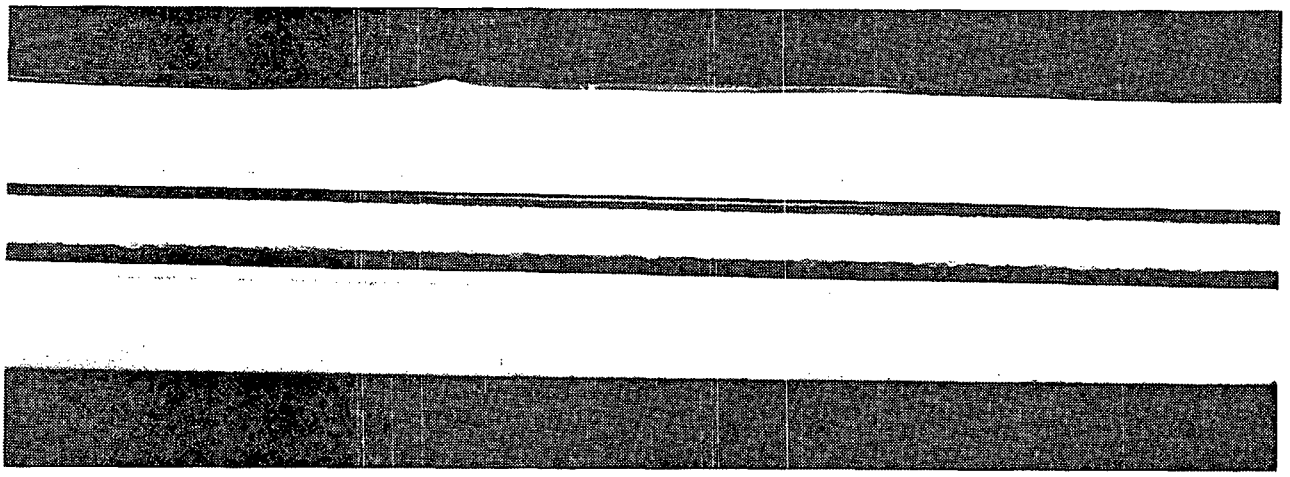

Figure 3.3. Photograph location 1, 1.0 m downstream; annular flow, little liquid.

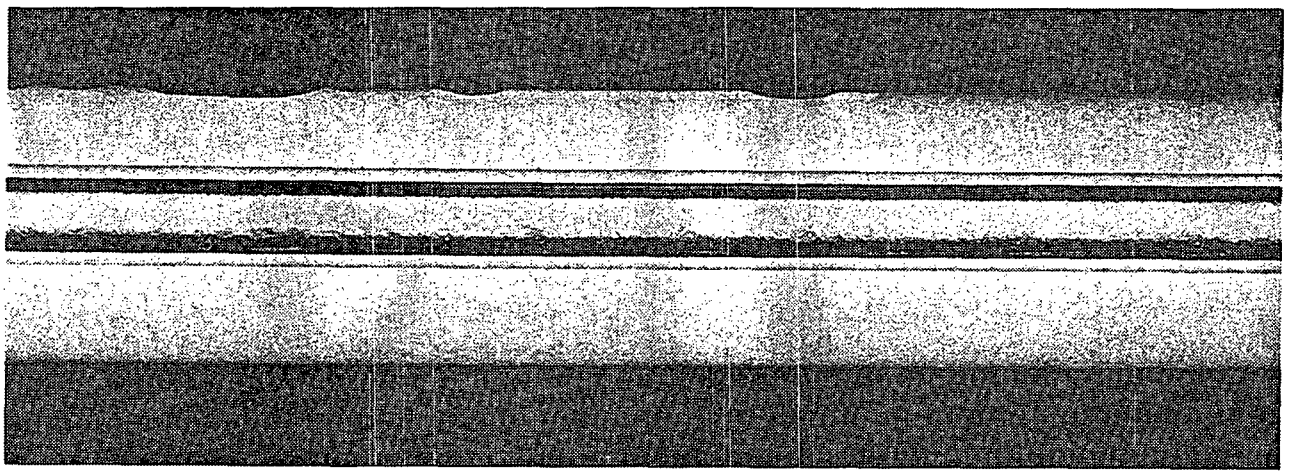

Figure 3.4. Photograph location 2, 2.6 m downstream annular flow.

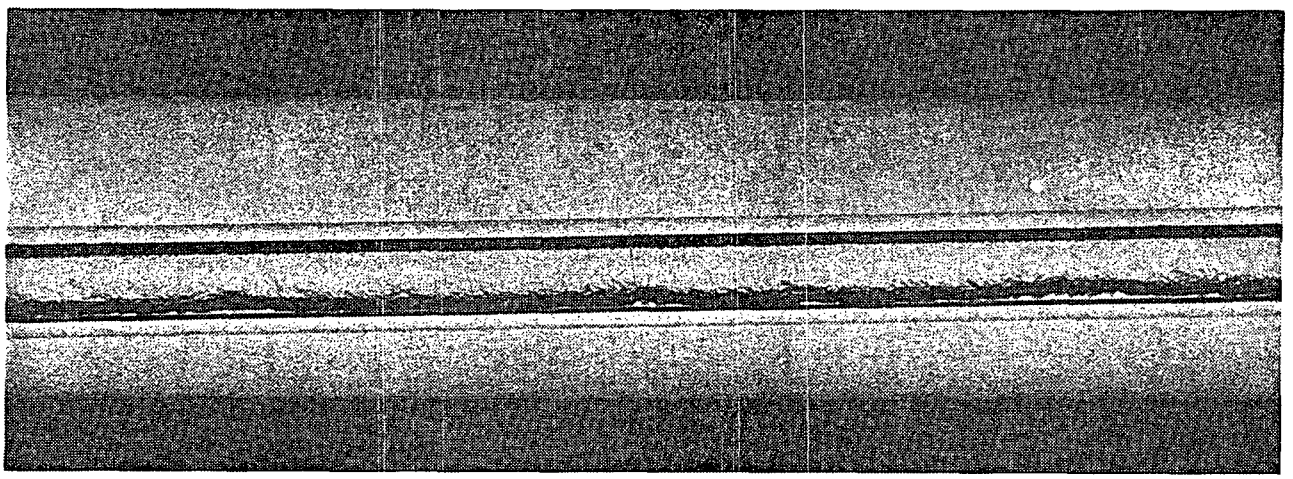

Figure 3.5. Photograph location 3, 4.0 m downstream; annular flow.

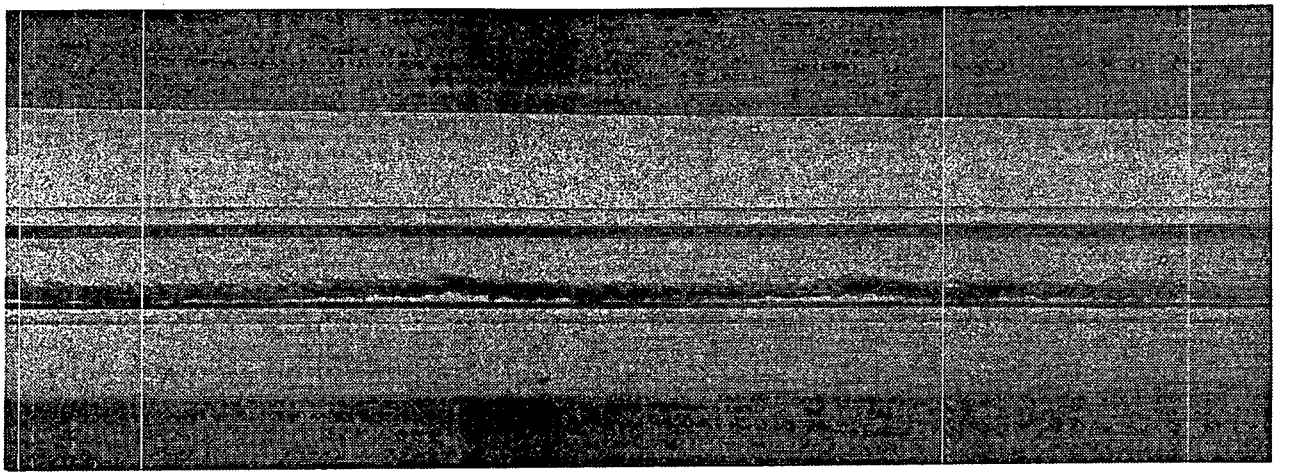

Figure 3.6. Photograph location 4, 5.9 m downstream; annular flow.

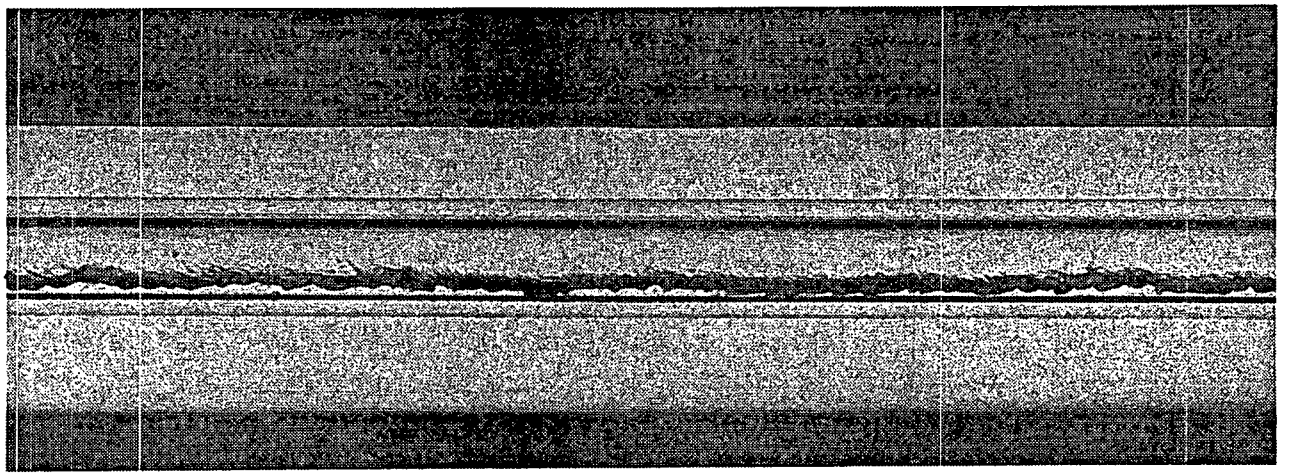

Figure 3.7. Photograph location 5, 7.5 m downstream; annular to wavy flow transition.

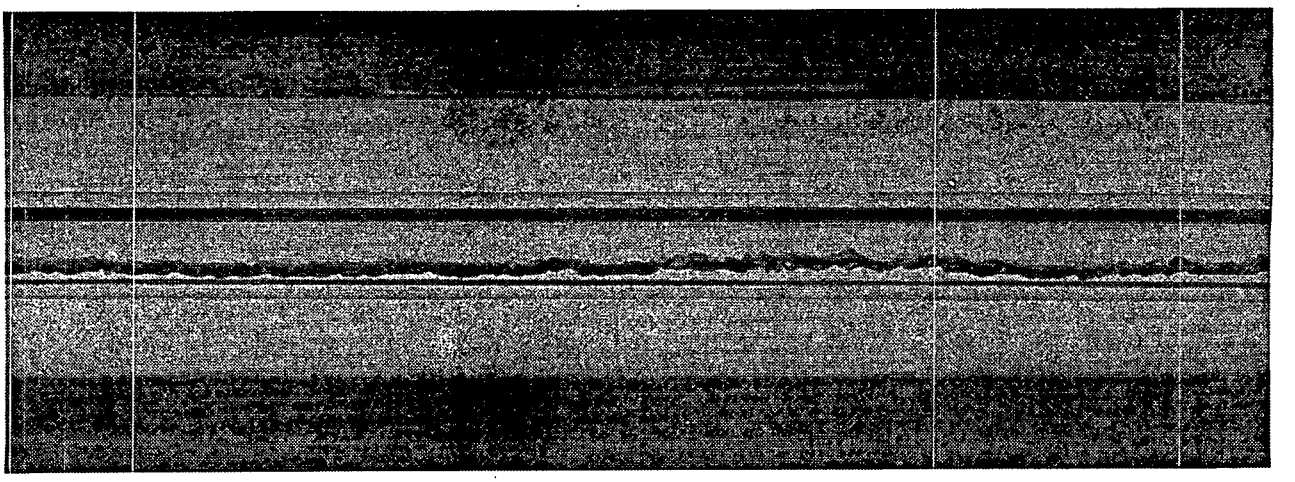

Figure 3.8. Photograph location 6, 9.0 downstream; annular to wavy flow transition.

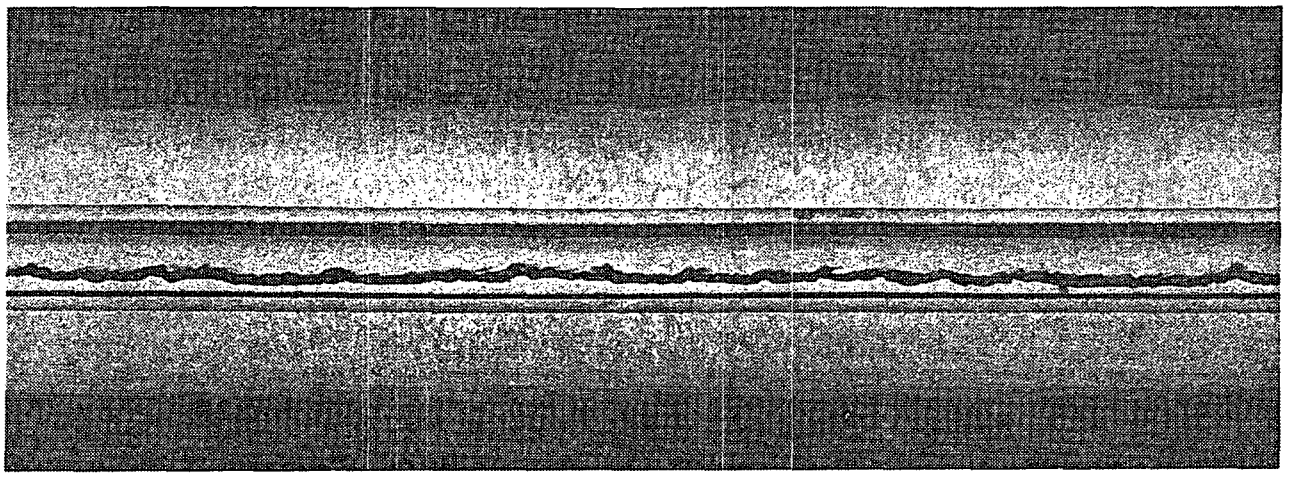

Figure 3.9. Photograph location 7, 12.0 m downstream; wavy flow.

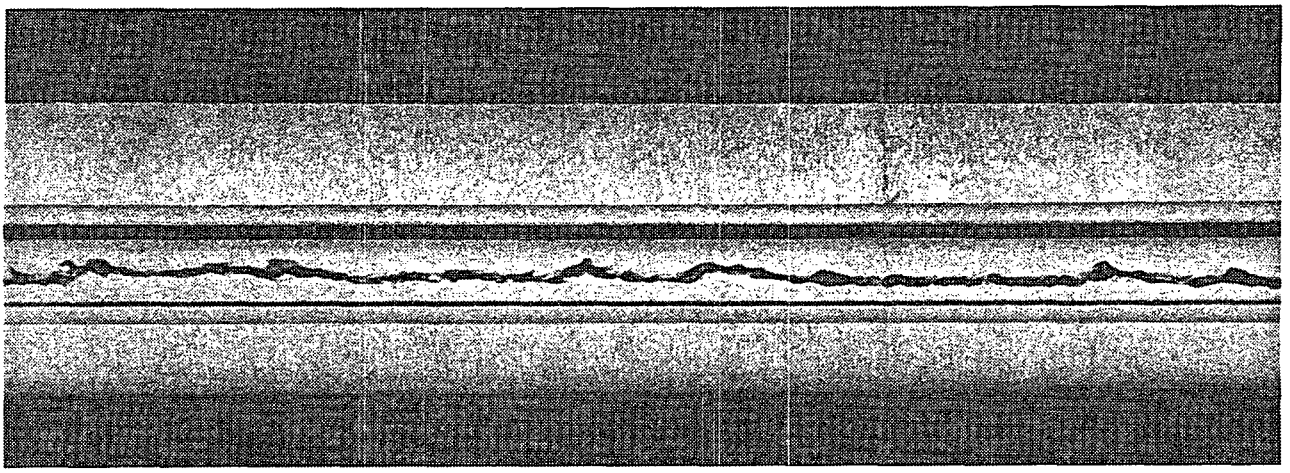

Figure 3.10. Photograph location 8, 13.6 m downstream; wavy flow.

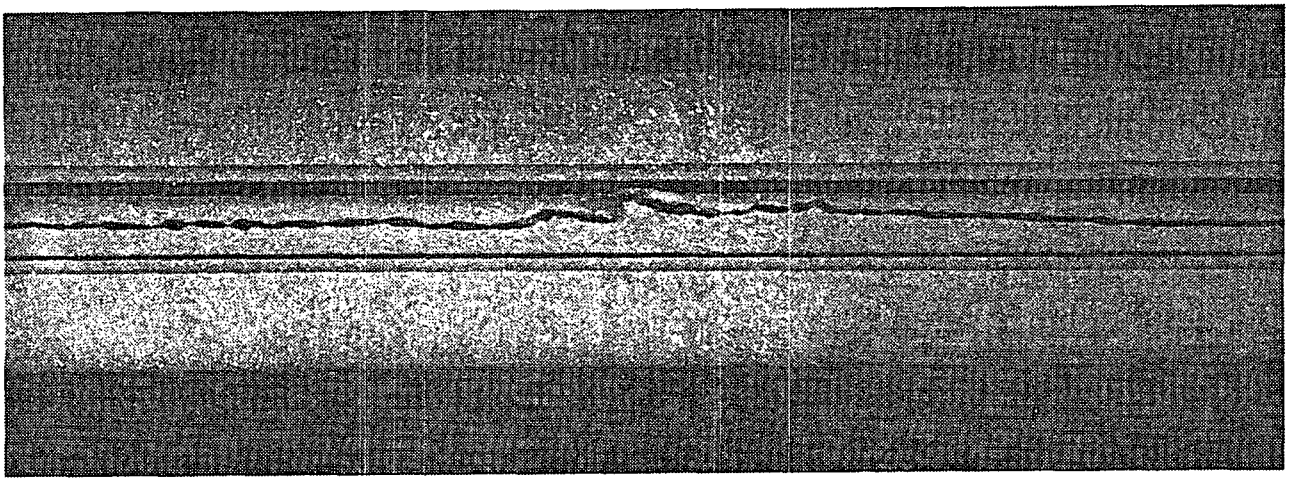

Figure 3.11. Photograph location 9, 15.3 m downstream; wavy flow.

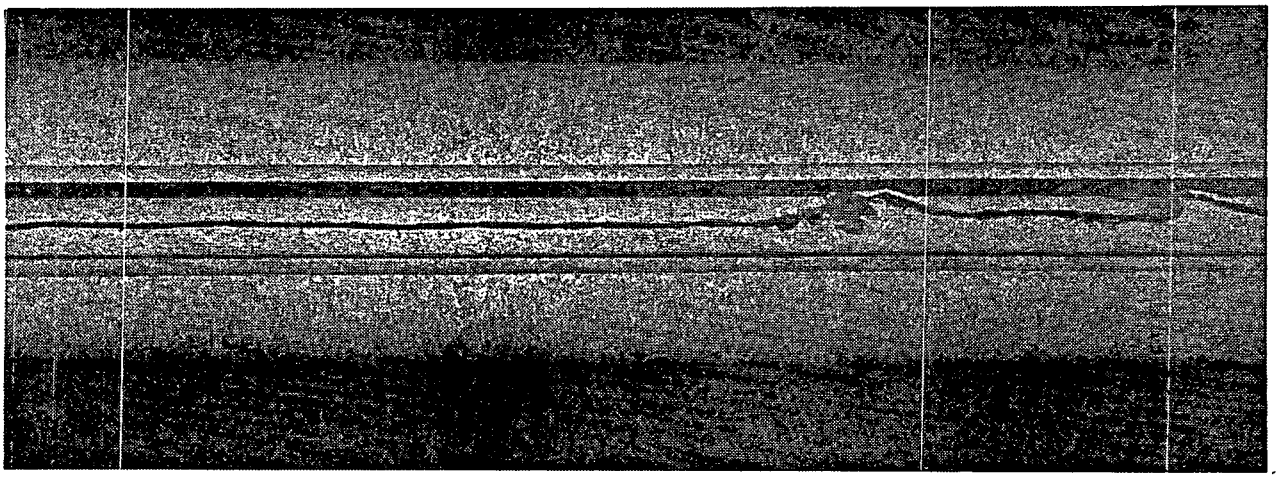

Figure 3.12. Photograph location 10, 17.1 m downstream; wavy flow.

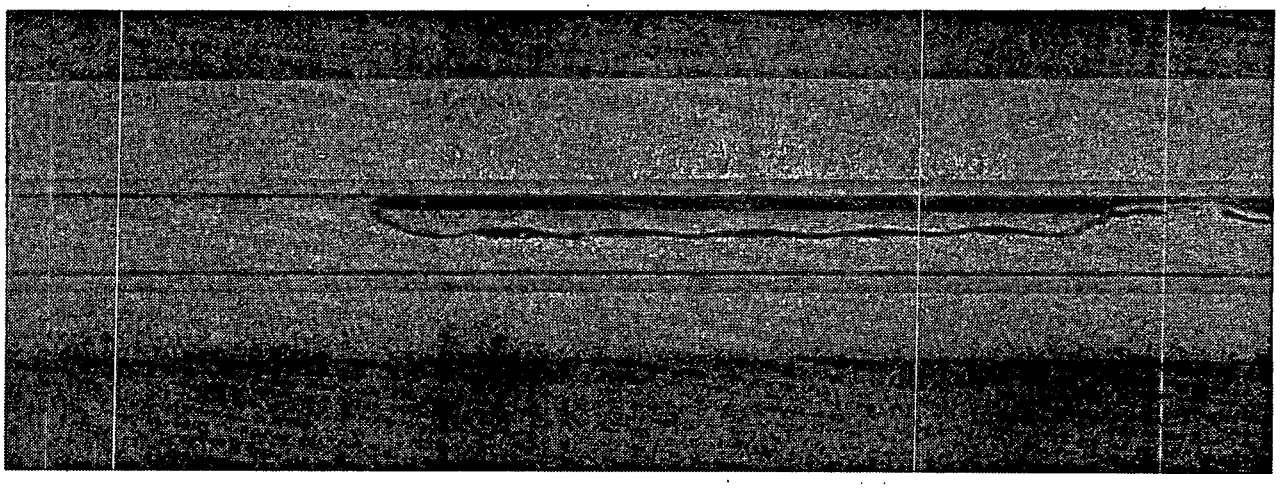

Figure 3.13. Photograph location 11, 18.7 m downstream; slug flow.

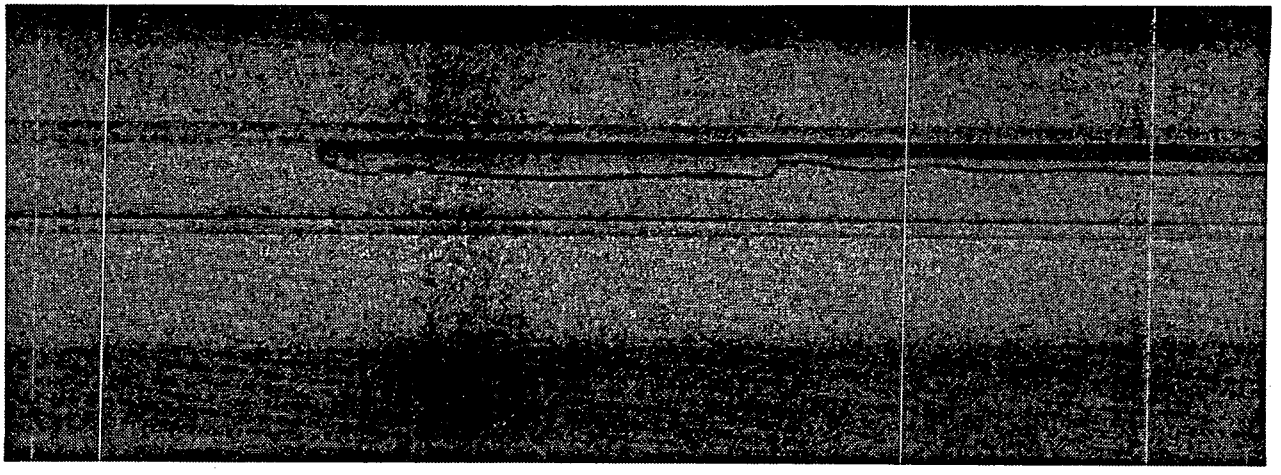

Figure 3.14. Photograph location 12, 20.1 m downstream; slug flow.

based on the vapor specific volumes, the correlation would predict the $\Delta p$ for R-114 to be approximately 2.3 times that for R-12.

The single-refrigerant profiles exhibited a decline in temperature around test sections 6 or 7, although saturated conditions still exist at these locations as well as points further downstream in the condenser. As mentioned by Kornota [10], this is due to the thermocouples being influenced by the temperature of liquid, which here began to be subcooled. The profile for pure R-12 exhibits 15.4°C of superheat and 10.1°C of subcooling. The profile for pure R-114 has 11.5°C of superheat and 16.7°C of subcooling. The mixture profile has 15.2°C of superheat and 3.5°C of subcooling.

### 3.3.3 Flow Regimes During Condensation

To show correlation of the data presented in subsequent sections to their associated flow patterns, the photographs from test 26, in which the mixture composition was 30.3 percent R-114 and 69.7 percent R-12 by mass, are shown in Figs. 3.3 and 3.14. The refrigerant entered the condenser with 15.2°C of superheat and left with 3.5°C of subcooling. Other information concerning the flow parameters can be found in Table 3.1.

The numbered locations along the condenser where photographs were taken are given in the photograph caption and correspond to position shown in circles in Fig. 2.4.

The glass condenser tube is the narrower horizontal band in the light-colored portion of each picture. At the entrance of the condenser, the flow is annular with vapor flowing in the center and condensation occurring on the tube surface. At these positions (Figs. 3.3 to 3.6), liquid coexists with superheated vapor. The flow regime changes from annular to wavy flow in Figs. 3.7 and 3.8 and is wavy in Figs. 3.9 through Fig. 3.12. Further downstream in the condenser, the flow turned to slug flow (Figs. 3.13 to 3.14) before becoming completely condensed. Similar flow patterns existed at approximately the same locations along the condenser for single refrigerant tests.

### 3.3.4 Temperature Gradient/Fluctuations

Nonequilibrium temperatures prevail in condensers, even when condensing a single refrigerant. In order for heat to be transferred, a temperature gradient must exist; and in order for vapor to condense, the vapor pressure of the liquid must be less than the actual pressure of the vapor. In tube-type condensers a phenomenon occurs, called slip, in which the vapor moves down the tube at a higher velocity than the liquid. When a refrigerant mixture condenses, the existence of slip shifts the vapor such that a higher temperature and a lower concentration of R-114 (in the R-12/R-114 mixture) is in contact with the liquid than would be true if no slip had occurred.

Some temperature measurements were taken using fine-gauge thermocouples to sense rapidly changing temperatures at two different elevations in the refrigerant tube. Figures 3.15 and 3.16 show the temperature fluctuations at test section 10 at the bottom of the tube (test 23) and at 9.22 mm from the tube bottom and 2/3 up the tube diameter (test 26), respectively. Tests 23 and 26 each had an approximate mass concentration of 30 percent R-114 and 70 percent R-12 charged into the system.

Figure 3.15 in itself does not give proof that slip was occurring. The temperature fluctuations were not large and did not show a dominant trend of upward or downward peaks. The above result was expected because the refrigerant was almost entirely condensed at test location 10. Thus the thermocouple at the bottom of the tube was in constant contact with liquid. Therefore, the actual liquid temperature would be given by the average temperature in Fig. 3.15, which turns out to be approximately 20.4°C.

Viewing Fig. 3.16, which gives temperature data two-thirds up the tube diameter at the same condenser location, a definite upward trend can be seen in the peaks of the graph. These upward peaks are due to periodic encounters of the thermocouple with vapor pockets in the refrigerant stream. The temperature of the vapor is at least as high as the uppermost points of the peaks. However, the temperature of the vapor could exceed that given by the peaks of the graph because all of the liquid must evaporate from the thermocouple bead before the actual temperature of the vapor can be obtained.

Figure 3.16 indicates that the temperature of the vapor is at least 22.0°C. The temperature of the liquid at this location would be given by the base of the peaks in Fig. 3.16. From this figure it can be seen that the

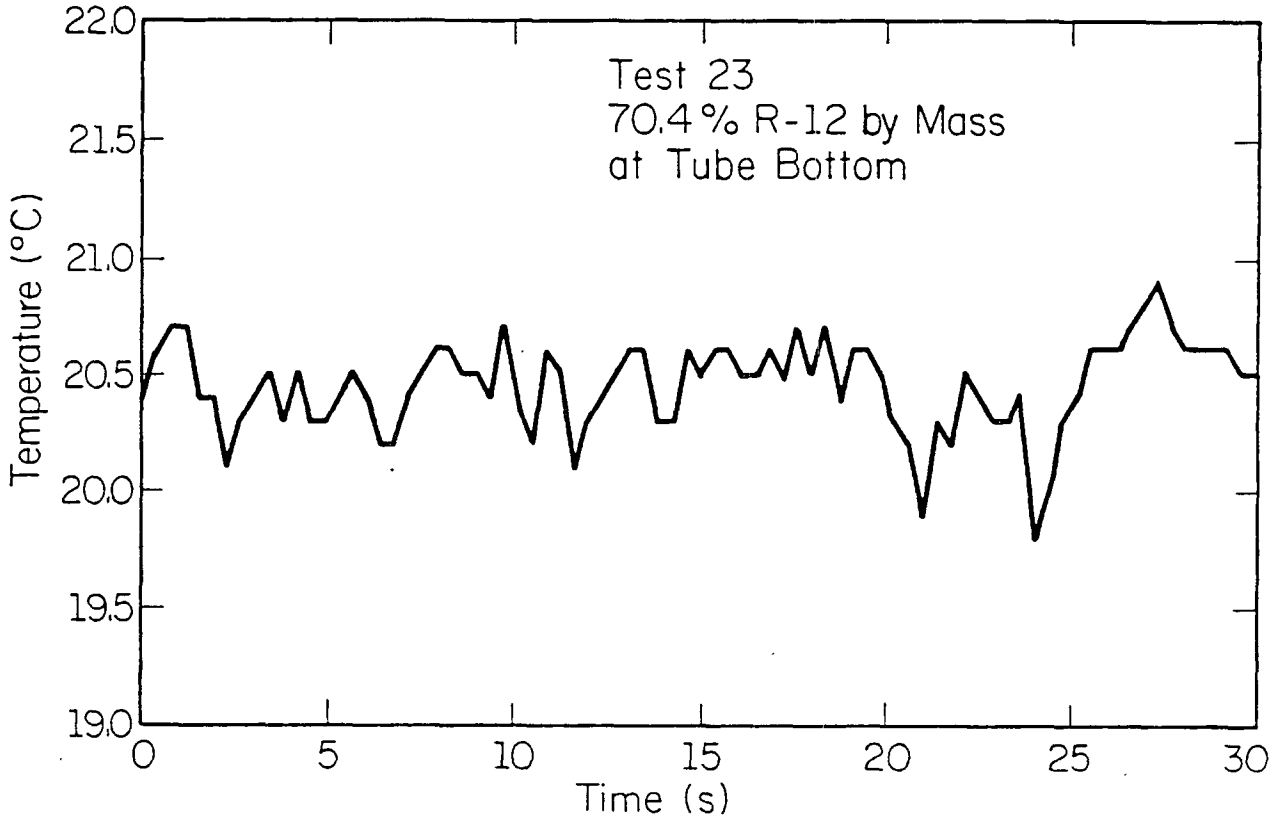


Figure 3.15. Temperature fluctuations at the tube bottom at test section 10 for test 23.

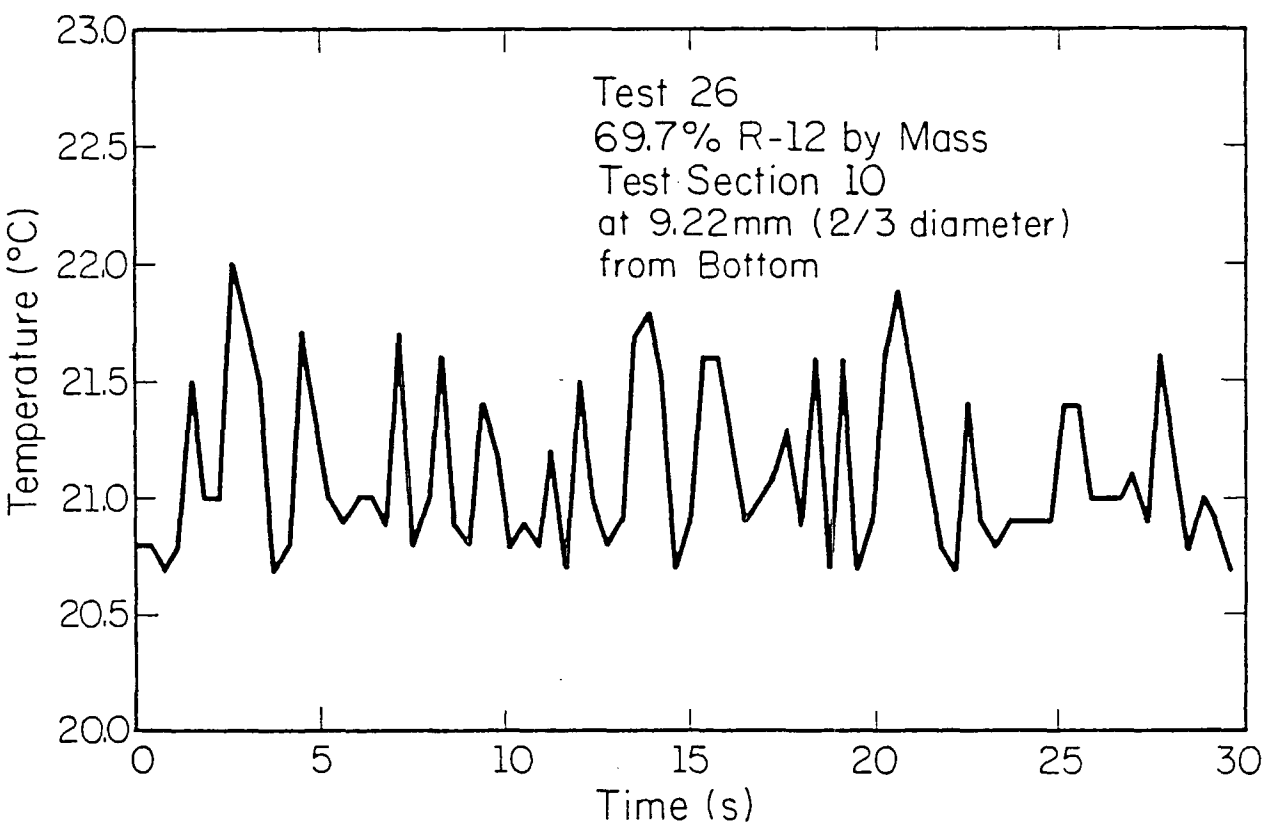


Figure 3.16. Temperature fluctuations 9.22 mm (2/3 diameter) from the tube bottom at test section 10 for test 26.

liquid temperature is approximately 20.7°C. Therefore there is at least a 1.3°C temperature difference between the vapor and the liquid. This is the type of nonequilibrium that would result due to slip. However, as mentioned earlier, the nonequilibrium depicted by the temperature gradient between the vapor and the liquid will exist without slip. It is a fact that the temperature difference between the two phases will be greater with slip than without. Unfortunately, there is no way to determine, for a specific set of flow conditions, what the magnitude of the $\Delta T$ should be to indicate slip.

The data presented in Figs. 3.15 and 3.16 were obtained at test section 10 located near the end of the condenser. From Figs. 3.13 and 3.14 it is seen that at test section 10 the flow regime is slug flow. Here the vapor pockets are entrained in the slower moving liquid. The magnitude of the slip encountered here is not as great as it would be in the wavy or stratified flow regime where the detached vapor is free to move across the top of the liquid flowing in the bottom half of the tube.

This fact is confirmed by differences between the temperature profiles from tests 23 and 26 at test section 8, which is in the wavy flow regime (Figs. 3.11 and 3.12). At this location in the condenser, there was a 2°C temperature difference between the vapor and the liquid, which is greater than the 1.3°C temperature difference encountered in the slug flow region.

Note that the liquid temperature shown in Fig. 3.15 is close but not equal to that shown in Fig. 3.16. The difference arises because the figures represent data that were obtained from two separate tests. Minor variations in test conditions such as condenser cooling water temperature are responsible for this temperature difference.

### 3.3.5 Refrigerant Concentration Measurements

Some data from gas chromatographic analyses are presented to provide additional insight into the mechanism of the condensing process with a refrigerant mixture. Figure 3.17 shows concentration measurements taken from three different tests, but all with a 30% R-114 and a 70% R-12 mixture by mass. Samples were extracted at four different positions along the condenser, and at each of these locations the sample probe was positioned at three different elevations within the refrigerant tube--at the bottom, 4.62 mm from the bottom, and 9.22 mm from the bottom. Figure 3.17 also shows lines of the

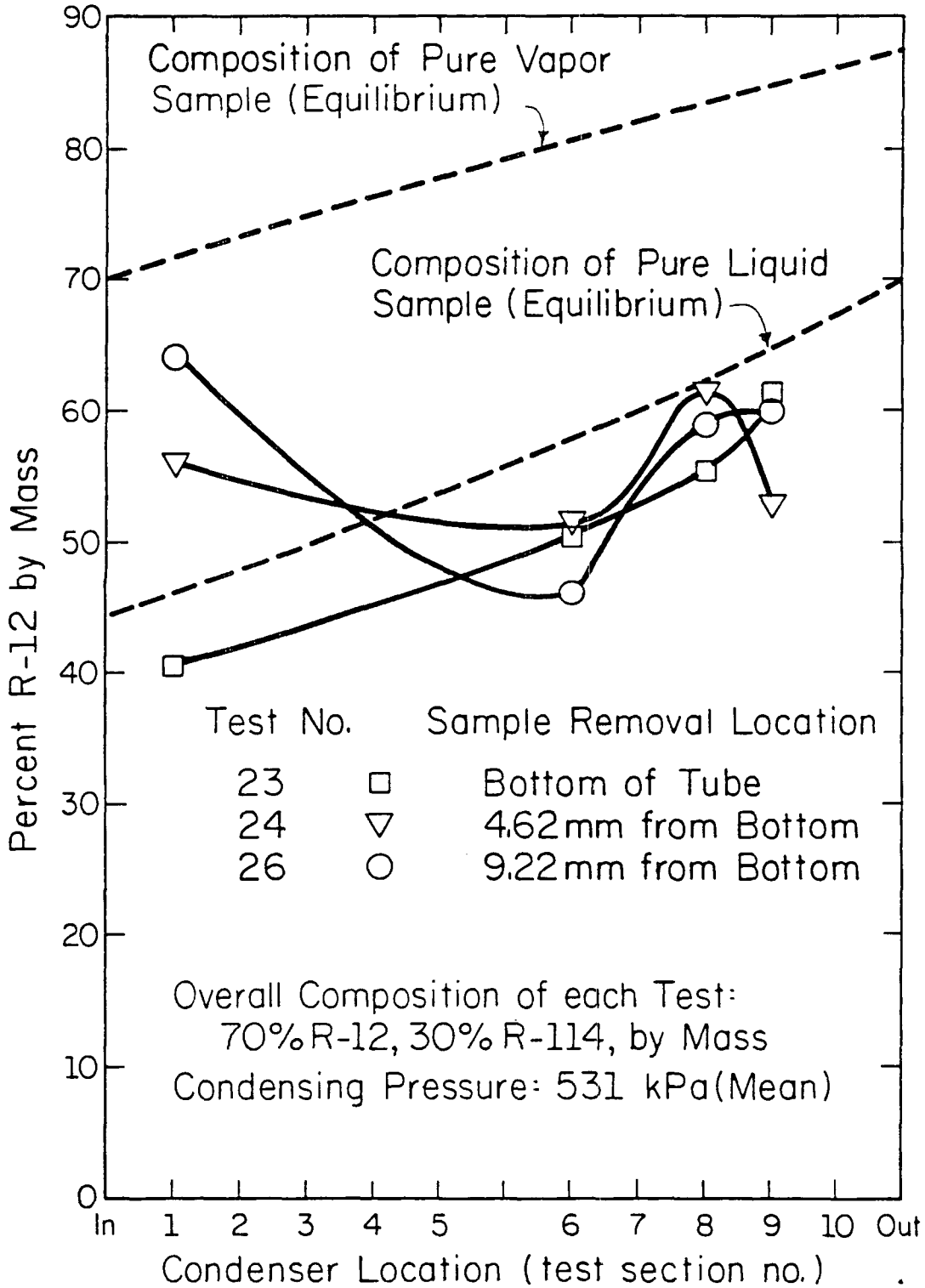


Figure 3.17. Experimental composition results compared to condensation occurring at a uniform rate over entire length of the condenser under equilibrium conditions.

calculated composition of the vapor fraction and the liquid fraction, assuming that liquid and vapor remained in equilibrium throughout the condensation process, and the heat flux was constant throughout the condensation or, in other words, that condensation occurred at a constant rate. The condensation process was assumed to begin at the entrance of the condenser, although the rate of condensation at that point is quite low.

The first observation relates to the overall magnitude of the measured concentrations in comparison to the ideal vapor and liquid compositions. There is a displacement of approximately 5 percent, with the ideal compositions determined from the measured charge being higher than the chromatographic readings. If this 5 percent correction were made, almost perfect agreement would result at position 1. At that location the reading from the sample taken at the bottom of the tube, which should be all liquid, agrees with the chromatograph. At the 9.22 mm distance from the bottom (2/3 of the diameter) the sample should be vapor, and its concentration would check the ideal expectation. The concentration of the sample taken at the 4.62 mm position is between the liquid and vapor concentrations, and may be a mixture of liquid and vapor. The one other consistent set of results in Fig. 3.17 is the concentration as determined by chromatography of samples taken at the bottom of the tube all along the condenser. If the 5 percent shift in concentration were allowed, the measured concentration of the liquid fraction agrees with the ideal.

The concentrations at positions 6, 8, and 9 at the 1/3 and 2/3 diameters from the bottom would have been expected to be much higher than those actually measured. If the samples were vapor alone and if slip did not exist, they would have been expected to parallel the ideal vapor concentration line. If the samples were completely vapor and there was some slip, then the vapor having a concentration reflecting that of an upstream position would prevail. Another reason that could be advanced for the low concentrations at these positions is that some liquid was also extracted along with the vapor. On a volume basis, only a small fraction of liquid would completely distort any expectation of accurate measurement of a vapor concentration.

Based solely on the concentration measurements, it is not possible to prove that slip plays a role in influencing condensing coefficients. Some combinations of the knowledge of the flow regimes and the measurements of the

coefficients that are reported in Chapter 5 probably give more convincing evidence of the influence of slip and/or concentration gradients reducing the heat-transfer coefficients.

# 4. COPPER CONDENSER TEST FACILITY

## 4.1 Introduction

The purpose of tests run on the copper condenser was to measure local heat-transfer coefficients and correlate these measurements with the flow regimes that were observed using the transparent condenser. The transparent condenser permitted visual observation of the flow regimes, but because tube temperatures could not be measured the heat-transfer coefficients could not be determined. Thermocouples could be mounted, however, on the copper condenser which along with measurements of the refrigerant temperature and heat flux permitted calculation of the condensing heat-transfer coefficients. Furthermore, because the inside tube diameters, the refrigerant flow rates, and the rates of heat transfer were correspondingly the same for both condensers, the heat-transfer coefficients could be correlated with the flow regime.

## 4.2 Overall Condenser Layout

In order to correlate condensing coefficients with their respective flow patterns and to avoid dimensional scaling adjustments, we constructed the copper condenser as close as possible to the same size as the transparent condenser. The condenser, whose configuration is shown in Fig. 4.1, is basically a tube-in-tube counterflow heat exchanger with refrigerant flowing inside the inner tube and water flowing in the annulus. The total length of the condenser is 19.8 m (64.8 ft).

The inner tube is supported with three supports for each pass. The six supports are made of pieces of brass tubing approximately 25 mm (1 in.) long. The tube pieces have small metal rods soldered into them around their circumference. Each support is fitted over the outside of the refrigerant tube and fastened to it at the proper locations with a small bead of solder. The small metal rods support the tube in the middle of the annulus while causing a minimal disturbance to the cooling water as it flows around them. The inner refrigerant tube is also supported wherever the refrigerant tube protrudes from the annulus, i.e. at the condenser entrance, exit, and in the middle of each pass.

The inner tube that carries the refrigerant is made of 15.9-mm OD (5/8-in.) copper tube. The tube has an inside diameter of approximately 12.7 mm (1/2 in.) which is also the size of the inner diameter of the refrig-

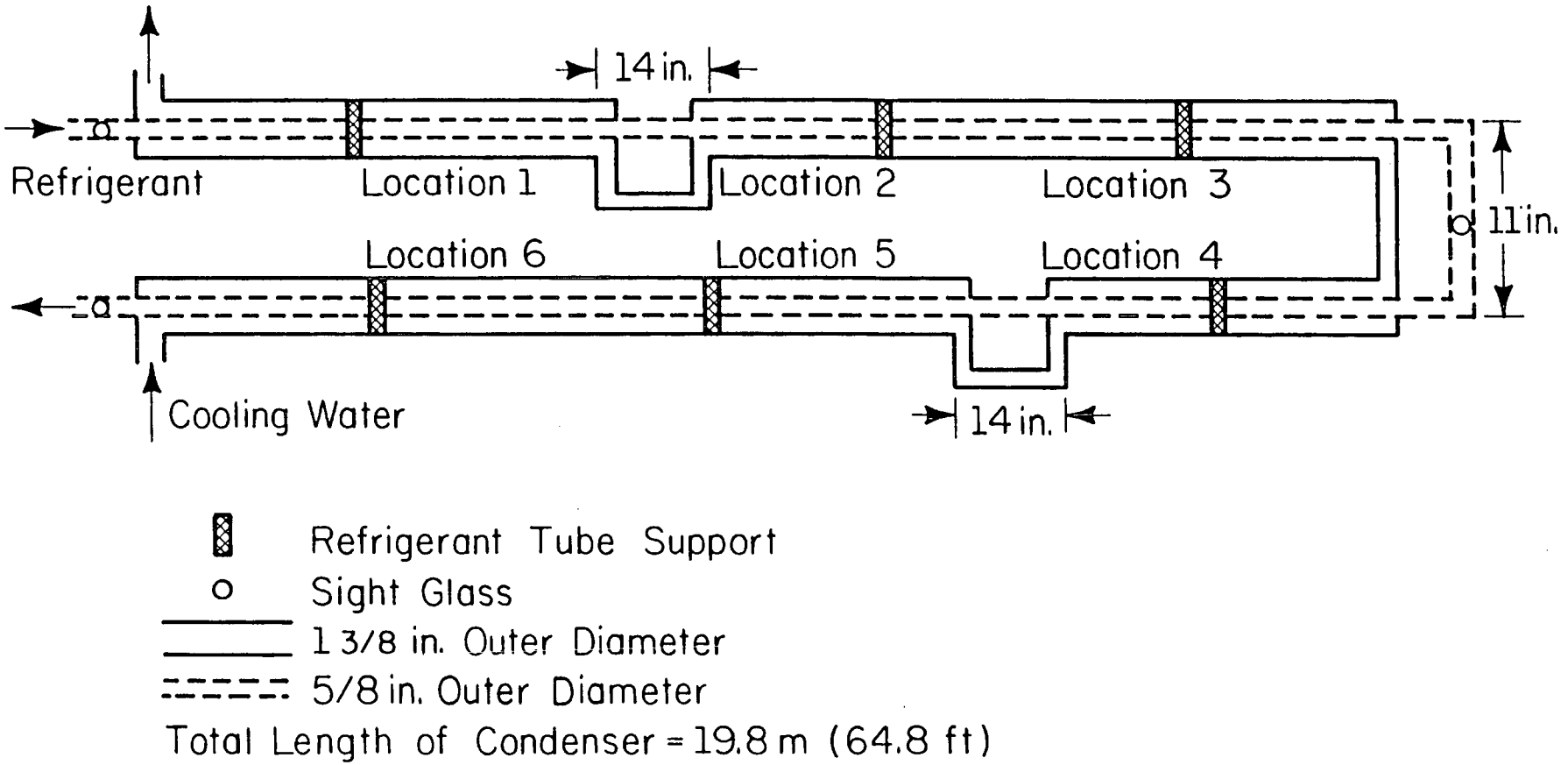


Figure 4.1. Schematic diagram of copper condenser.

erant tube in the transparent condenser. Due to the greater conductivity of copper compared with glass, the cooling water velocity in the copper condenser should be less than that in the transparent condenser to achieve the same heat-transfer rate. Therefore, it was necessary to downsize the annulus of the copper condenser from the 63.5-mm ID (2 1/2-in.) annulus of the transparent condenser. Through calculation of the heat-transfer coefficient, it was decided that a 34.9-mm OD (1 3/8-in.) copper tube would be adequate for the annulus. A 12.7-mm (1/2-in.) rotameter is used to measure the cooling water flow rate.

The outside of the annulus is insulated with a 12.7-mm thick (1/2-in.) layer of foam rubber insulation. In places where the refrigerant tube protrudes from the outer annulus, it is insulated with a 9.5-mm thick (3/8-in.) layer of insulation. Figure 4.1 shows that the inner tube has three sight glasses--one each at the condenser entrance, exit, and midpoint--to give rough indications of refrigerant quality at these points.

## 4.3 Copper Condenser Instrumentation

The copper condenser is instrumented with type T (copper-constantan) thermocouples measuring refrigerant, condenser cooling water, and condenser tube wall temperatures. Pressure taps are provided to measure the pressure of the refrigerant at various points along the condenser.

Instrumentation locations are numbered in succession starting with the one closest to the condenser entrance as shown in Fig. 4.1. It was decided that heat-transfer coefficients should be determined at least once in each of the different flow patterns that occur during the condensation process. To accomplish this, there are six test locations in the condenser at distances of 2.4, 4.6, 7.1, 12.3, 14.6, and 17.1 meters from the condenser entrance.

## 4.4 Thermocouples

The entire system includes a total of 50 copper-constantan thermocouples, with ten of these located outside the copper condenser to measure system temperatures around the pump/boiler loop. The copper condenser has a total of 40 thermocouples implemented along its length. A datalogger is used to measure the analog voltages and to convert these voltages to temperatures. Temperatures are given with an accuracy of 0.1°C. The stated accuracy when measuring copper-constantan voltages is equivalent to ±0.5°C.

### 4.4.1 Refrigerant Thermocouples

Temperature measurements of the refrigerant are made at nine locations along the copper condenser: at each of the six test locations and at the condenser entrance, exit, and midpoint. Figure 4.2 shows the instrumentation on the refrigerant side of the condenser. The thermocouples are located in the center of the refrigerant tube encased in 0.318-cm OD (1/8-in.) stainless steel tubes as illustrated in Fig. 4.3. The thermocouples are placed in the stainless steel sheaths to steady the temperature readings. Also, the tips of the stainless steel tubes are sealed to prevent refrigerant leaks.

The stainless steel sheaths are positioned with a wire helix in the center of the cross-section of the refrigerant tube to obtain representative readings of the bulk temperature of the refrigerant. To minimize the error in refrigerant temperature measurement due to conduction along the stainless steel sheaths, we located as much tube as possible within the refrigerant stream leading to the point where the temperature is measured. At each of the six test locations, a minimum of 70.0 cm (24 in.) of stainless steel tube is inserted into the refrigerant stream. At the midpoint and ends of the condenser, a minimum of 30.5 cm (12 in.) is located in the refrigerant stream.

### 4.4.2 Refrigerant-Tube Temperature Measurement

Another quantity necessary in the calculation of the local condensing coefficients at a particular location is the refrigerant tube temperature. It has been shown that the heat-transfer coefficients vary around the circumference of the condenser tube [14,15]. Noting this fact it was decided that a representative local condensing coefficient could be obtained using an average refrigerant tube temperature. Therefore, thermocouples were soldered at four points around the refrigerant tube circumference, approximately 90 degrees apart on the top, bottom, and sides. The tube temperature at location i, $T_{p_i}$, is obtained as an arithmetic average of the four temperatures around the circumference.

Figure 4.4 illustrates the placement of the thermocouples that measure the refrigerant tube temperature. The greater the size of the thermocouple solder bead that rises above the surface of the refrigerant tube, the greater the error in the temperature measurement due to convection to the condenser

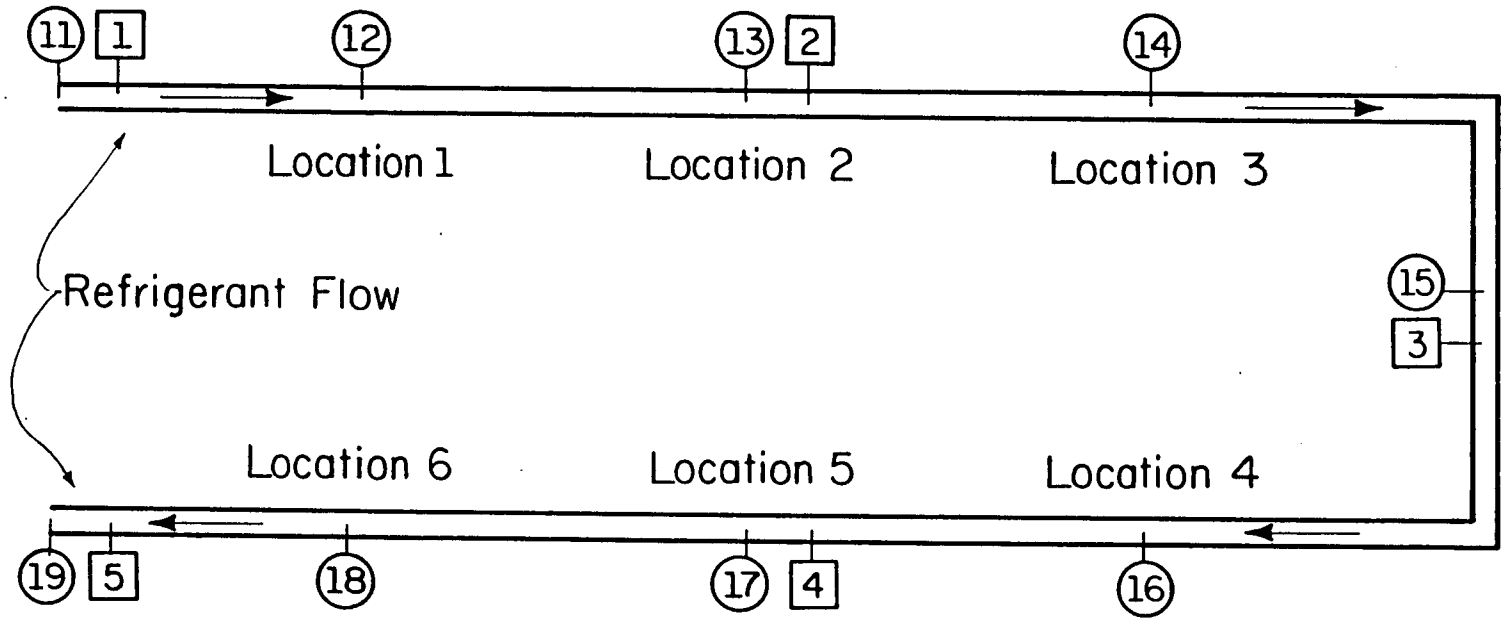


○ Location of Thermocouple in Refrigerant Stream
□ Pressure Tap
Total Length of Condenser = 19.8 m (64.8 ft.)

Figure 4.2. Refrigerant-side instrumentation.

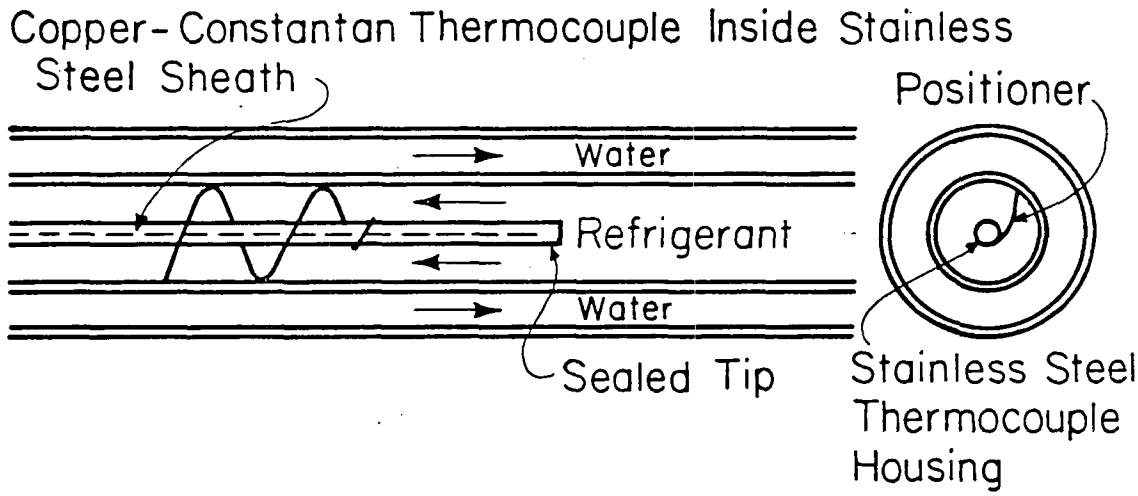


Figure 4.3. Refrigerant temperature measurement.

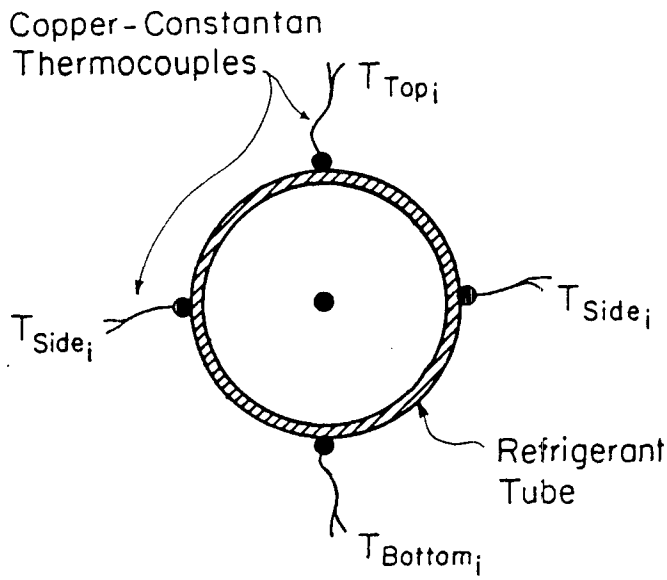


$$Tp_i = (T_{Top_i} + T_{Bottom_i} + T_{Side_i} + T_{Side_i})/4$$

Figure 4.4. Determination of tube temperature $T_{p_i}$ at location i (i = 1,6).

cooling water. This error was reduced by notching the refrigerant where each thermocouple was to be affixed and then soldering the thermocouples to the tube in the notches, minimizing the area protruding above the tube surface. Figure 4.5 shows the location and numbering of the thermocouples.

### 4.4.3 Temperature Measurement of Cooling Water

The cooling water temperature, like that of the refrigerant, is measured at nine different locations along the condenser. As shown in Fig. 4.5, the temperature of the cooling water is measured at the six test locations and at the condenser entrance, exit, and midpoint. A piece of rigid wire fastened to the refrigerant tube was used to center the thermocouple in the annulus where the cooling water flowed as illustrated in Fig. 4.6. Omitted from the figure, for clarity, are the four thermocouples used to measure the refrigerant tube temperature and the thermocouple used to measure the refrigerant temperature.

## 4.5 Pressure Measurements

Figure 4.2 shows all the locations where the condensing pressures of the refrigerant are obtained along the copper condenser. The pressure is measured at five locations: the condenser entrance, exit, halfway point, and at the midpoint of each pass. The five condenser pressures are fed to a manifold on the control panel (Fig. 2.2) where each pressure can be read individually from a single pressure gauge. The pressure gauge used to measure condenser pressures has a range of 0 to 1000 kPa and scale divisions of 10 kPa.

Pressure taps at the inlet and outlet of the refrigerant pump and the outlet of the expansion valve were connected to the manifold of a second pressure gauge. By appropriate settings of the valves, each pressure could be read individually on the same gauge. The gauge used to measure these pressures also has a range of 0 to 1000 kPa with scale divisions of 10 kPa.

## 4.6 Calculations During and Following Tests

A small desktop computer was used during tests to compute some of the quantities needed to guide adjustments of the test facility. Following completion of the test the data reduction was performed using a program in a mainframe computer.

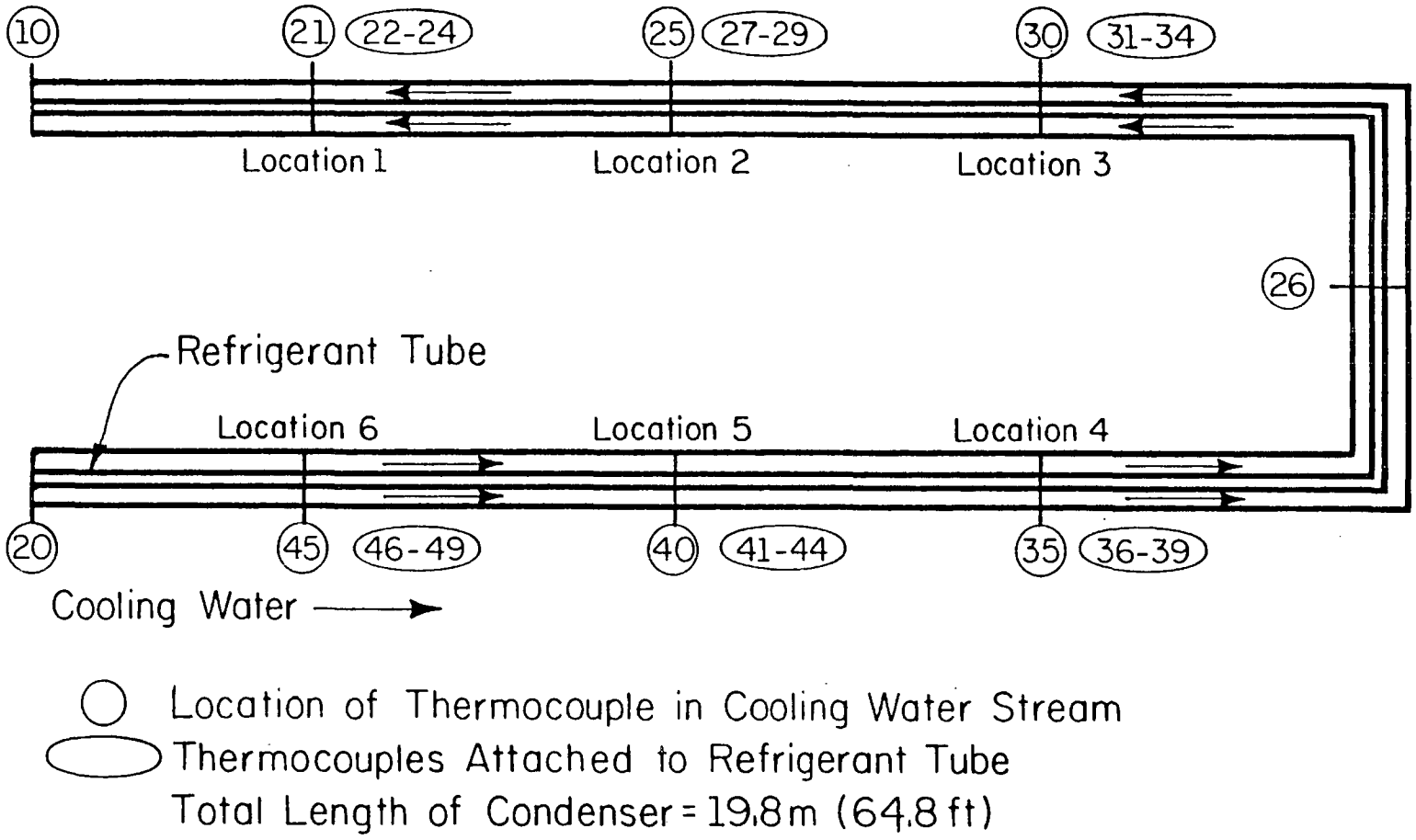


Figure 4.5. Water-side instrumentation.

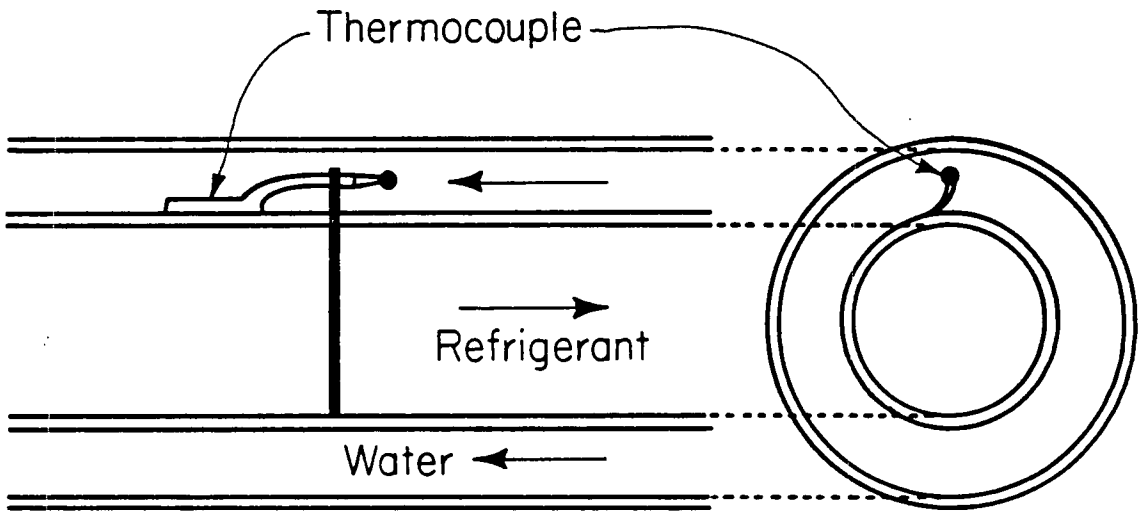


Figure 4.6. Temperature measurement of the condenser cooling water.

One of the programs run frequently during a test was that of calculating the dew-point and bubble-point temperatures based on the measured pressure and the refrigerant composition. The same program computed enthalpies at any desired position in the condenser. The equations used in this program were taken from Downing [16]. Another program available for the desktop computer converted the reading of the refrigerant rotameter to the mass-flow rate which, in combination with the enthalpies determined above, permitted computation of the rate of heat transfer--a quantity that was kept constant for each series of the tests.

At the end of a test, the raw data were reduced using an interactive program on a mainframe computer. One of the main tasks of this program was the calculation of the local heat-transfer coefficients, which were computed according to the methods outlined in Fig. 4.7. In the figure, $T_{p_i}$ represents an average of four tube temperatures, and the temperatures used in computing the log mean temperature difference, were obtained from the nearest temperature measurement location on each side of location i. The refrigerant temperature fluctuated, as shown in Figs. 3-15 and 3-16, so the time-averaged temperature was used for $T_{1_i}$. In those sections where the slope of the curve of the refrigerant temperature changed abruptly, such as when desuperheating stopped and condensation began, the use of the entering and leaving temperatures of refrigerant gave a slightly distorted log-mean-temperature difference. The distortion was approximately constant for all concentrations, however, so the observed effect of the concentration on the heat-transfer coefficient was still valid.

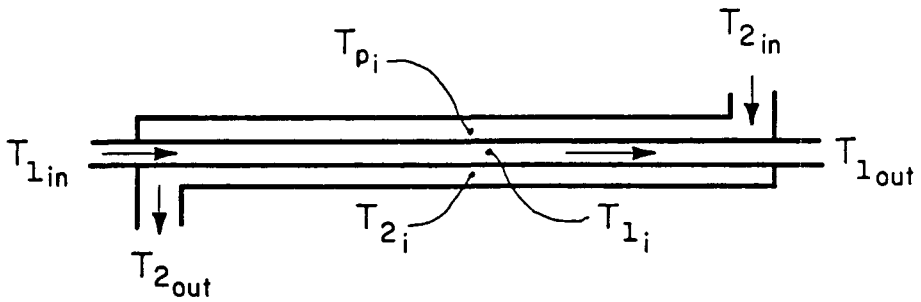


Let: $Q$ = heat transfer rate (kW) for this section

$q = Q/\text{area}$ on refrigerant side of pipe

LMTD = log mean temperature difference

$$= \frac{(T_{1_{in}} - T_{2_{out}}) - (T_{1_{out}} - T_{2_{in}})}{\ln[(T_{1_{in}} - T_{2_{out}})/(T_{1_{out}} - T_{2_{in}})]}$$

Then: $q_{local} = q \times (T_{1_i} - T_{2_i})/\text{LMTD}$

$h_i\ (W/(m^2K)) = q_{local}/(T_{1_i} - T_{p_i})$

Figure 4.7. Calculation of local heat-transfer coefficients $h_i$ at test location i (i = 1,6).

# 5. COPPER CONDENSER TEST RESULTS

## 5.1 Test Objectives

All of the results presented herein are from tests with refrigerant compositions of pure R-12, pure R-114, or mixtures of the two. As mentioned earlier, one of the functions of the copper condenser was the experimental determination of circumferentially averaged local condensing coefficients at various points along the condenser. The intent was then to correlate these coefficients with the flow regimes along the condenser.

Another objective was to identify any trend(s) in the local condensing coefficients that resulted from varying the concentration of R-114 in the R-12/R-114 mixture while keeping the other test parameters constant. In particular, an attempt was made to verify the results obtained by Stoecker and McCarthy [11], which showed that midway through the condenser, the condensing coefficients dropped as the R-114 percentage was increased from zero, reaching a minimum in the range of 50 to 70 percent R-114. Finally it was desired to observe the effect of varying the overall heat transfer rate on the condensing coefficients.

## 5.2 Test Conditions

A total of 31 tests were run with the copper condenser; however, the results of only 20 of these tests are discussed here. The 11 tests not discussed were used to determine system limitations such as the overall heat-transfer rate in the condenser. Two series of test tests were run, series A and B, each with a different overall heat-transfer rate in the condenser. The refrigerant mixture concentrations used in the tests were 0, 30, 50, 70, and 100 percent R-114 by mass. Each series contained two tests at each mixture concentration to replicate the data obtained. Series A consisted of tests 2, 5, and 7 through 14. Series B consisted of tests 21 through 27 and 29 through 31. Test conditions for both series of tests are given in Table 5.1.

The control of the tests was such that the entire condensation process was spread over the complete length of the condenser. To accomplish this task it was necessary for the refrigerant to be superheated upon entering the condenser and subcooled at the exit. Furthermore, the superheat must be removed from the refrigerant within a short distance from the condenser entrance. Likewise, the subcooling must start near the condenser exit. The

Table 5.1 Summary of Test Conditions for Test Series A and B

| Test No. | % R-114 by Mass | Heat Transfer Rate in Condenser (kW) | Refrig. Flow Rate (kg/s) | Condenser Entering/ Exiting Refrig. Temp. (°C) | Superheat/ Subcooling of Refrig. (°C) | Pressure Drop in Condenser (kPa) |
|---|---|---|---|---|---|---|
| | | | Series A | | | |
| 2 | 50 | 3.43 | 0.0232 | 45.0/22.7 | 4.1/7.2 | 20 |
| 5 | 50 | 3.37 | 0.0230 | 45.0/24.3 | 3.6/6.1 | 23 |
| 7 | 0 | 3.50 | 0.0243 | 45.0/29.3 | 8.1/7.1 | 15 |
| 8 | 0 | 3.47 | 0.0240 | 45.0/29.4 | 9.7/5.6 | 10 |
| 9 | 30 | 3.38 | 0.0234 | 45.0/27.4 | 4.5/4.7 | 15 |
| 10 | 30 | 3.41 | 0.0234 | 45.0/26.0 | 4.3/6.4 | 14 |
| 11 | 100 | 3.52 | 0.0249 | 45.0/25.5 | 11.5/5.1 | 28 |
| 12 | 100 | 3.53 | 0.0249 | 45.0/24.4 | 11.5/6.5 | 31 |
| 13 | 70 | 3.44 | 0.0236 | 45.0/23.8 | 6.2/4.2 | 20 |
| 14 | 70 | 3.46 | 0.0237 | 45.0/23.4 | 6.2/4.2 | 22 |
| | | | Series B | | | |
| 21 | 70 | 4.34 | 0.0305 | 45.8/26.8 | 3.6/3.5 | 35 |
| 22 | 50 | 4.33 | 0.0295 | 47.7/25.6 | 5.4/5.4 | 20 |
| 23 | 30 | 4.30 | 0.0291 | 49.1/26.5 | 5.9/8.0 | 22 |
| 24 | 50 | 4.32 | 0.0295 | 47.0/25.6 | 4.8/5.3 | 24 |
| 25 | 30 | 4.40 | 0.0292 | 49.1/23.4 | 6.0/10.6 | 29 |
| 26 | 70 | 4.36 | 0.0305 | 45.8/26.2 | 2.4/5.8 | 27 |
| 27 | 100 | 4.40 | 0.0299 | 49.8/22.6 | 14.3/8.4 | 34 |
| 29 | 0 | 4.48 | 0.0317 | 37.9/28.2 | 5.2/3.6 | 21 |
| 30 | 100 | 4.40 | 0.0299 | 49.9/23.0 | 14.0/7.5 | 35 |
| 31 | 0 | 4.45 | 0.0315 | 37.9/28.2 | 5.6/3.4 | 25 |

refrigerant temperature profiles in the condenser show that the superheat is removed between the condenser entrance and test location 1. The profiles also show that the subcooling begins after test location 6 and before the condenser exit.

The tests in series A were run under conditions similar to those run with the transparent condenser by Kornota [10] and those cited in Chapter 3. The conditions for the tests in series A were as follows: refrigerant temperature entering the condenser of 45°C, refrigerant subcooled 4 to 12°C at the condenser exit, and an approximate heat-transfer rate in the condenser of 3.45 kW.

The tests run with the transparent condenser allowed visualization of the various flow patterns and where they occurred along the condenser. Because of the physical similarity between the copper and transparent condensers as well as the similarities among the three groups of tests, similar flow patterns should exist in the copper condenser at approximately the same locations as in the transparent condenser. Thus, any trends in the test data at any of the six locations along the copper condenser from test series A might possibly be correlated to a specific flow pattern.

The tests in series B were run to note the effects of changing the overall heat-transfer rate in the condenser. Tests in series B were conducted with a heat-transfer rate of 4.35 kW, which was the maximum attainable heat-transfer rate for the system. The amount of superheat and the temperature of refrigerant entering the condenser were not specified for this series of tests. The subcooling at the condenser exit was maintained between 4 and 12°C. Because of the increased heat-transfer rate in the condenser, it would be inadvisable to draw any conclusions about the exact locations of the various flow patterns. A summary of test conditions is given in Table 5.1. The reduced data for each of the tests has been condensed for convenience and is included in the Appendix.

## 5.3 Test Reproducibility

It was mentioned in the previous section that two tests were run at each mixture concentration. The tests were duplicated in order to increase confidence in the data obtained. The two ways in which test reproducibility was judged was by comparing refrigerant temperature profiles along the condenser and the heat-transfer coefficients obtained at the various test

locations. We found that all of the tests in both series were very reproducible. Figure 5.1 shows the greatest deviation in temperature profiles between any pair of tests of similar R-114 concentration. On the horizontal axis in Fig. 5.1, 0 m corresponds to the condenser entrance and 19.8 m to the condenser exit. The pair of tests shown are 50 percent R-114 from test series A. The greatest deviation in temperature on Fig. 5.1 at any location was 1.6°C. The temperature profiles exhibited the same shape but deviated slightly in numerical values. The slight shift in temperature profiles between similar tests can be attributed to minor variations in the condenser cooling water temperature. The condenser cooling water was fed to the system directly from the city water supply and any variation in its temperature directly affected the condensing pressure which, in turn, controlled the refrigerant condensing temperatures.

Figure 5.2 exhibits the greatest deviation in heat-transfer coefficients between any pair of similar tests. The data shown were obtained from 30 percent R-114 tests in series B. The greatest deviation between heat-transfer coefficients was 173 $W/(m^2\ K)$, which occurred approximately 7.1 m downstream from the condenser inlet representing 10 percent difference. Again, all of the heat-transfer coefficient curves from similar tests exhibited similar shapes to that depicted in Fig. 5.2. The differences in condensing coefficients are due to temperature variations in the refrigerant, the condenser tube wall, and/or the condenser cooling water. The variation in condensing coefficients with respect to all of these temperatures is examined more closely in the error analysis section later in this chapter.

## 5.4 Refrigerant Temperature Profiles Along Condenser

Figure 5.3 shows representative temperature profiles in the condenser for each of the mixture composition tests in series A. The figure shows that the condensation of mixtures occur over a range of temperatures as expected, while the condensation of single refrigerants occurs at approximately a constant temperature. A slight drop in saturation temperature is also apparent along the condenser for the single refrigerant tests, which is caused for the pressure drop along the condenser. The R-114 vapor has a greater specific volume than R-12, so the pressure drop and thus the change in saturation temperature along the condenser is greater for pure R-114 as shown in

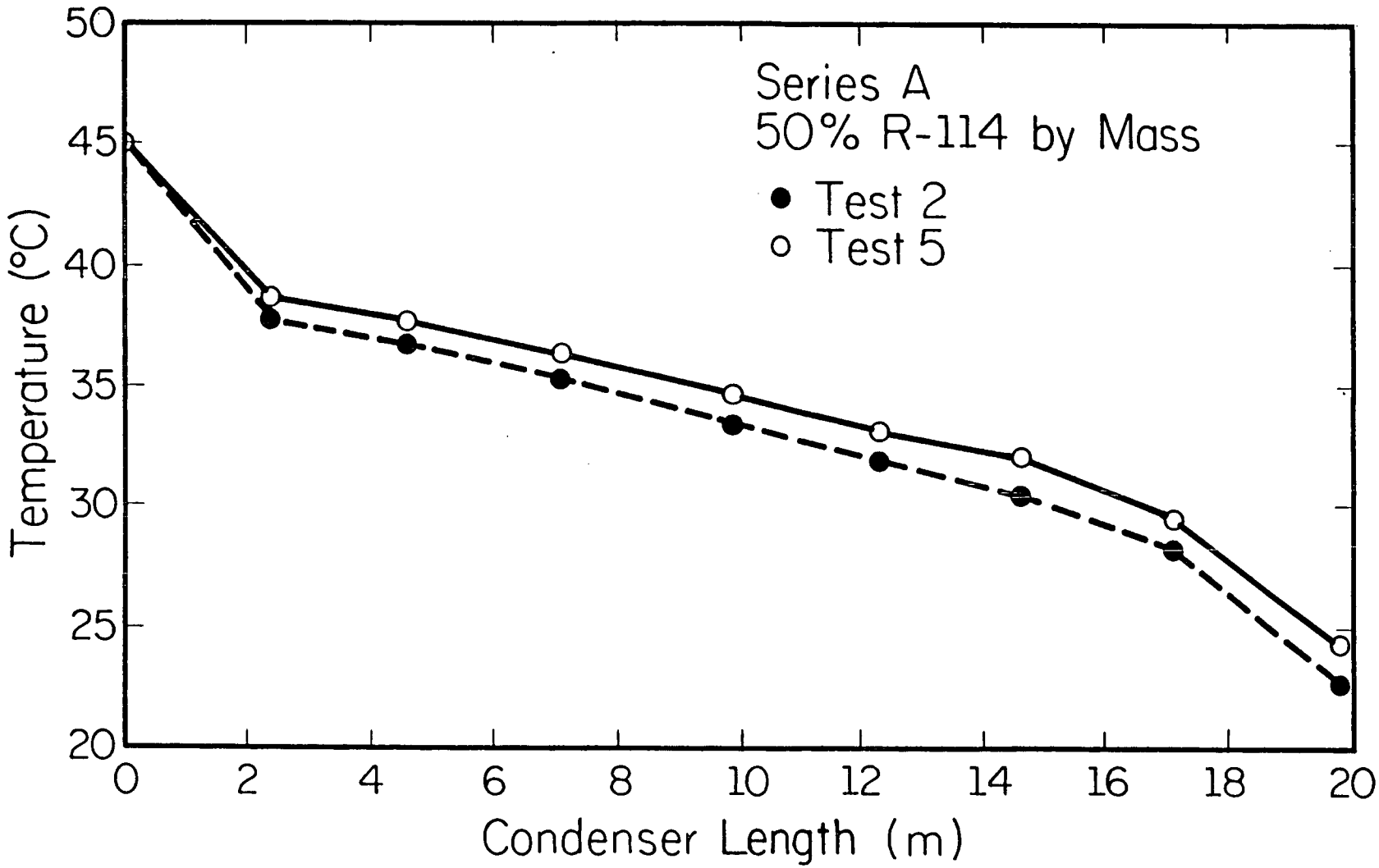


Figure 5.1. Test reproducibility: temperature profiles in R-12/R-114 mixtures.

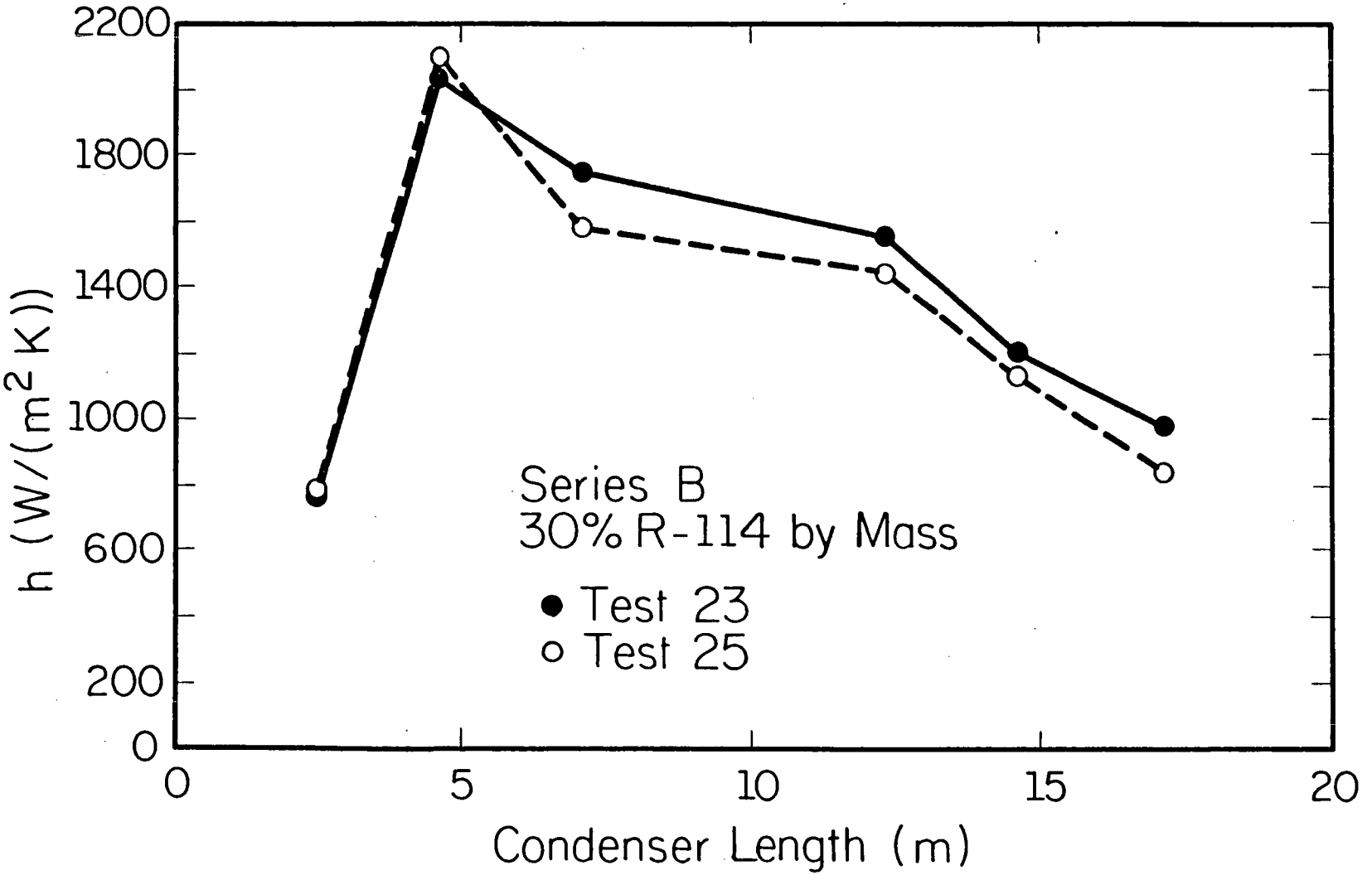


Figure 5.2. Test reproducibility: condensing coefficients in R-12/R-114 mixtures.

Fig. 5.3. The saturation temperatures and condensing temperature ranges in Fig. 5.3 do not fall in succession with respect to R-114 concentration because each mixture concentration had its own unique condensing pressure.

Figure 5.4 depicts a condensing refrigerant temperature profile from the series A test with a 30 percent R-114 by. This temperature profile is representative of the other temperature profiles from different mixture concentrations. Three distinct regions can be identified on the profiles. Region 1 is the entrance region of the condenser where all of the superheat is removed from the refrigerant vapor. Region 2, which makes up the major portion of the condenser length, is where the condensation process occurs. The slope of the graph in region 2 depends on both concentration of R-114 in the mixture and on the drop in condensing pressure. Region 3 is the exit region of the condenser, where the liquid refrigerant is subcooled.

Because measurements were taken at discrete points along the condenser, it was possible for all of the superheat to be removed from the refrigerant before the first temperature measurement in the condenser. Likewise it was possible for subcooling to begin somewhere between test location 6 and the condenser exit. These occurrences would have the effect of reducing the lengths of regions 1 and 3 in Fig. 5.4. It should be pointed out that the shape of the temperature profile shown in Figure 5.4 is similar to all other profiles except those of a 70 percent R-114 by mass mixture concentration. In each of the four 70 percent R-114 tests (two in series A and two in series B) the slope of the temperature curve in region 2 was so nearly equal to the slope in region 3 that it was difficult to identify where condensation ended and subcooling began.

## 5.5 Condensing Coefficients Along Condenser

### 5.5.1 Condensing Coefficient Profiles

In Chapter 4 it was stated that the condensing coefficients were experimentally determined at six different locations along the copper condenser. From these six points the pattern of the condensing coefficient profile in the condenser can be obtained. The condensing coefficient profiles for 0 and 100 percent R-114 tests from series A are shown in Figs. 5.5 and 5.6, respectively. The shapes of these profiles are very similar. Note that for the single refrigerants the condensing coefficients at test locations 2, 3, and 4 stay fairly constant.

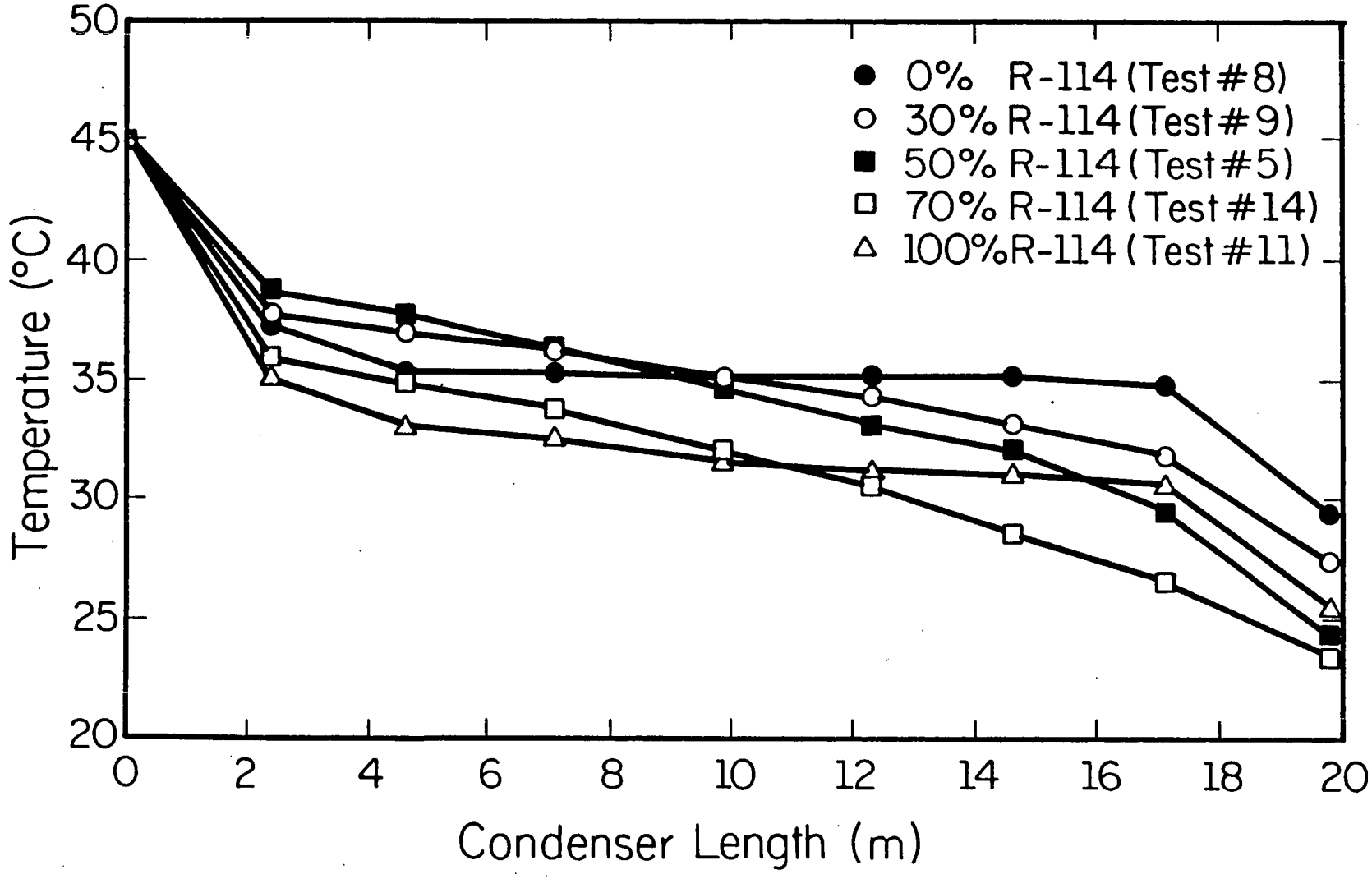


Figure 5.3. Temperature profiles for the various R-12/R-114 mass concentrations from test series A.

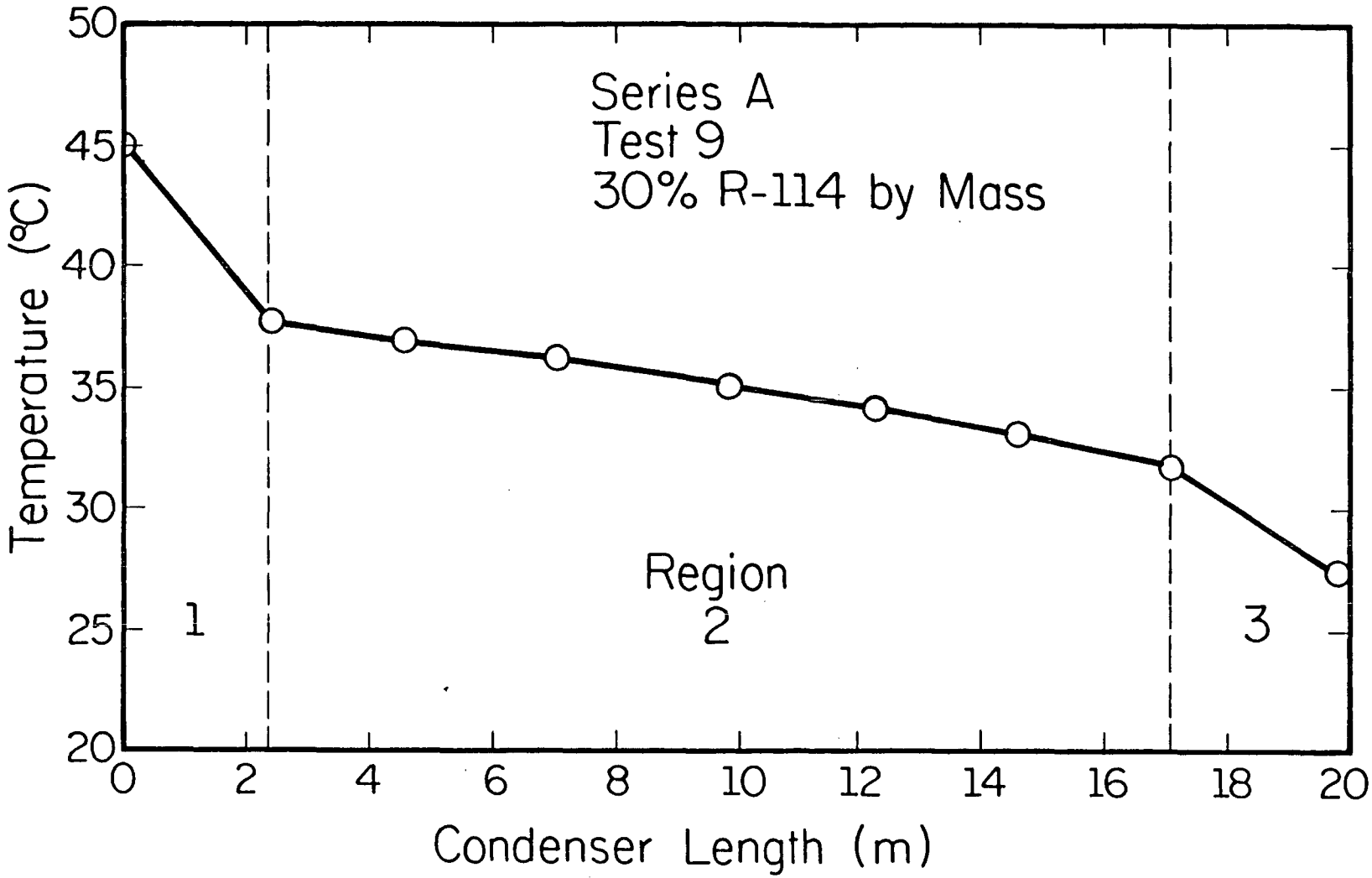


Figure 5.4. Typical refrigerant temperature profile along condenser.

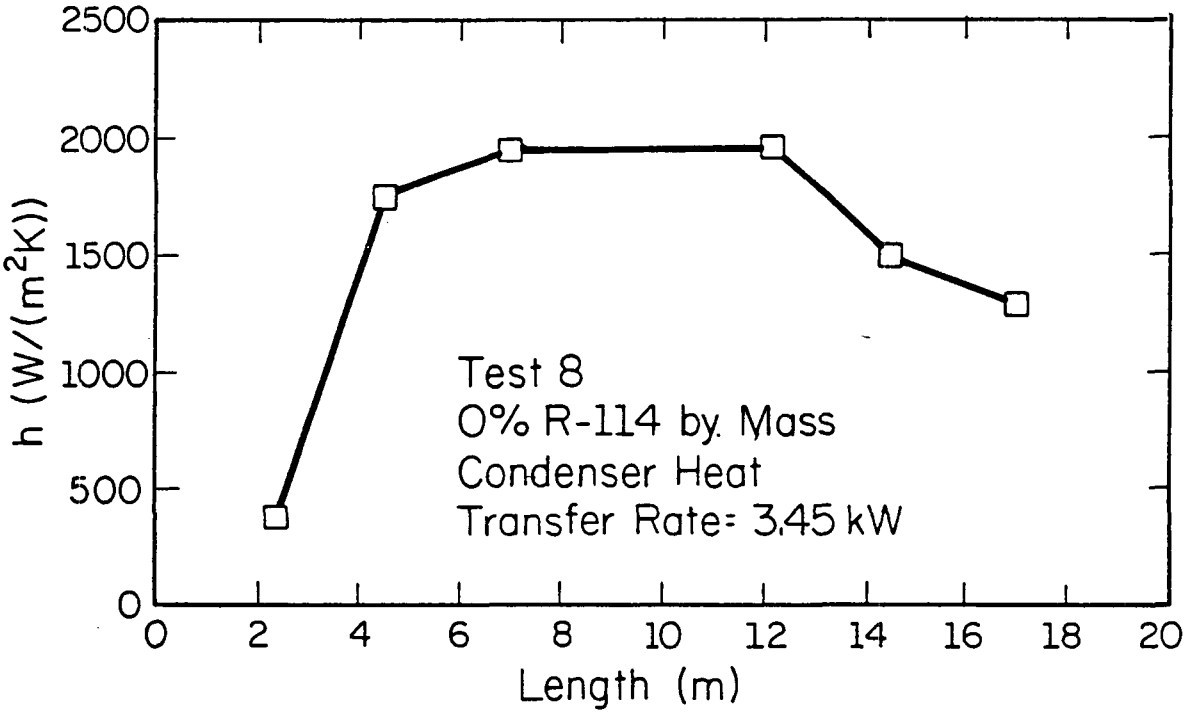


Figure 5.5. Condensing coefficient profile for pure R-12 (test series A).

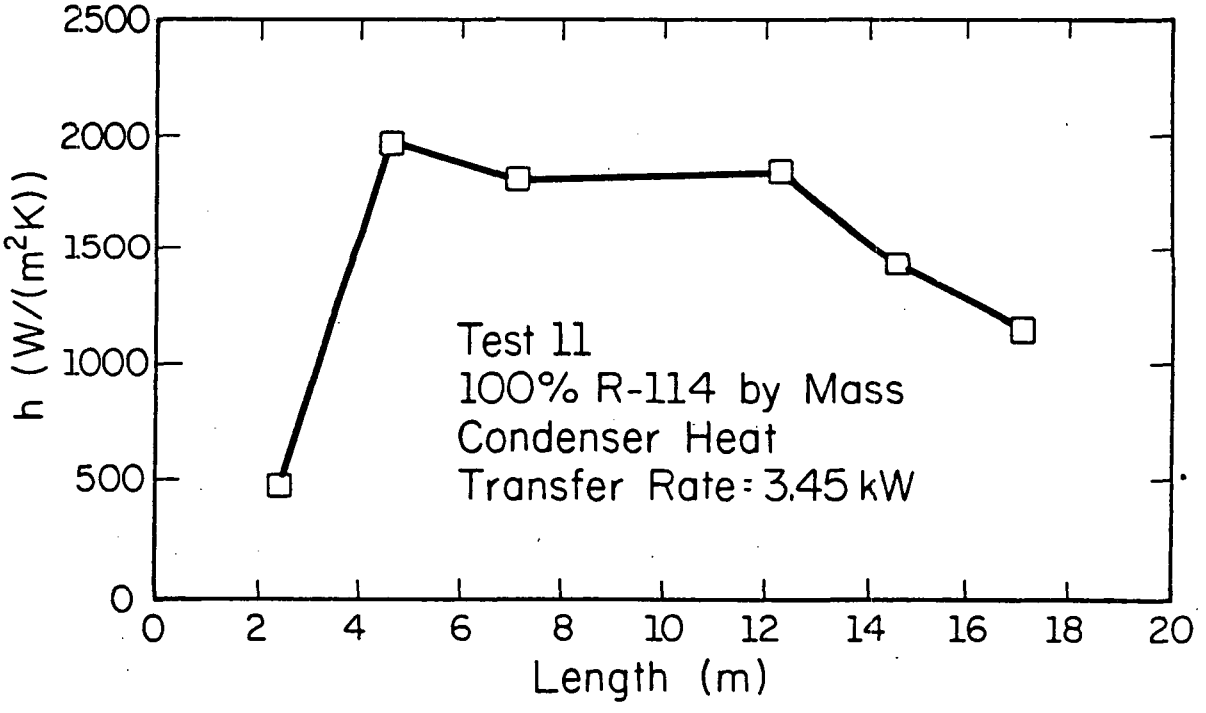


Figure 5.6. Condensing coefficient profile for pure R-114 (test series A).

Figures 5.7, 5.8, and 5.9 show, respectively, the condensing coefficient profiles for tests of 30 percent, 50 percent, and 70 percent mass concentrations of R-114 from series A. These profiles are very similar. The major difference between the mixture profiles and the single-refrigerant profiles can be seen at test locations 2, 3, and 4. For the mixture tests, the condensing coefficients steadily decreased after the maximum was reached at test location 2. The single-refrigerant tests, on the other hand, exhibited approximately constant coefficients at these locations. By analogy to the tests run with the transparent condenser, the flow regime at test locations 3 and 4 was wavy (see Figs. 3.7 and 3.9).

### 5.5.2 Effect of Concentration on Condensing Coefficients

Figure 5.10 shows variations in the condensing coefficients with concentration at test locations 1 and 2 in test series A. There was a slight increase in condensing coefficients with the mixtures compared to single refrigerants at test location 1. The increase in local heat-transfer coefficient with concentration at high vapor qualities has been noted by other experimenters [17]. The heat-transfer coefficients are approximately constant for all R-114 concentrations except at test location 2. Figures 3.4 and 3.5 indicate that the flow regime at test locations 1 and 2 was annular.

Figure 5.11 shows the change in condensing coefficients with concentration at test locations 3 through 6 from the tests in series A. From this figure it is clear that there is a definite decrease in heat-transfer coefficients of the mixtures compared with those of the pure refrigerants. It appears that at these locations the minimum condensing coefficients occur at R-114 mass concentrations between 50 percent and 70 percent. The largest drop in condensing coefficients at any location is at test location 4 where there was a reduction of 828 $W/(m^2K)$ between the 0 percent and 70 percent R-114 tests which was approximately a 40 percent drop. Again, based on the photographs from Chapter 3, the predominant flow pattern existing at these locations was wavy.

### 5.5.3 Effect of Increasing Heat-Transfer Rate in Condenser

As mentioned earlier in this chapter, the second group of tests, series B, had an overall heat-transfer rate in the condenser of 4.35 kW. This

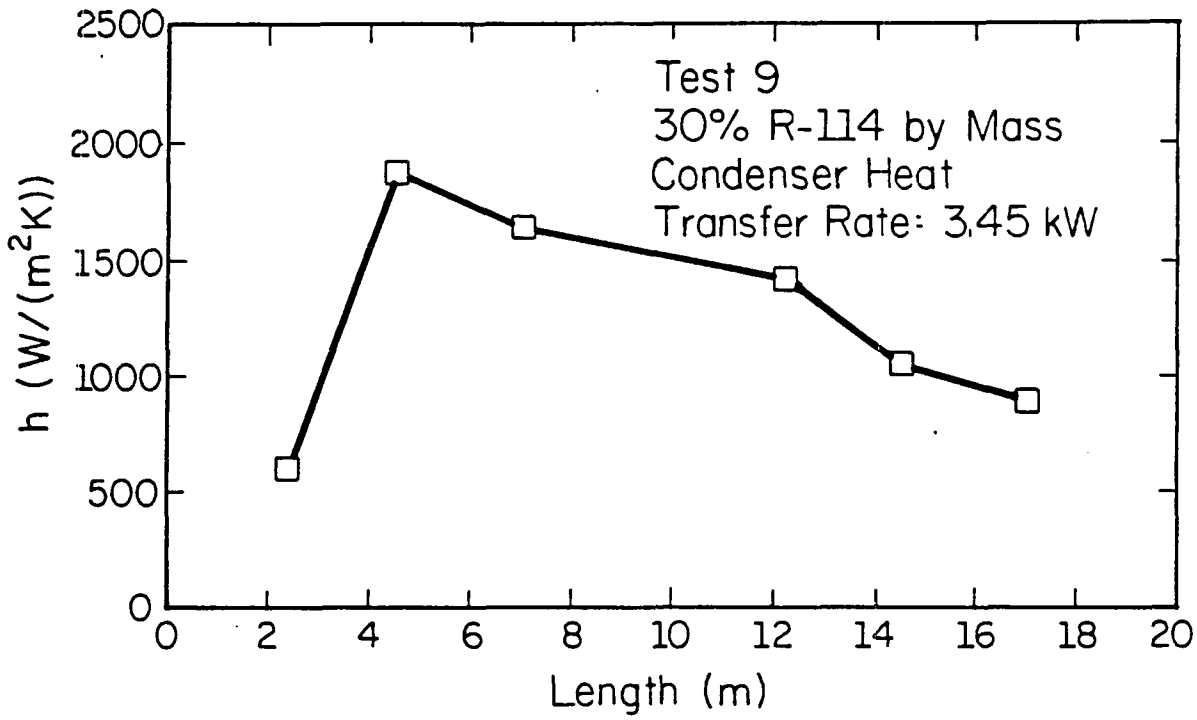


Figure 5.7. Condensing coefficient profile for 30% R-114 (test series A).

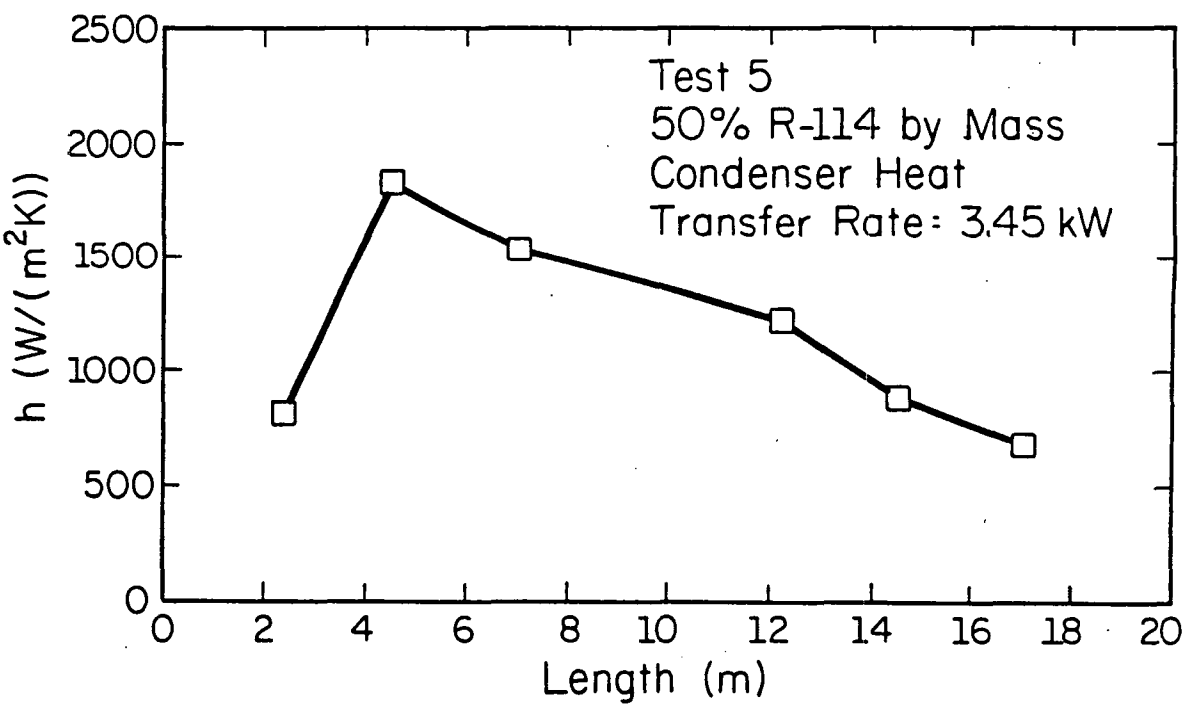


Figure 5.8. Condensing coefficient profile for 50% R-114 (test series A).

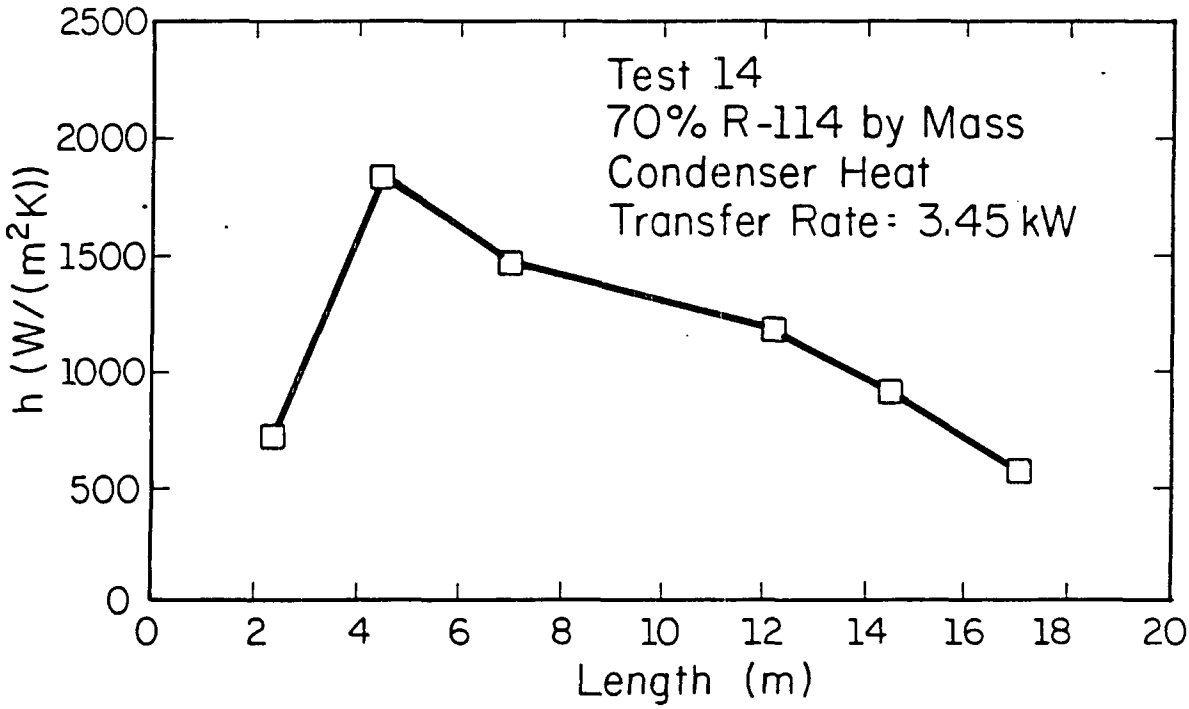


Figure 5.9. Condensing coefficient profile for 70% R-114 (test series A).

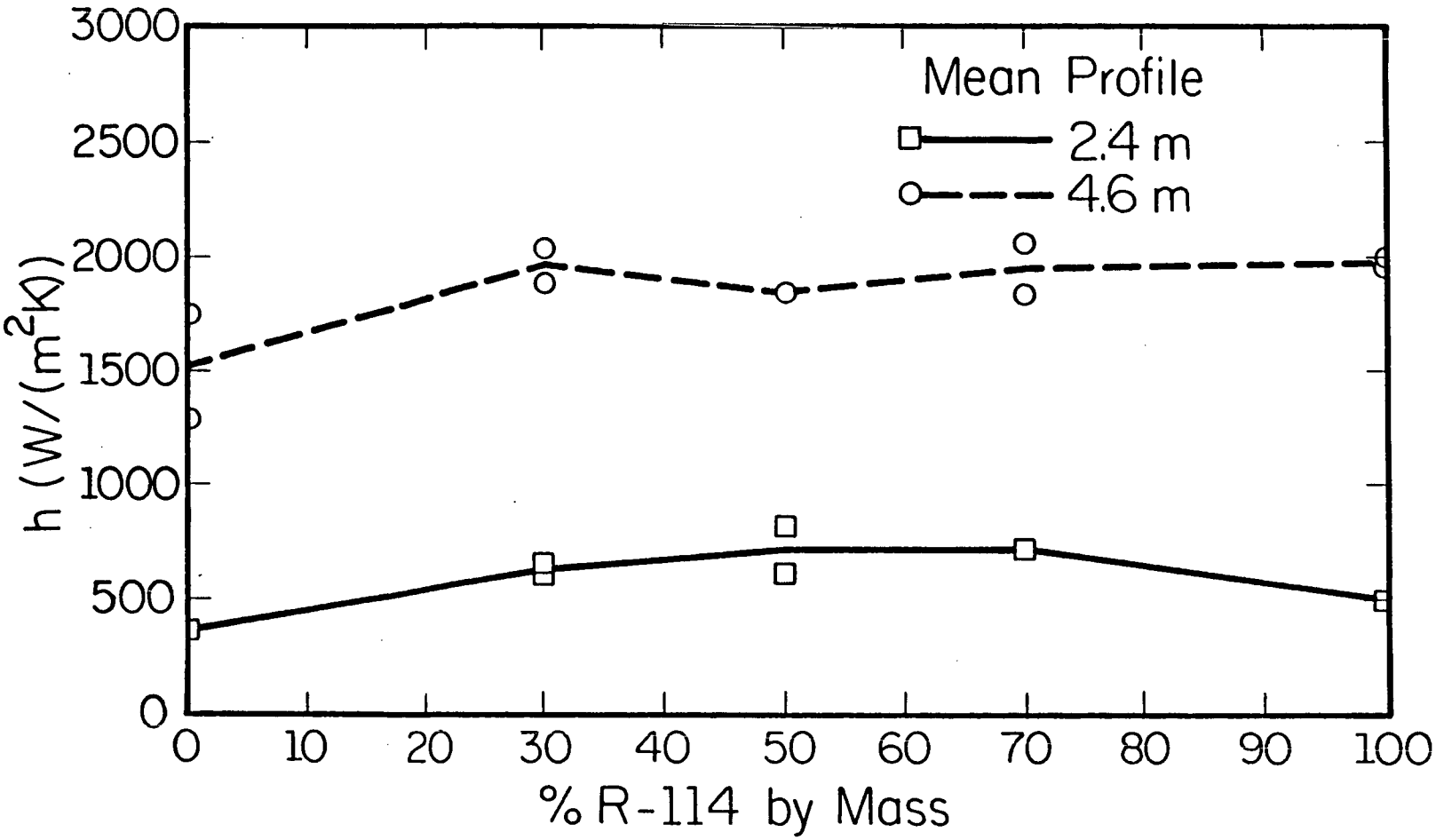


Figure 5.10. Variation in condensing coefficients with concentration at 2.4 and 4.6 m downstream (test series A).

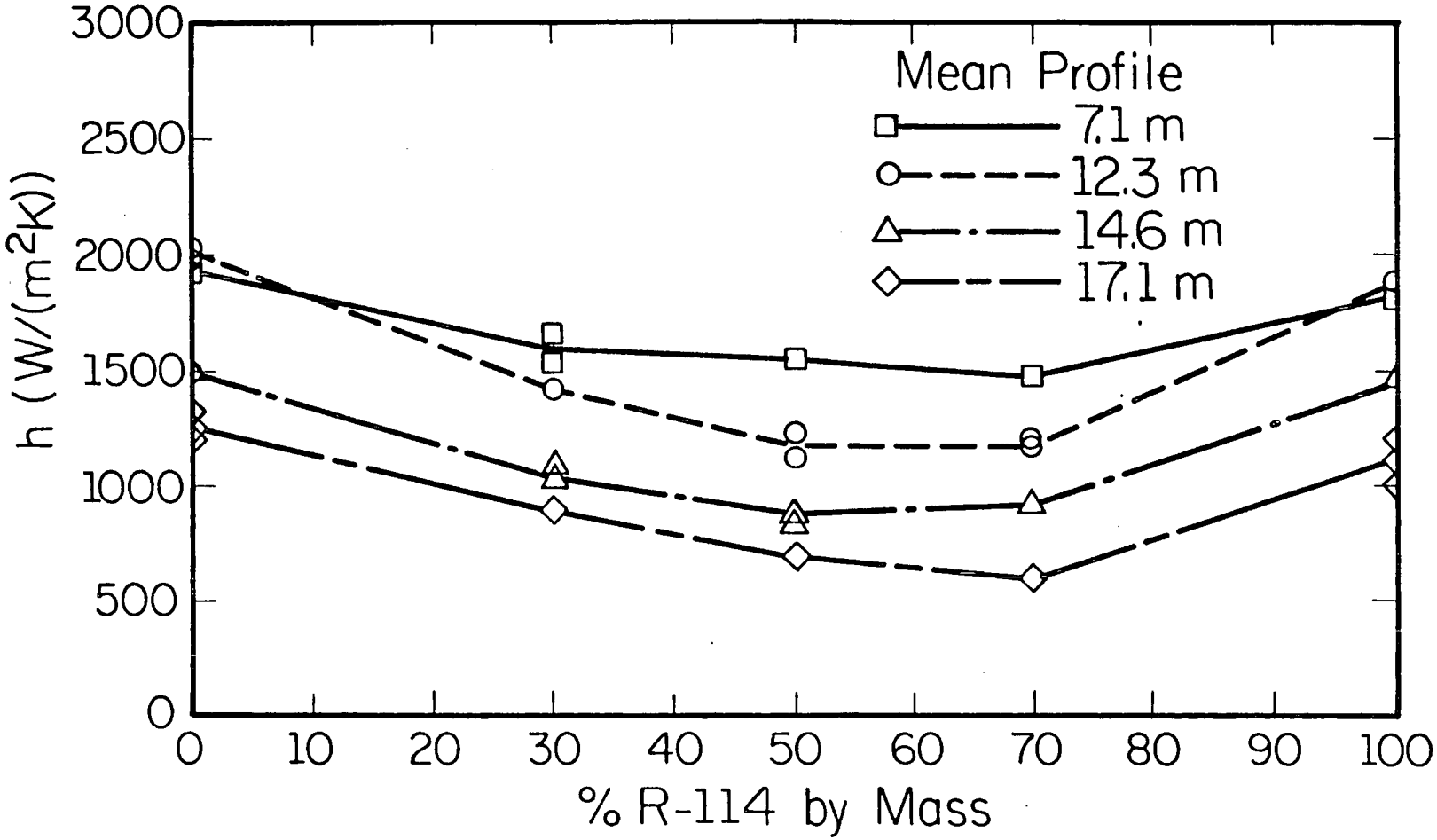


Figure 5.11. Variation in condensing coefficients with concentration at 7.1, 12.3, 14.6, and 17.1 m downstream (test series A).

is approximately a 26 percent increase in heat transfer rate compared with tests in series A. The refrigerant temperature profiles in the condenser from the tests in series B are similar to their counterparts in series A. The only significant differences between the profiles in the two series are the amounts of superheating and subcooling.

One of the objectives of conducting test series B with higher heat fluxes was to determine whether the higher heat transfer rates would blunt the reduction in heat-transfer coefficients occurring with mixtures. A potential method of preventing the reduction in heat-transfer coefficient when using mixtures may be to provide artificial agitation. We were interested in knowing if the increased turbulence that naturally occurs with the higher refrigerant flow rates in series B would influence pure refrigerants and refrigerant mixtures differently. Figures 5.12 through 5.16 show the condensing coefficients for series B for both single-refrigerant tests as well as for mixtures. When the values in these figures are compared with the results of series A, it is seen that in general the heat-transfer coefficient is higher in all tests for series B at location 2, but are only slightly higher at all other locations. Figure 5.17 shows a comparison of the coefficient through the condenser for a 50 percent by mass mixture.

For pure R-12 the increase in heat flux results in a noticeable improvement in the heat-transfer coefficient at the 2.5 and 5-m positions where the coefficient is improved by approximately 25 percent. Near the outlet of the condenser the values of heat-transfer coefficients in series B are approximately 5 percent higher than in series A. In the midsection of the condenser there is virtually no change in the heat-transfer coefficient. It can be concluded, then, that the increased flow rate associated with the high heat fluxes result in greatest improvement in the portions of the condenser where the convective mode of heat transfer is significant (the desuperheating and the subcooling sections).

Figure 5.17 shows a comparison of the coefficent through the condenser for a 50 percent by mass mixture. The heat-transfer coefficients of test series B are 10 to 15 percent higher throughout, except for the one position at 7-m. At least in a portion of the midsection of the condenser the high heat flux increases the coefficient, which gives at least modest support to the idea that increased turbulence in the midsection inhibits the reduction in

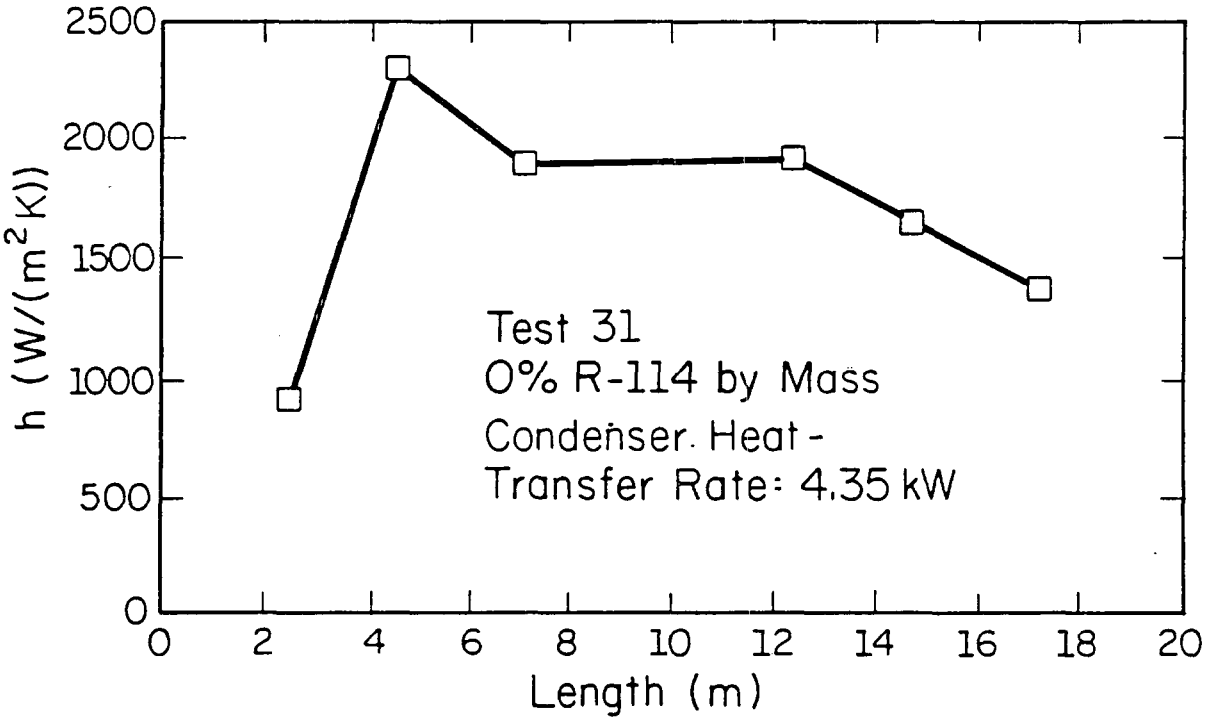


Figure 5.12. Condensing coefficient profile for pure R-12 (test series B).

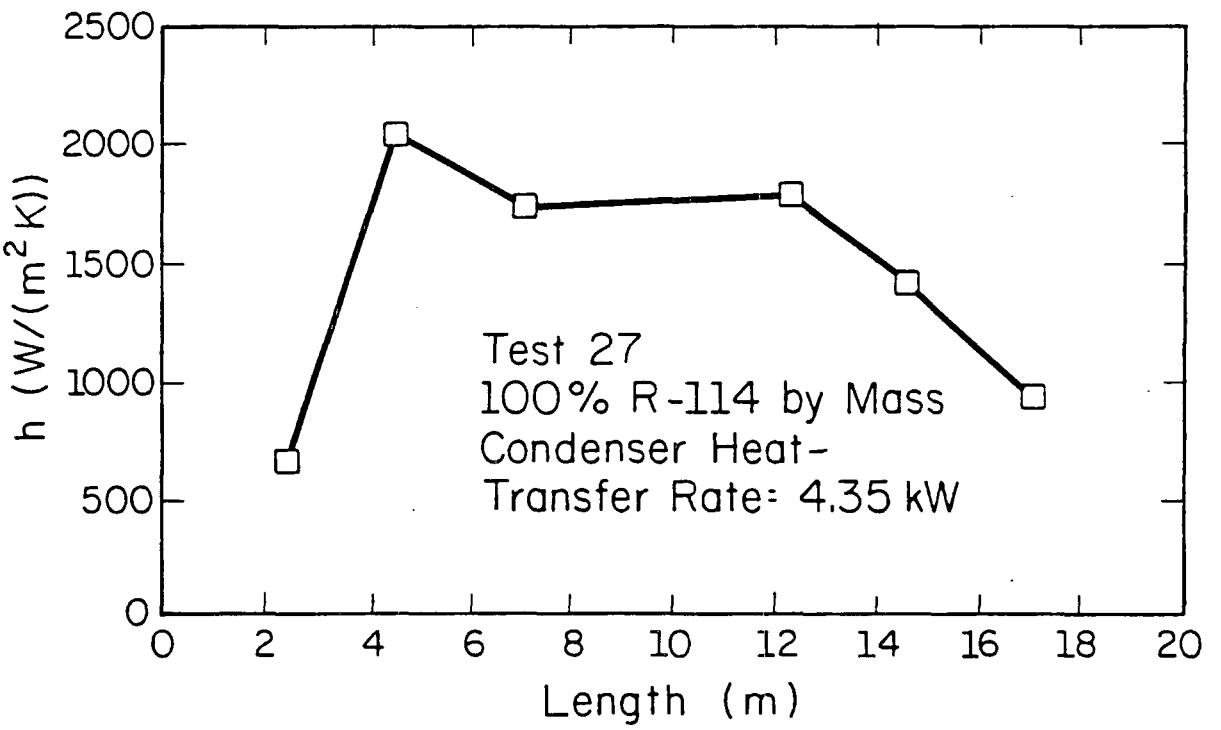


Figure 5.13. Condensing coefficient profile for pure R-114 (test series B).

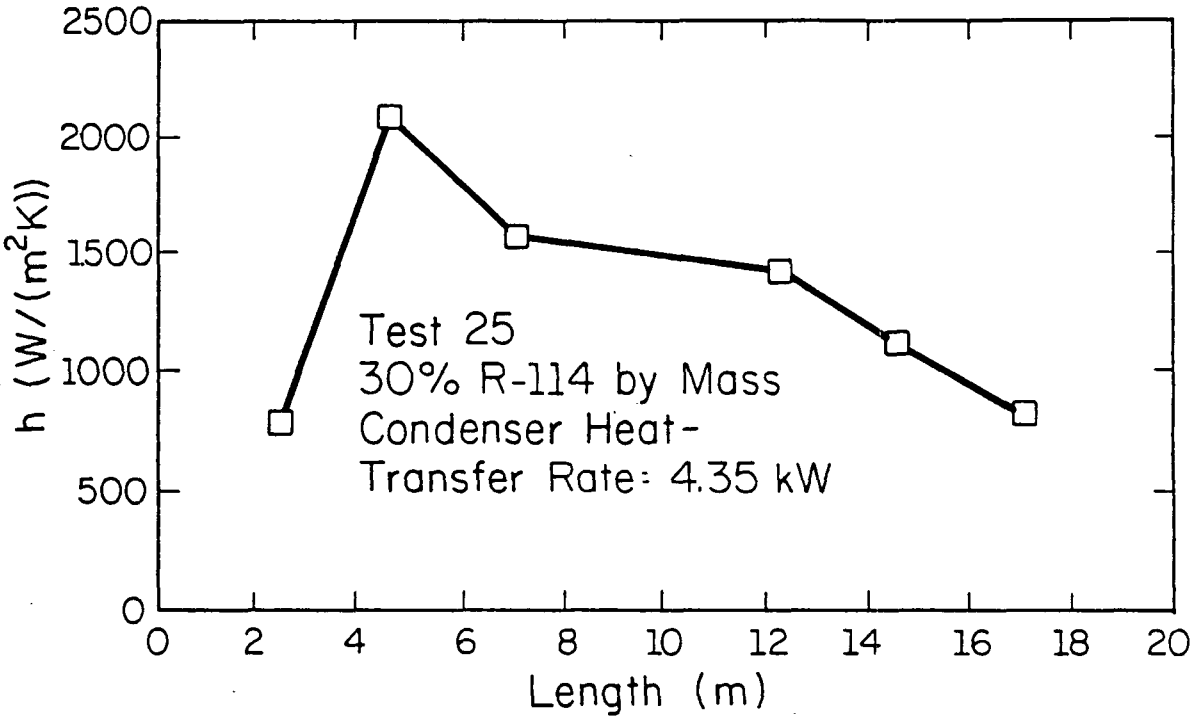


Figure 5.14. Condensing coefficient profile for 30% R-114 (test series B).

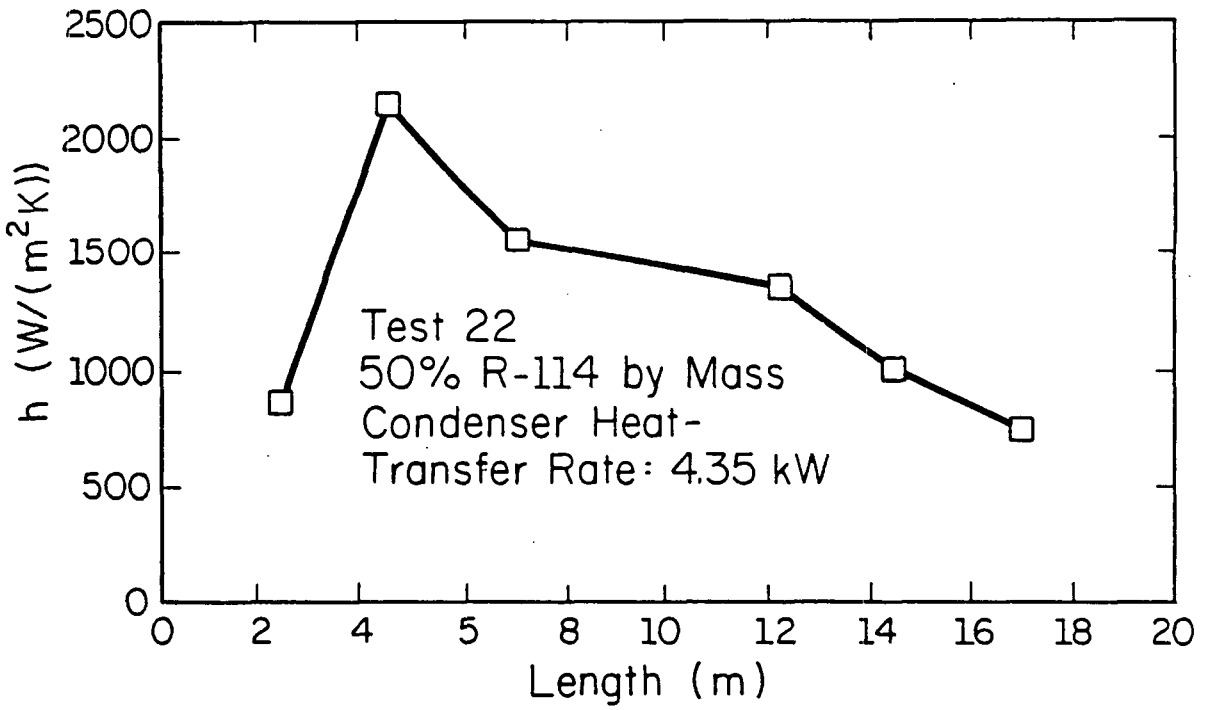


Figure 5.15. Condensing coefficient profile for 50% R-114 (test series B).

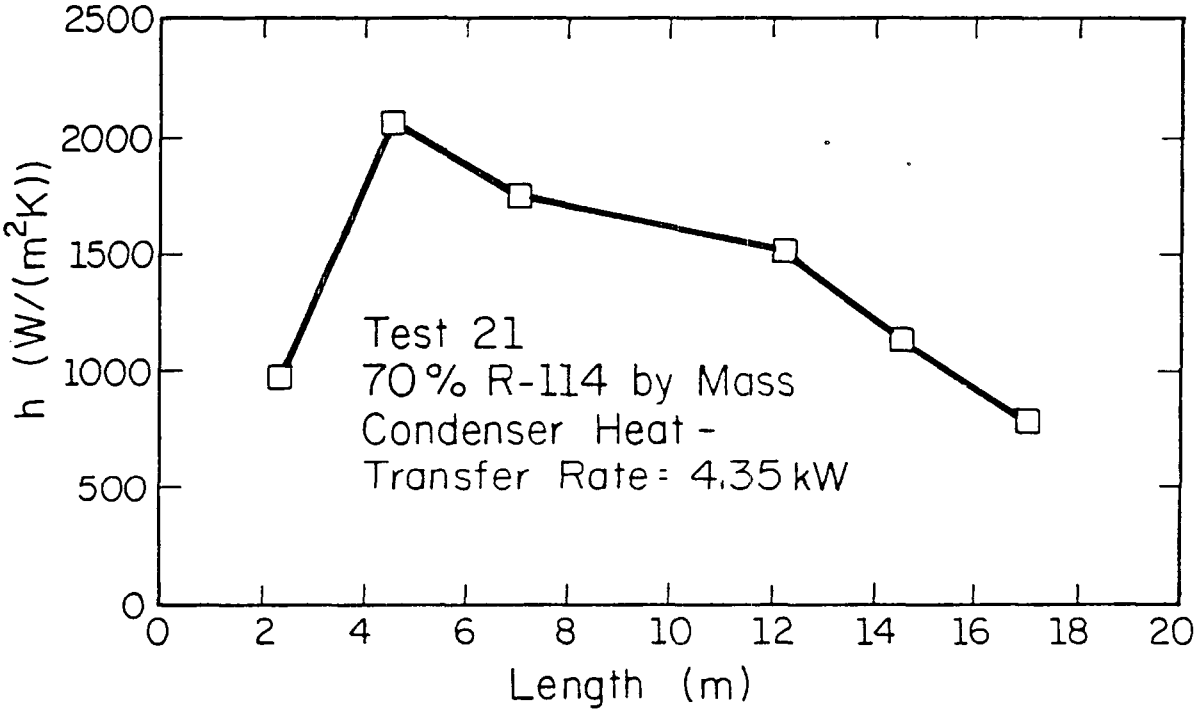


Figure 5.16. Condensing coefficient profile for 70% R-114 (test series B).

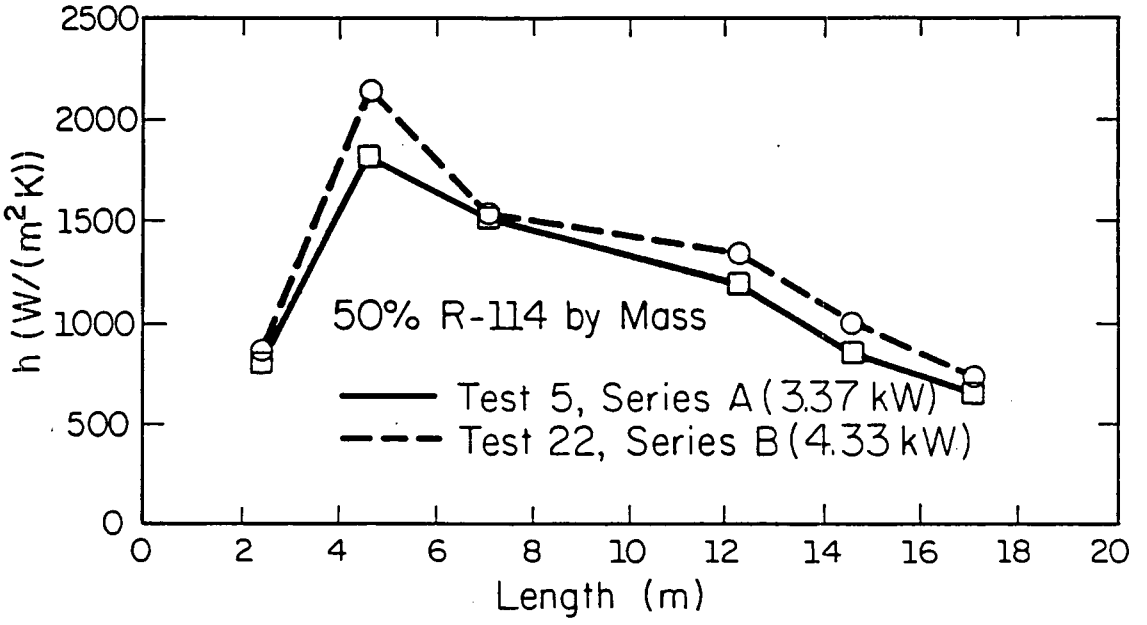


Figure 5.17. Increase in condensing coefficient with increasing heat flux at 4.6 m downstream from condenser entrance (test location 2).

heat-transfer coefficient when using a mixture. If the data at the 5-m position had also shown improvement in the coefficient in series B, the evidence would be stronger. Figure 5.18 for a 70 percent R-114 mixture that the coefficient is improved throughout the condenser, so it is possible that the measurement at the 5-m position for the 50 percent mixture is slightly in error.

The optimum choice of condenser loading is a study unto itself, but the comparison of series A and B suggests that high loadings (and perhaps more turbulence) results in greater improvement of the heat-transfer coefficients in the midsection of the condenser when the refrigerant is a mixture rather than when it is a pure one.

The effects of concentration on the tests of series B are illustrated first in Fig. 5.19, which shows the effect of the concentration on the condensing coefficients at locations 1 through 3. The flow patterns existing at these locations in the condenser were probably annular in transition to wavy. Figure 5.20 shows some definite trends in the coefficients in the second half of the condenser at locations 4, 5, and 6. It appears that the lowest coefficients occur at a concentration of approximately 50 to 70 percent R-114 where the reduction was between 20 and 35 percent of that of a linear relation between the pure constituents. At similar locations in test series A, the lowest condensing coefficients occurred at R-114 concentrations between 50 and 70 percent. The flow patterns at these locations were probably wavy and slug flow. The decrease in local heat-transfer coefficients with concentration in the middle and latter stages of the condenser has been noted by others [10,11,17].

## 5.6 Experimental Error

Many sources of experimental error accompany the test facility and test procedure. Fortunately, much of the error associated with the instrumentation and measurements does not affect the determination of the local heat-transfer coefficients but only the description of parameters applicable to a given test. Errors not affecting the heat-transfer coefficient measurements will be discussed followed by the measurements and error associated with the determination of the heat-transfer coefficients.

The heat input to the boiler water loop of the system was measured using voltage and current meters. The voltmeters have scaled divisions of 5 V, and

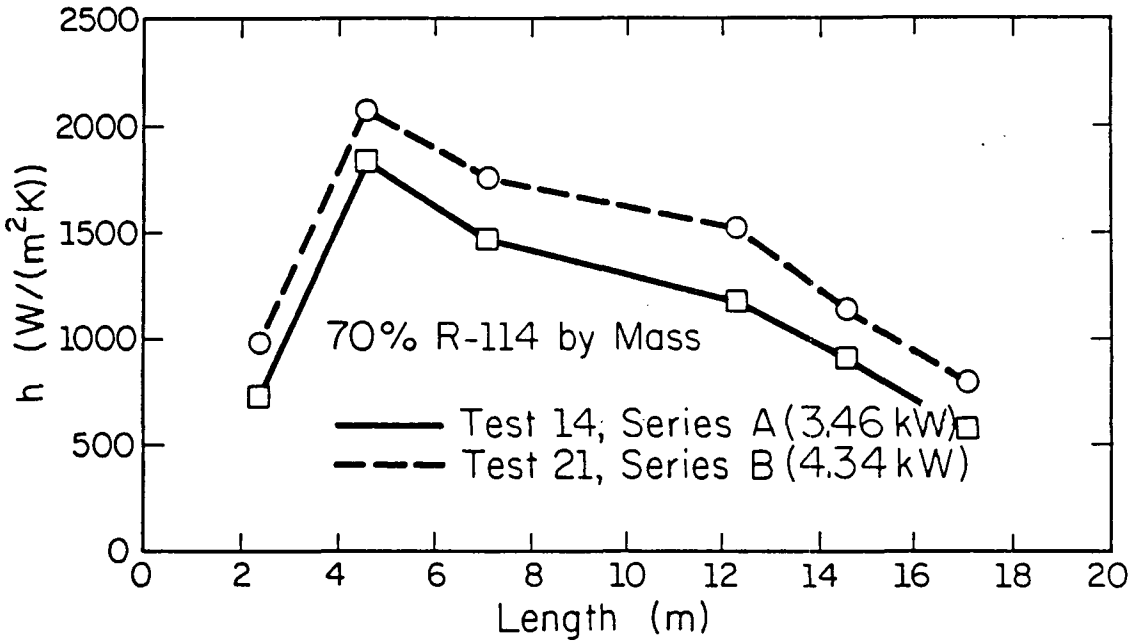


Figure 5.18. Uniform increase in condensing coefficients with increasing heat flux for 70% R-114.

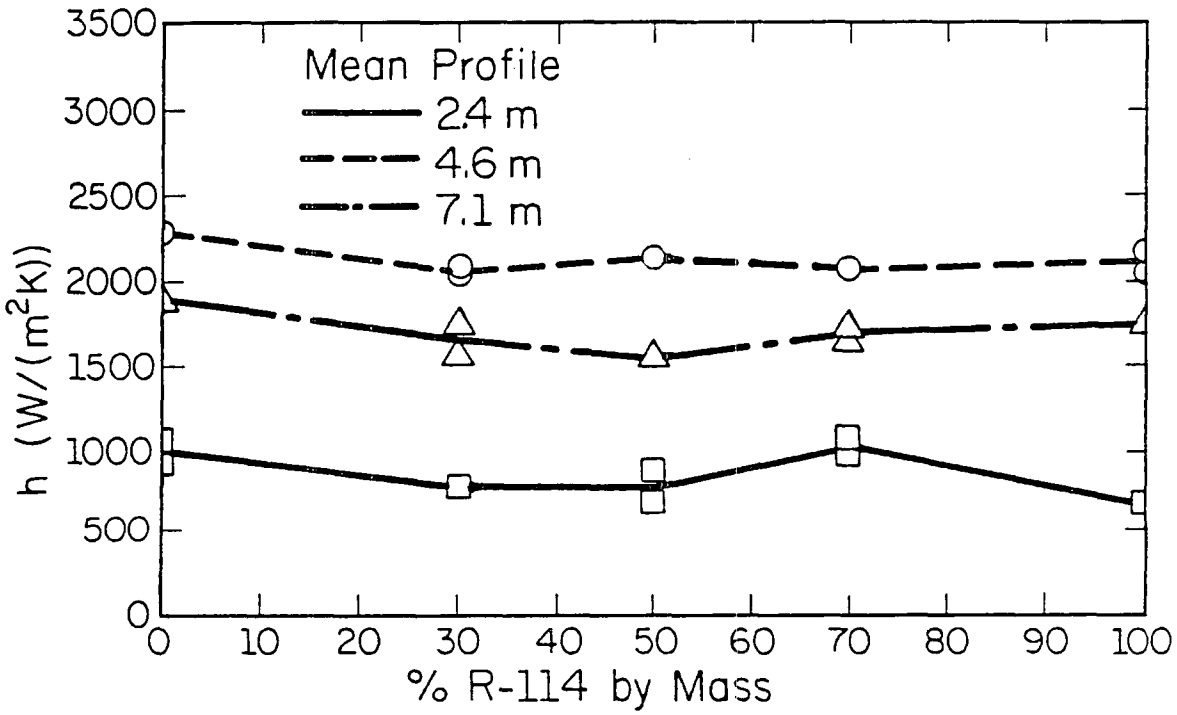


Figure 5.19. Variation in condensing coefficients with concentration at 2.4, 4.6, and 7.1 m downstream (test series B).

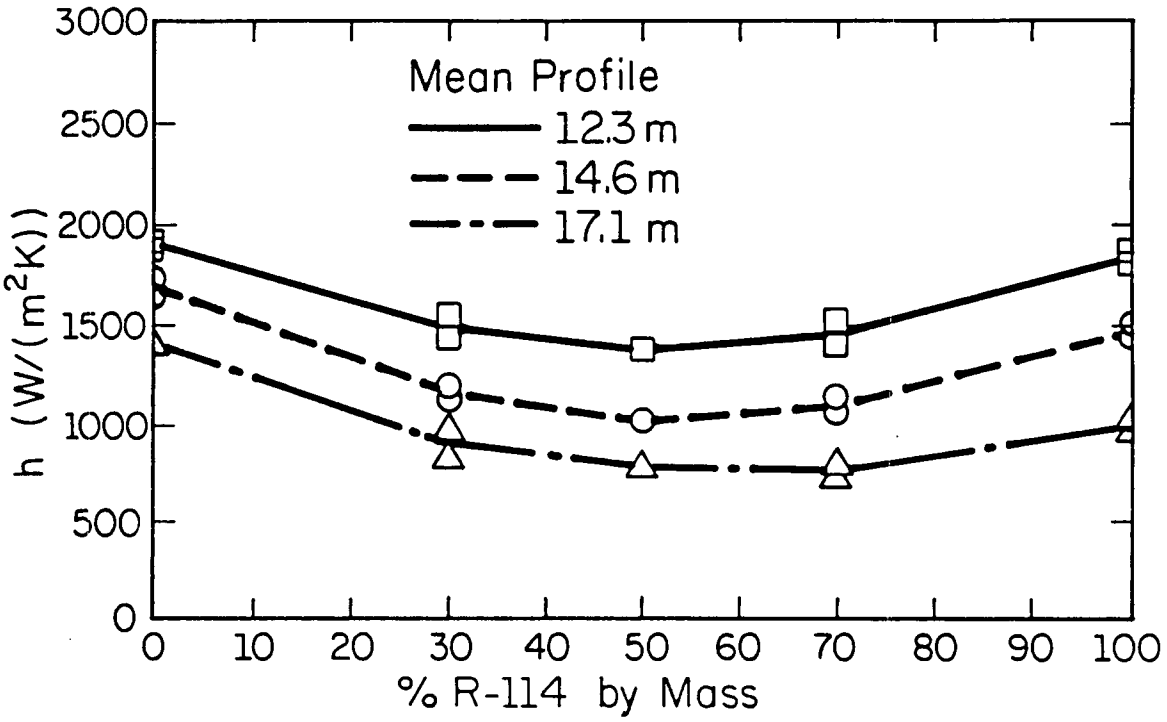


Figure 5.20. Variation in condensing coefficients with concentration at 12.3, 14.6, and 17.1 m downstream (test series B).

the ammeters have divisions of 0.2 A. Most of the voltmeter readings were above 200 V. For a voltage measurement of 200 V, an error of 2.5 percent could be introduced. The smallest ammeter readings were approximately 6.5 A, and most of the readings were over 10 A. Thus, a reading of 6.5 A could result in an error of as much as 3.1 percent.

The refrigerant flow rate was measured with a rotameter that has an error of 2 percent of the full scale. The boiler water flow rate was measured with a rotameter that also has an error of 2 percent of full scale. Both flow meters had at least a 50 percent (of scale) flow through them; therefore, the maximum error in flow rate measurement for both the refrigerant and boiler water was less than 4 percent each.

The refrigerant charge put into the system was measured by weighing it on a double-beam balance. The balance has scaled divisions of 0.02 lb. Approximately 6.3 kg of refrigerant was charged into the system during start up. Measurements were made of each refrigerant for a test, and the error in concentration measurement was less than 0.5 percent.

Pressure measurements were made using two different pressure gauges. All of the condenser pressures were read from one gauge and the rest of the system pressures were read from the other gauge. Both gauges have scaled divisions of 10 kPa. Thus the error in pressure measurement could be as much as 6.8 percent when using pure R-114 and as much as 1.4 percent when using pure R-12 in the system.

All of the temperature measurements were made using copper-constantan thermocouples. A great deal of effort was involved in positioning the thermocouples within the system (described in Chapter 4) to minimize the error due to their locations. Assuming that the thermocouples were positioned correctly, the only other error present was due to variations in construction of the thermocouples and the datalogger, which could amount to approximately 0.5°C. Temperature measurements throughout the system ranged from 15 to 55°C. Thus maximum errors in temperature measurements could vary between 0.9 and 3.3 percent.

Of primary interest to this study is the error present in the experimentally determined heat-transfer coefficients. An assumption critical to the calculation of the heat-transfer coefficients is that there is no heat trans-

fer between the condenser cooling water and the surroundings. The cooling water enters the condenser at about 15°C and exits around 35°C. Therefore, while flowing through the condenser the water is warmed to a temperature above ambient. The adiabatic assumption is taxed mostly at the inlet and outlet of the cooling water flow stream. At these locations the temperature difference between the water and its surroundings is greatest.

To estimate the error associated with the above heat transfer, we assumed an ambient temperature of 20°C (68°F). As mentioned earlier, the points of interest in the condenser were the two ends. The lengths of the condenser segments used in the analysis were those used to calculate the condensing coefficient at each end of the condenser.

The length used at the cooling water inlet was that used to calculate the coefficient at test location 6. Within this part of the condenser, the cooling water was warmed to a temperature above the ambient. Analysis shows that approximately 0.3 percent of the heat gained by the water in this part of the condenser was from the surroundings. The maximum heat transfer will occur at the cooling water exit. The length of the condenser used to determine the heat transfer at this end was that used to calculate the heat-transfer coefficient at test location 1. It was found that the amount of heat gained by the water in this section of the condenser could be in error by as much as 11 percent due to heat lost to the surroundings.

The measured quantities that directly influence the determination of the heat-transfer coefficients were various temperatures and the condenser water flow rate. The temperatures used in the calculation of the local coefficients were noted in Chapter 4. The flow rate of the condenser cooling water was measured with a rotameter that was accurate to within 2 percent of full scale. Since the rotameter was operated at around 70 percent capacity, the flow rate had a maximum error of about 3 percent.

Using the maximum temperature measurement error of 0.5°C previously given, the temperatures and water flow rates were analyzed in such a way as to obtain the worst case error in local heat-transfer coefficient measurement. Analyses were done on tests with differing R-114 mass concentrations. Also the condenser was divided into entrance, midrange, and exit regions for the analysis.

The greatest percent deviation in transfer coefficients would exist at the condenser entrance (test location 1). At this location the coefficients could conceivably deviate between +116 percent and -76 percent. The reasons for the great variation are two-fold. First, all of the temperatures used in the calculation of the coefficients appear as differences. In general, these temperature differences are smaller near the condenser entrance. Thus the 0.5°C offset of each temperature will more greatly affect the $\Delta T$ at the condenser entrance. Second, the heat-transfer coefficients at this location are much smaller than those at the other test locations. Thus, a uniform variation in the coefficients will show up as a larger percentage difference at location 1 than at any of the other locations.

In the midrange of the condenser (test locations 2, 3, and 4), the worst-case variations in condensing coefficients are estimated to be between +39 percent and -31 percent. At the condenser exit (locations 5 and 6), the worst-case variations are estimated to be between +48 percent and -39 percent. Here the temperature differences are large, but the coefficients themselves are not as high as in the middle of the condenser.

The error found in the heat transfer between the condenser cooling water and its surroundings was not included in the above worst case error estimates. This error, had it been included, would tend to reduce the calculated worst case error. The heat lost to the environment was greatest at test location 1. Also, this location was where the greatest percent deviation in the heat-transfer coefficient occurred. Including the heat lost to the environment would have increased the measured value of the coefficient. It would also have enlarged some of the temperature differences such that the 0.5°C shift in temperatures would have had less effect on the augmented coefficient value. Both of the above factors would reduce the percent deviation between the measured and augmented heat-transfer coefficients.

## 5.7 Reasons for Reduction in Heat-Transfer Coefficient

One benefit of being able to explain why the heat transfer coefficient drops when condensing a mixture is to try to minimize this disadvantage. Kornota and Stoecker [10] calculated an example of concentrations of R-12 that existed in the vapor at one point during the condensation and also the concentration condensing at that point. That situation, shown in Fig. 5.21

showed that while the vapor above the liquid had an R-12 concentration of 60.8%, the vapor condensing only had a 47.6% concentration of R-12. Near the liquid-vapor interface the counterdiffusion process of R-12 and R-114 may explain the reduction in coefficient occurring during condensation of a mixture.

Figure 5.21 was calculated for a no-slip condition, and it is reasonable to ask whether the existence of slip would cause a greater disparity between the vapor concentration existing above the liquid and the concentration actually condensing. The opposite is the case, however, because if slip occurs the vapor now existing in the upper portion of the tube is that which should exist in the upstream part of the condenser. This vapor has a lower concentration of R-12 than the 60.8% shown in Fig. 5.21 and thus a concentration closer to the 47.6% that is condensing.

The above observation suggests that vapor-liquid slip may not be the culprit in the reduction of heat-transfer coefficient. The fact that the midsection of the condenser suffers most from the degradation of the coefficient could be attributable mostly to the low turbulence there not overcoming the counterdiffusion barrier.

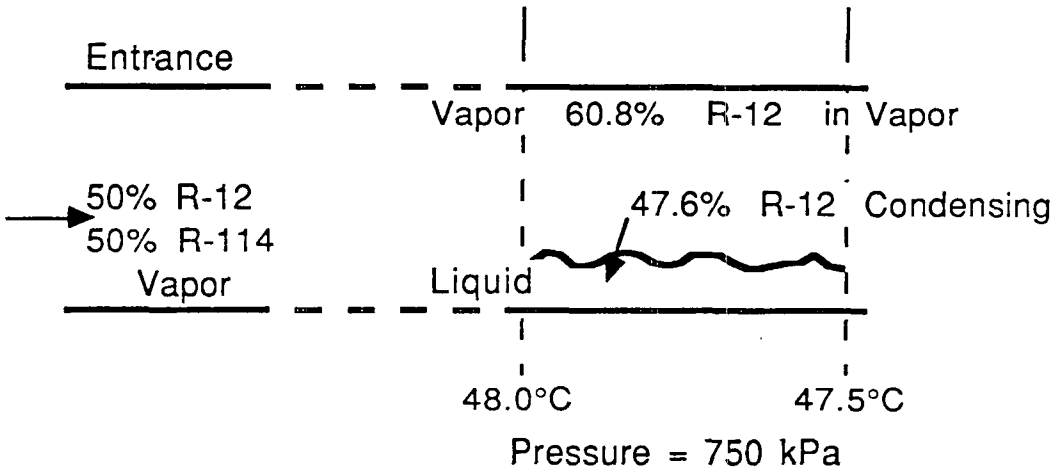


Figure 5.21. Vapor concentrations existing and condensing at one position in a condenser tube.

# 6. CONDENSING COEFFICIENT CORRELATIONS

## 6.1 Introduction

As a complement to the experimental study of condensing coefficients the theoretical determination of condensing heat-transfer coefficients was examined. A review of the literature was performed, and several of the popular correlations predicting condensing coefficients were selected for comparison. These correlations have undergone varying amounts of experimental comparison by other experimenters in order to test their accuracy, and the amount of verification will be noted. The correlations were developed from either a theoretical, semitheoretical, or empirical basis. All of the equations were formulated and tested using single fluids. The expressions are used here to predict the condensing coefficients for nonazeotropic mixtures of R-12/R-114 as well as the condensing coefficients for pure R-12 and pure R-114.

When one is working with two-phase flows during a condensation process, the calculation of fluid properties and flow conditions can be difficult. Calculation of the two-phase flow velocity requires knowledge of the quality. The quality of a nonazeotropic refrigerant mixture can be estimated when the pressure and temperature of the fluid are known. However, such information is not adequate to determine the quality for a pure refrigerant. Therefore, the quality of pure refrigerant is determined at various points along the condenser using an energy balance with the condenser cooling water. The refrigerant enters the condenser superheated and the amount of heat needed to be removed from the refrigerant to form saturated vapor is calculated. This heat is then added to the condenser and determines the location along the condenser where condensation begins. From this point on, all of the heat added to the water indicates the amount of refrigerant condensed, thus yielding the quality.

A total of eight correlations are presented here. All of the expressions are applicable only within a certain range of parameters and thus will be used within these ranges. Some of the correlations have certain applicability criteria that prohibit their use in predicting condensing coefficients for the experimentation done herein. The experimental verification by others of these correlations is noted. All of the quantities used in the expressions are defined in the NOMENCLATURE.

The comparison of each correlation is presented graphically with the predicted experimental heat-transfer coefficient. Each graph has a 45 degree dashed line which serves as a reference line denoting predictions that match the experimental values. It seemed desirable to include some reference lines that would enclose an area within which the predicted data points would be said to be "accurate," even though the term is subjective and also depends on the application at hand. For design purposes, we felt that an adequate prediction would fall within 20 percent of the actual value. Thus, solid lines marking predictions of ±20 percent are included on the graphs for reference.

The locations of the flow patterns at various points along the condenser are assumed to be known for series A but may be slightly different in series B with its higher heat flux only be approximated for series B. When the application of a correlation depends on a specific flow pattern, it is assumed that similar flow patterns exist at similar locations for the tests in both series. Therefore, when available, the results for series B will be presented at the same condenser locations as those for series A. The results presented for series B tests do not necessarily imply that the correlation is inaccurate.

None of the results at test location 1 are presented. All of the correlations grossly overpredicted the condensing coefficients at this location. The errors in the predictions are due to entrance effects in the condenser which are not addressed by any of the correlations. A more detailed discussion of entrance effects is given later in this chapter.

## 6.2 Individual Correlations

### 6.2.1 Akers and Rosson Correlation

The first correlation presented here was proposed by Akers and Rosson [18] and developed from a "semitheoretical" approach. The expression is to be applicable to both semistratified and laminar annular flows, only when the liquid Reynolds number ($Re_\ell$) does not exceed 5000. Two equations are given for different ranges of the vapor Reynolds number ($Re_v$).

For $1000 < Re_v < 20{,}000$,

$$h = 13.8 \left(\frac{k_\ell}{D}\right) Pr_\ell^{1/3} \left(\frac{i_{\ell v}}{C_{p_\ell} \Delta T}\right)^{1/6} Re_v^{0.2} \; ; \tag{6.1}$$

and for $20{,}000 < Re_v < 100{,}000$,

$$h = 0.1 \left(\frac{k_\ell}{D}\right) Pr_\ell^{1/3} \left(\frac{i_{\ell v}}{C_{p_\ell} \Delta T}\right)^{1/6} Re_v^{2/3} \; . \tag{6.2}$$

A correlation used to cover ranges of $Re_\ell$ not covered by Eqs. 6.1 and 6.2 was proposed by Akers et al [19].

For $Re_\ell > 5000$ and $Re_v > 20{,}000$,

$$h = 0.026 \left(\frac{k_\ell}{D}\right) Pr_\ell^{1/3} \left(\frac{D\, G_e}{\mu_\ell}\right)^{0.8} \; . \tag{6.3}$$

For the tests in series A, annular and semistratified flow patterns are assumed to have existed at test locations 1 through 4 in the condenser. Figure 6.1 shows the comparison of the Akers and Rosson correlations (Eqs. 6.1 and 6.2) with our experimental data for the mixture tests in series A. The figure shows that the correlations accurately predict the condensing coefficients at test locations 2 and 3.

Figure 6.2 shows that Eqs. 6.1 and 6.2 overpredict the condensing coefficients for the pure refrigerant tests in series A at test location 2. Downstream of location 2, particularly at location 3, the magnitude of the predicted coefficients drew closer to the experimental values. The expressions underpredict the experimental values at location 4. Some results were obtained at location 5; however, the flow pattern suggests that this regime is beyond the range of applicability of these equations.

Figures 6.3 and 6.4 show that the Akers and Rosson correlations predict favorably the experimental results from the mixture and single refrigerant tests from series B at test locations 2 and 3. The flow conditions were out of the range of applicability for correlations at locations 4, 5, and 6.

In the formulation of these expressions, the temperature drop across the condensate film, $\Delta T$, appears in the denominator of Eqs. 6.1 and 6.2. This quantity was not measured but was calculated using the temperature difference between the refrigerant and the refrigerant tube, a quantity that is likely to be larger than the $\Delta T$ across the condensating film. The use of this

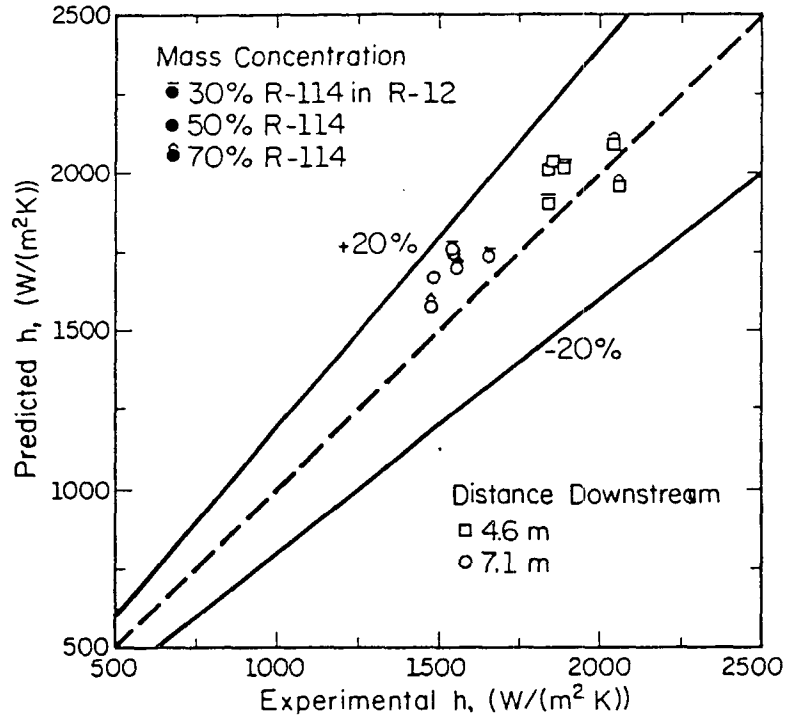


Figure 6.1. Akers and Rosson correlation [18] applied to R-12/R-114 mixture tests of series A.

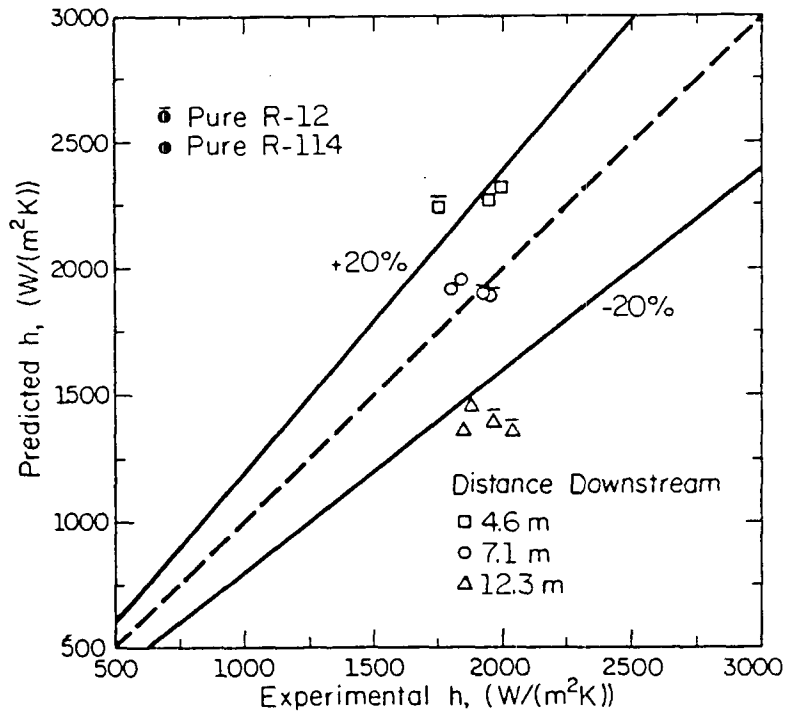


Figure 6.2. Akers and Rosson correlation [18] applied to R-12 and R-114 tests of series A.

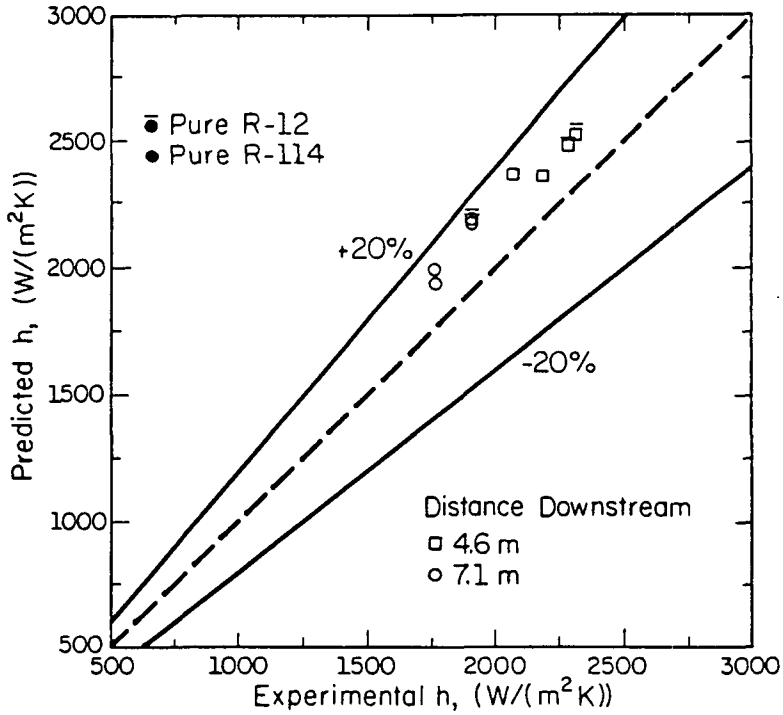


Figure 6.3. Akers and Rosson correlation [18] applied to R-12/R-114 mixture tests of series B.

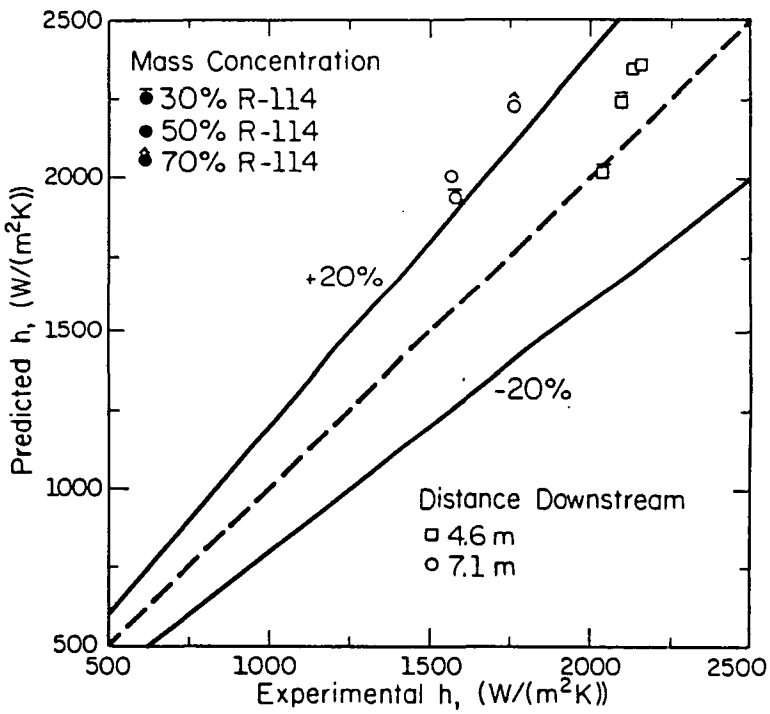


Figure 6.4. Akers and Rosson correlation [18] applied to R-12 and R-114 tests of series B.

estimated $\Delta T$ causes the predicted heat-transfer coefficients to be smaller than actual. Therefore, any underpredictions from these correlations can be at least partially accounted for by this cause. From Figs. 6.1 through 6.4, it is seen that only the data at test location 4 from the single refrigerant tests of series A were underpredicted by the expressions. As a result using the correct $\Delta T$ would be more detrimental than beneficial to the predictions.

The relationship proposed by Akers et al. (Eq. 6.3) for higher liquid Reynolds numbers was not applicable to the flow parameters used in these tests. The expression did give some marginal results at condenser location 4 and downstream. Since an annular flow pattern does not exist at these locations; the data points are not meaningful.

Akers and Rosson obtained over 300 experimental data points while condensing pure methanol and pure R-12 [18]. They found that the mean deviation between the coefficients predicted by Eqs. 6.1 and 6.2 and the experimentally determined coefficients was less than 5 percent. The maximum deviation was less than 20 percent. Akers et al. [19] experimented with pure propane and pure R-12 in a horizontal tube. They found Eq. 6.3 to predict the condensing coefficients to within 20 percent of the experimental values. Tandon et al. [15], ran condensing experiments with the pure refrigerants R-12 and R-22. They found Eqs. 6.1 and 6.2 to correlate to the experimental data to within 20 percent for the R-12 and within 25 percent for the R-22.

### 6.2.2 Azer Correlation

A condensing-coefficient correlation was developed by Azer et al. [20] from a theoretical analysis using an analogy between the equations of momentum and heat transfer across a liquid film, and its use is recommended only for annular flow condensation

$$h = 0.039 \left(\frac{k_\ell}{D}\right) Pr_\ell^{0.337} \, Re_{vT}^{0.9} \left(\frac{\mu_v}{\mu_\ell}\right) \left(\frac{\rho_\ell}{\rho_v}\right)^{0.5} \left(\frac{x^{0.9}}{4.67-x}\right) \phi_v \, , \tag{6.4}$$

where

$$\phi_v = 1 + 1.09 \, X_{tt}^{0.0399} \, . \tag{6.5}$$

The annular flow requirement of Eq. 6.4 limits its use in predicting condensing coefficients to the first half of the condenser. For the tests in series A, the flow pattern at test location 3 could be described as semiannular. Downstream of condenser location 3, the refrigerant flow becomes stratified. Figure 6.5 shows the results of using this equation to predict the condensing coefficients for the mixture tests in series A. The predictions are in excellent agreement with the experimental data at locations 2 and 3, but the results given by Eq. 6.4 deteriorate as it is applied downstream of test location 3.

Figure 6.6 shows that when Eq. 6.4 is applied to the single-refrigerant tests from series A, the comparison is good at location 3; however it overpredicts at location 2. Again the expression breaks down when applied to non-annular flow regimes as, for example, at location 4.

Figure 6.7 shows the series B mixture test results compared with Eq. 6.4. The expression closely predicts the experimentally determined values at location 2 but only marginally at location 3; however, the degree of correlation deteriorates. Deteriorating results are again apparent at location 4 and all downstream locations. Figure 6.8 shows that the equation overpredicts the experimental values from the single-refrigerant tests of series B. For this group of tests Eq. 6.4 is most accurate at test location 4, where it underpredicts the experimental values. As expected, the underpredictions become progressively worse downstream of location 4.

Azer et al. [20] did not provide experimental results to verify Eq. 6.4, however, Bae et al. [21] obtained results from two studies where pure R-12 and pure R-22 condensed inside horizontal tubes. The experimentally determined coefficients found by Bae fall within 30 percent of those predicted by Eq. 6.4.

A condenser study done by Tandon et al. [15] using pure R-12 found Eq. 6.4 to overpredict the experimental values by as much 125 percent. One reason offered for the large deviations between experimental and predicted coefficients was that the experimentally determined coefficients were average values determined over a 1-m length of tube as opposed to true local values. Also, the experimental data included points from the semiannular flow regime.

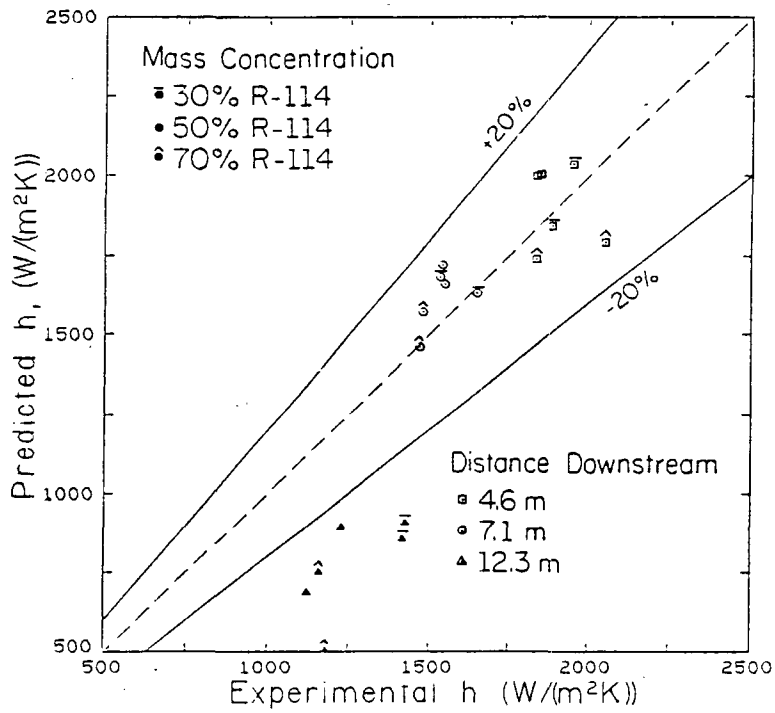


Figure 6.5. Azer et al. correlation [20] applied to R-12/R-114 mixture tests of series A.

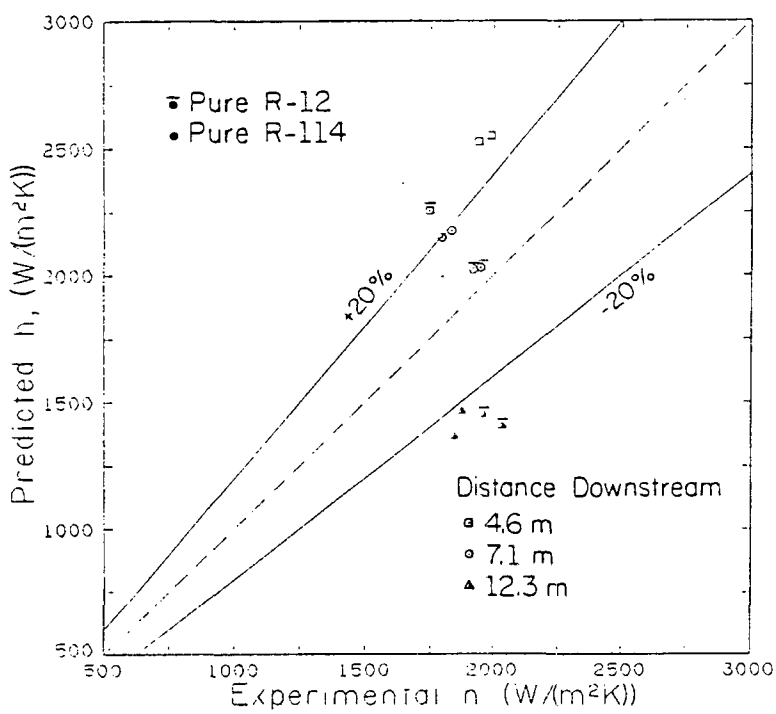


Figure 6.6. Azer et al. correlation [20] applied to R-12 and R-114 tests of series A.

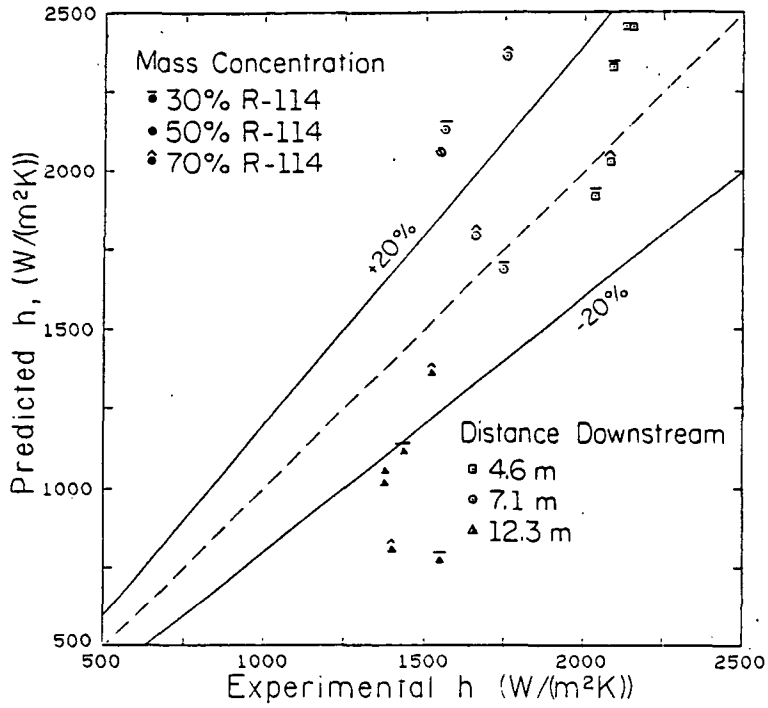


Figure 6.7. Azer et al. correlation [20] applied to R-12/R-114 mixture tests of series B.

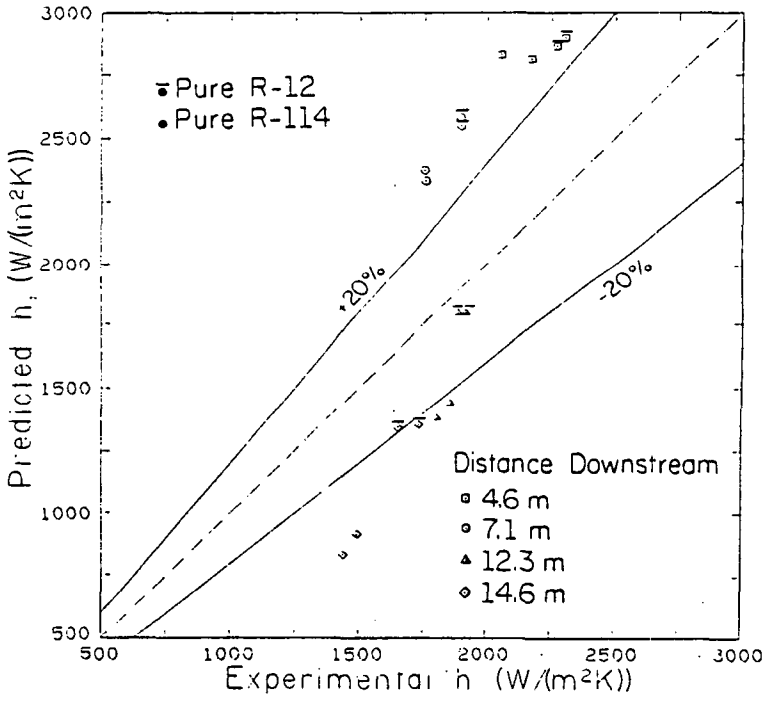


Figure 6.8. Azer et al. correlation [20] applied to R-12 and R-114 tests of series B.

### 6.2.3 Traviss Correlation

Again using the analogy between momentum and heat transfer, an equation to predict local condensing coefficients was developed by Traviss et al. [22], who recommended its use for the annular and dispersed flow regimes:

$$h = \left(\frac{k_\ell}{D}\right) \left(\frac{Pr_\ell \; Re_\ell^{0.9}}{F_2}\right) F(X_{tt}) \; , \tag{6.6}$$

where for $Re_\ell < 50$,

$$F_2 = 0.707 \; Pr_\ell \; Re_\ell^{0.5} \; , \tag{6.7}$$

for $50 < Re_\ell < 1125$,

$$F_2 = 5Pr_\ell + 5 \; \ln[1 + Pr_\ell \; (0.09636 \; Re_\ell^{0.585} - 1)] \; , \tag{6.8}$$

for $Re_\ell > 1125$,

$$F_2 = 5Pr_\ell + 5 \; \ln(1 + 5Pr_\ell) + 2.5 \; \ln(0.00313Re_\ell^{0.812}) \; , \tag{6.9}$$

and

$$F(X_{tt}) = 0.15 \; [X_{tt}^{-1} + 2.85X_{tt}^{-0.476}] \; . \tag{6.10}$$

The annular and dispersed flow pattern requirements of Eq. 6.6 should limit its applicability to our condenser test locations 1 through 3. Figure 6.9 shows the correlation favorably predicting the condensing coefficients for the mixture tests of series A at locations 2 through 4, but underpredicting the coefficients at location 5. It is not applicable at location 6.

Equation 6.6 yielded interesting results for the single-refrigerant tests of series A. The correlation accurately predicts the condensing coefficients at locations 2 through 6 as shown in Fig. 6.10. Surprisingly, the correlation deviates at condenser location 4 and improves further downstream.

Figures 6.11 and 6.12 depict the predictive quality of Eq. 6.6 for the mixture and single refrigerant tests of series B, respectively. The figures

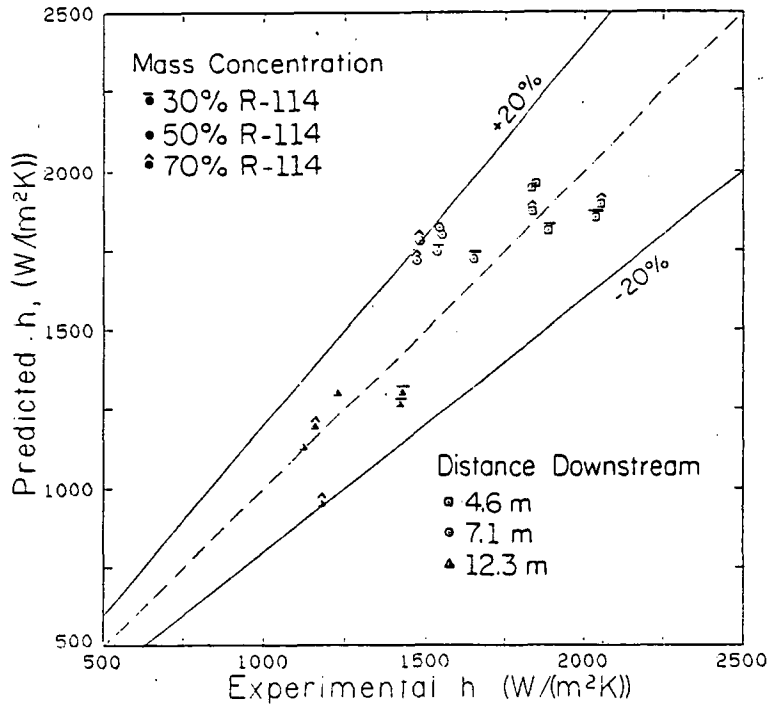


Figure 6.9. Traviss et al. correlation [22] applied to R-12/R-114 mixture tests of series A.

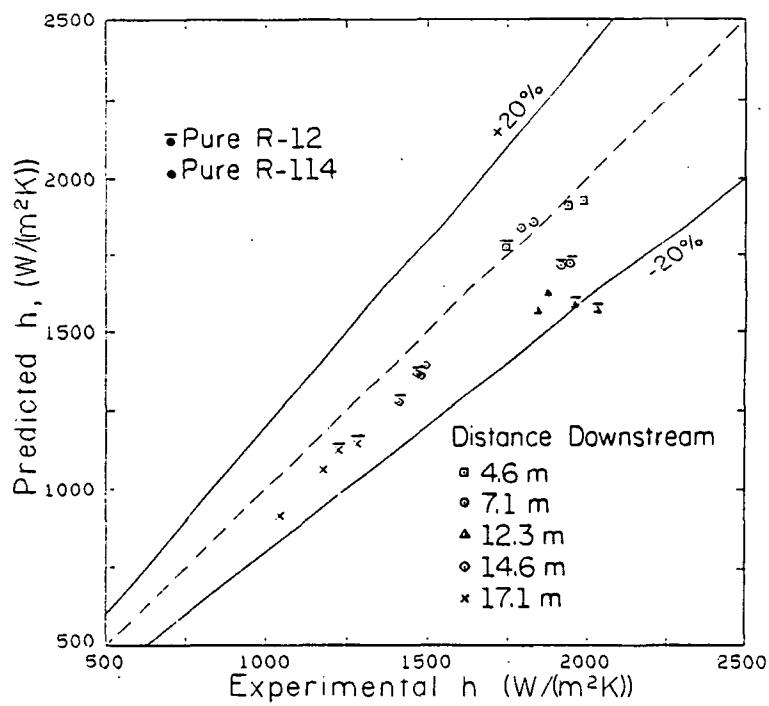


Figure 6.10. Traviss et al. correlation [22] applied to R-12 and R-114 tests of series A.

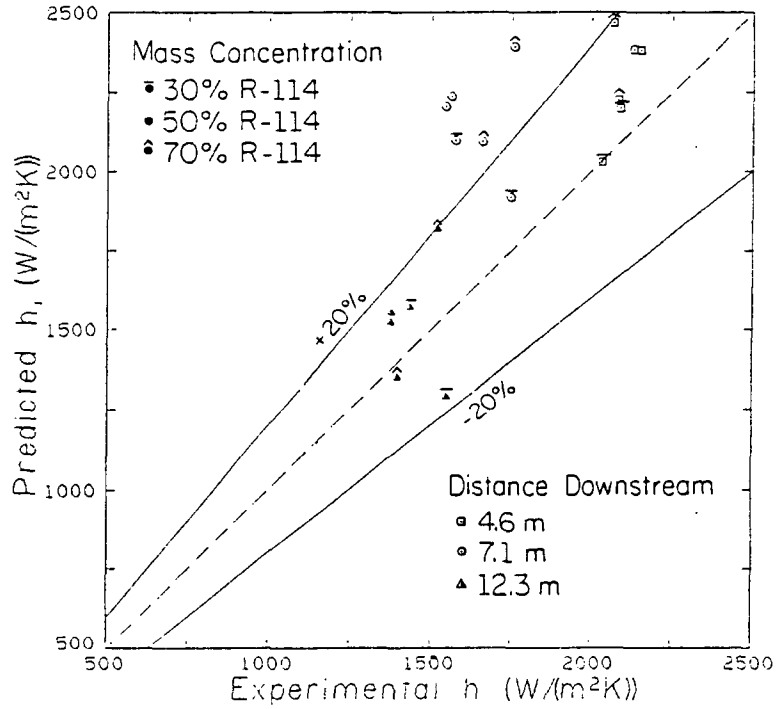


Figure 6.11. Traviss et al. correlation [22] applied to R-12/R-114 mixture tests of series B.

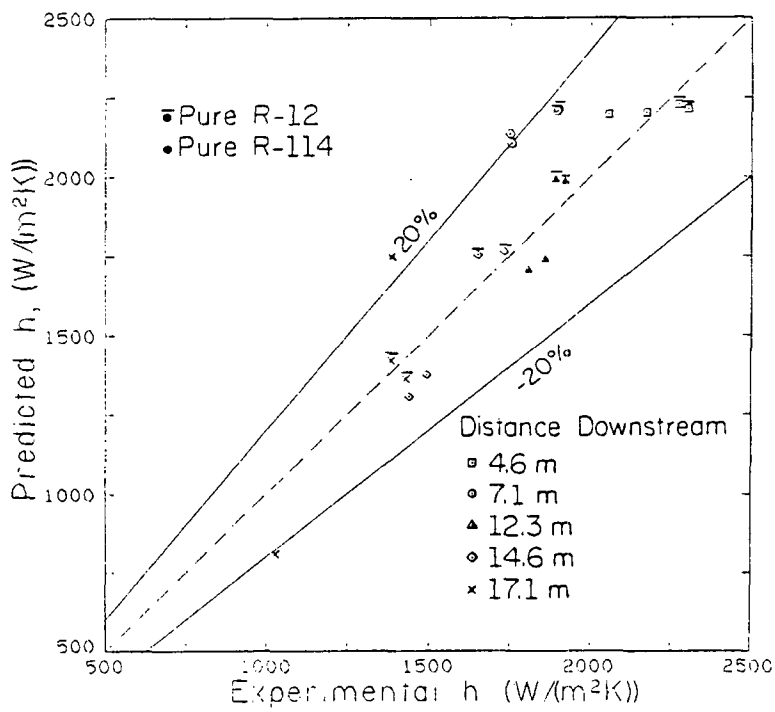


Figure 6.12. Traviss et al. correlation [22] applied to R-12 and R-114 tests of series B.

show nearly the same results as were obtained for the series A tests. The one major difference is that there was a noticeable degradation in the correlation at test location 3 for the series B tests, especially in the mixture tests. Also there is great deviation between the predicted and experimental values at location 6 for the pure R-114 tests of series B.

Traviss et al. [22] experimenting with single refrigerants R-12 and R-22, found the predicted coefficients from Eq. 6.6 to agree reasonably well with experimental values at high vapor qualities. This result reinforces the applicability of the correlation to the annular flow regime. Tandon et al. [15] used pure R-12 and pure R-22 did not find good agreement between experimental values and those predicted by Eq. 6.6. Again it was noted that some semiannular flow data were used and the experimental coefficients were not true local values. Also, Tandon applied the above correlation to the experimental data of Abis and found differences ranging from -30 percent to +100 percent.

### 6.2.4 Chato and Shah Correlations

Two correlations, one developed by Chato and the other by Shah, are used together to cover a wider range of flows as suggested by Shah [23]. Chato developed a correlation to predict local condensing coefficients during laminar condensation inside both horizontal and inclined tubes [24]. The relationship was developed using a momentum-energy method for the condensate forming in the tube. The equation developed by Chato for the horizontal tube is as follows:

for $U_v < 3$ m/s, $Re_{\ell T} < 1800$ and $Re_{vT} < 35{,}000$,

$$h = 0.5583 \left(\frac{\rho_\ell(\rho_\ell - \rho_v) g \, i_{\ell v} \, k_\ell^3}{D \, \mu_\ell \, TD}\right)^{0.25} . \qquad (6.11)$$

Another paper by Shah [25] developed a correlation to predict local condensing coefficients during film condensation inside pipes, which also complements Eq. 6.11 in that it covers a different range of flow conditions.

For $U_v > 3$ m/s, $Re_{\ell T} > 350$ and $Re_{vT} > 35{,}000$.

$$h = h_\ell \, (1 - x)^{0.8} \, (1 + \frac{3.8}{Z^{0.95}}) \, , \tag{6.12}$$

where

$$Z = (\frac{1}{x} - 1)^{0.8} \, P_r^{0.4} \tag{6.13}$$

and

$$h_\ell = 0.023 \, (\frac{GD}{\mu_\ell})^{0.8} \, Pr_\ell^{0.4} \, \frac{k_\ell}{D} \, . \tag{6.14}$$

The quantity $h_\ell$ is the heat-transfer coefficient calculated assuming all the mass flowing is liquid. Equation 6.14 is known as the Dittus-Boelter equation.

The Shah correlation was developed to predict condensing coefficients for film condensation; therefore the correlation should be applicable at condenser locations 1 through 3 for series A tests. Figure 6.13 shows that the Shah equation predicts low coefficients for mixtures in series A tests at location 2, but the agreement is better at location 3. The equation is not applicable at condenser locations 4 through 6.

Figure 6.14 shows the results of Eq. 6.12 when applied to the single-refrigerant tests of series A. The expression applies only to R-12 at condenser location 2, however, it is applicable at locations 2, 3, and 4 for the R-114 tests. Except for one data point, the correlation gives excellent results at locations 2 and 3 and good results at location 4.

Figures 6.15 and 6.16 show the results of Eq. 6.12 when it is applied to the mixture and single-refrigerant tests of series B. Figure 6.15 shows that the correlation gave better agreement in predicting the coefficients for the series B mixture tests than those for series A. Figure 6.16 shows that good results were obtained at locations 2 and 3 for both the pure R-12 and pure R-114 tests of series B. Also, good results were obtained at location 4 for the R-114 tests. The equation does not apply at locations 5 or 6 for the single-refrigerant tests of series B and at location 4 for the R-12 tests.

The Shah correlation, when compared with some 777 data points from a number of fluids including halocarbons, showed a mean deviation of approximately 15 percent [23].

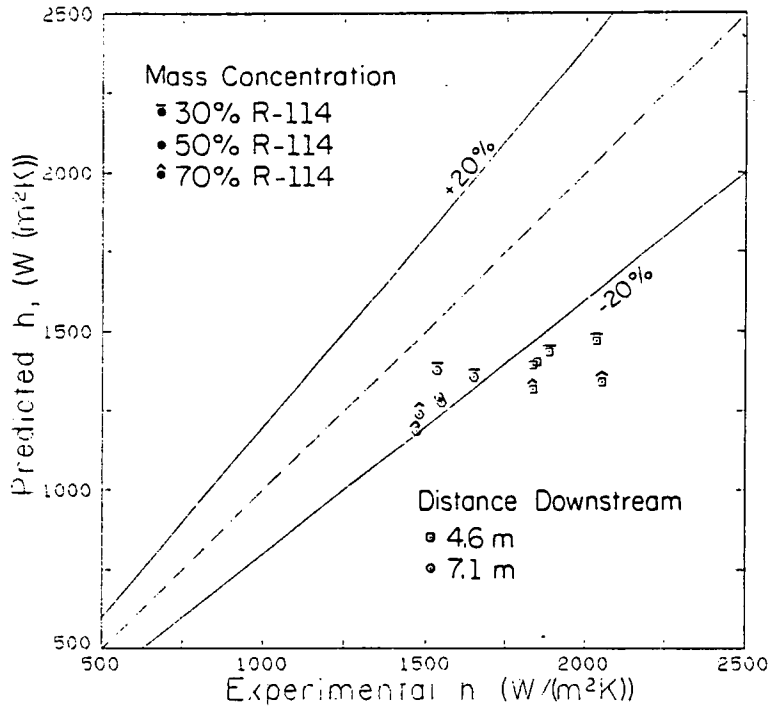


Figure 6.13. Shah correlation [25] applied to R-12/R-114 mixture tests of series A.

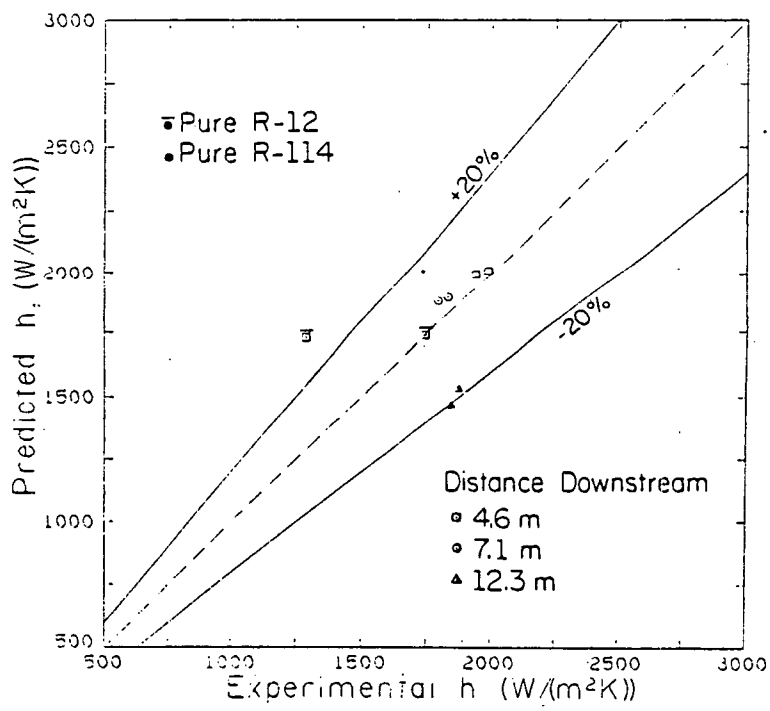


Figure 6.14. Shah correlation [25] applied to R-12 and R-114 tests of series A.

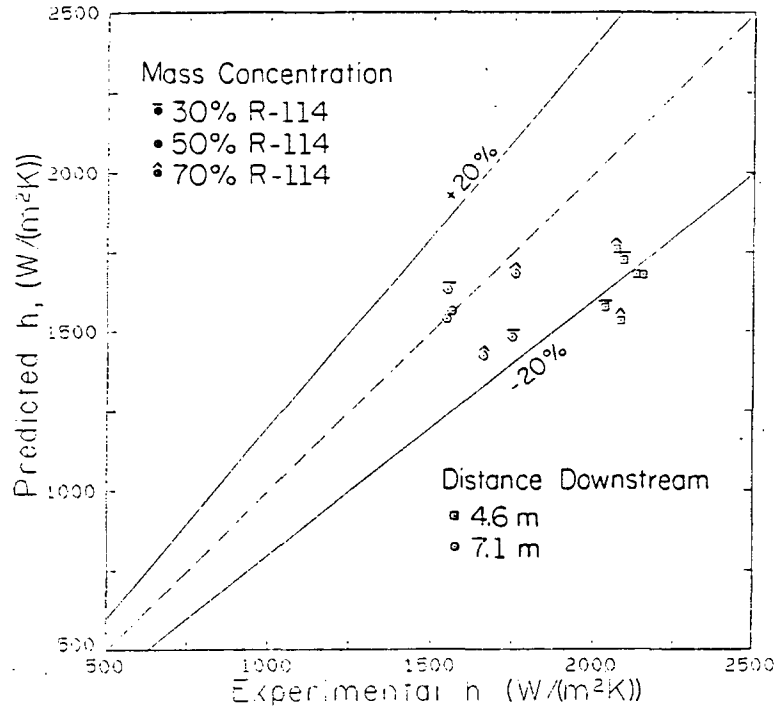


Figure 6.15. Shah correlation [25] applied to R-12/R-114 mixture tests of series B.

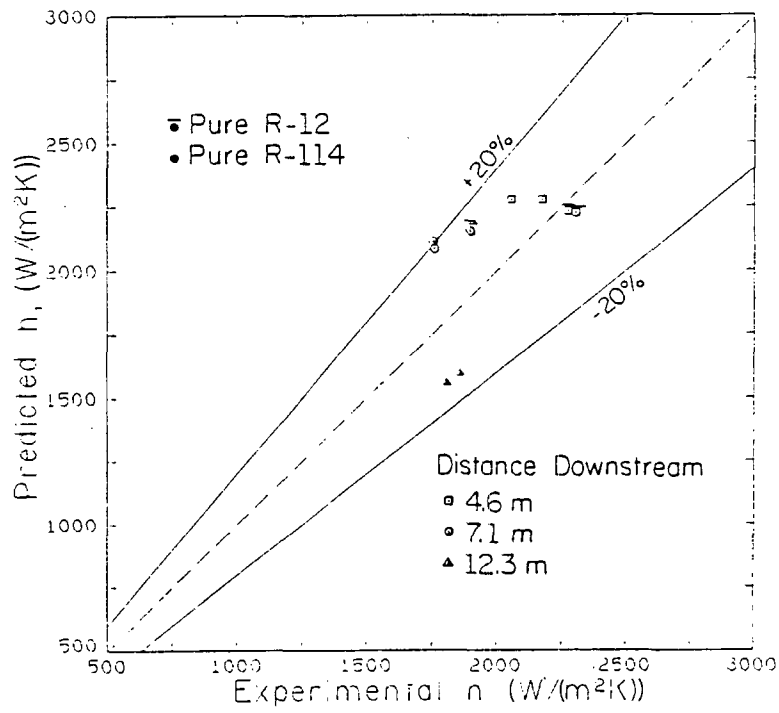


Figure 6.16. Shah correlation [25] applied to R-12 and R-114 tests of series B.

The flow conditions for our experimentation were such that the Chato correlation was not applicable. Chato condensed R-113 and found good agreement between the results given by Eq. 6.11 and the experimentally determined values [23]. Kroger [23] recommended that the results given by Eq. 6.11 be reduced by 10 percent for condensing R-12.

### 6.2.5 Tandon Correlation

Using the Akers and Rosson correlations, Eqs. 6.1 and 6.2, as a basis, Tandon et al. [15] developed equations to predict local condensing coefficients for annular and semiannular flow. Like the Akers and Rosson correlation, the equation from Tandon et al. is independent of the liquid Reynolds number.

For $Re_v < 30{,}000$:

$$h = 23.1\ Pr_\ell^{1/3} \left(\frac{i_{\ell v}}{C_{p_\ell}\ \Delta T}\right)^{1/6} Re_v^{1/8} \ . \tag{6.15}$$

For $Re_v > 30{,}000$,

$$h = 0.084\ Pr_\ell^{1/3} \left(\frac{i_{\ell v}}{C_{p_\ell}\ \Delta T}\right)^{1/6} Re_v^{0.67} \ . \tag{6.16}$$

Due to the annular and semiannular flow pattern requirements of Eqs. 6.15 and 6.16, their applicability would be limited to condenser locations 1 through 4. Figure 6.17 shows that the equations were quite accurate in predicting the condensing coefficients for the series A mixture tests at locations 2 through 5. The equations did not apply at location 6.

Figure 6.18 shows the results of Eqs. 6.15 and 6.16 when they are applied to the single-refrigerant tests of series A. The equations predicted coefficients at condenser locations 2 and 3. Fair results were obtained at locations 4 through 6. The results from the correlations should deteriorate downstream from location 4; however, Fig. 6.18 shows that the worst results occur at location 4 and results improve at locations 5 and 6.

Figure 6.19 depicts the results of the equations when they are applied to the mixture tests of series B. These results are similar to those obtained for the mixture tests of series A except that the percent deviations are

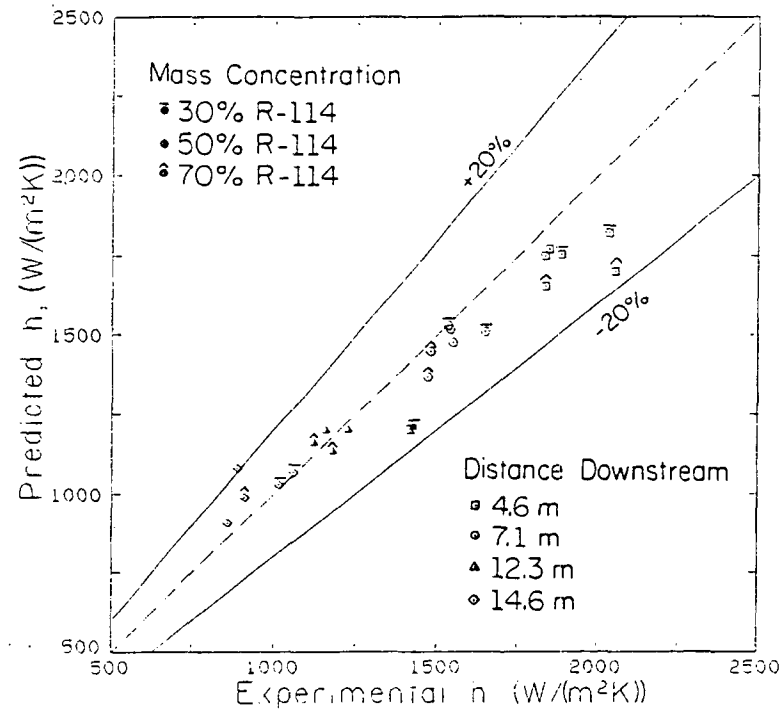


Figure 6.17. Tandon et al. correlation [15] applied to R-12/R-114 mixture tests of series A.

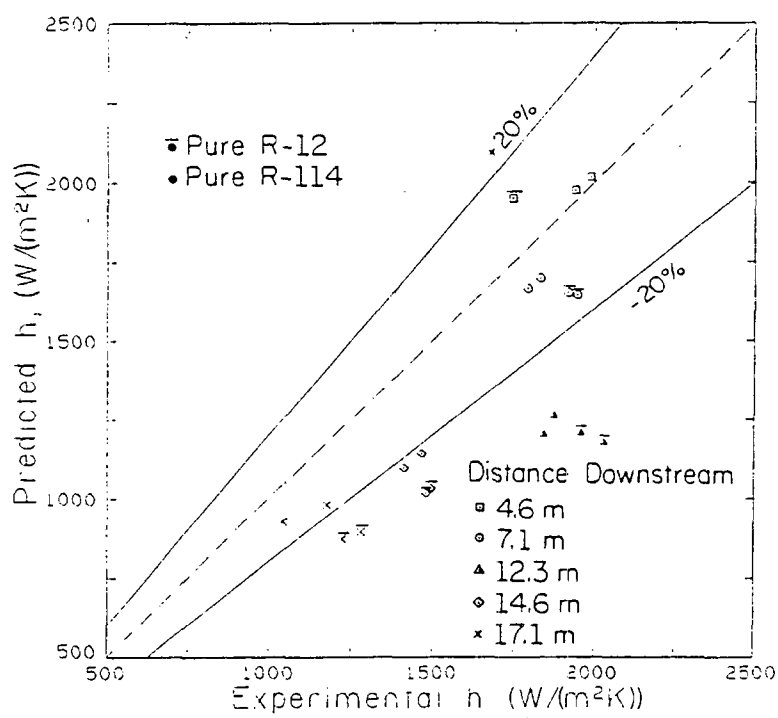


Figure 6.18. Tandon et al. correlation [15] applied to R-12 and R-114 tests of series A.

generally a little larger for the series B tests, especially in the second half of the condenser.

The correlations did much better at predicting the coefficients at condenser locations 2 and 3 for the single refrigerant tests of series B than for those of series A. The results from the series B refrigerant tests are shown in Fig. 6.20. The series B results were better at location 4, however, they were still only marginal. Unlike the series A results, the results for series B did not improve downstream of test location 4.

Like the Akers and Rosson expressions, Eqs. 6.15 and 6.16 employ $\Delta T$ in the denominator in one of their terms. As mentioned earlier this may explain, to some unknown extent, underpredictions by these equations. It is seen from the figures that the data points at condenser locations 2 and 3 are fairly close to the experimental values with no definite trend of underpredictions. However, the data at test location 4 is, in general, underpredicted, and the inclusion of the correct $\Delta T$ would improve the predictions.

Condensing experiments were conducted by Tandon et al. [15] with pure R-12 and pure R-22. Equations 6.15 and 6.16 predicted the condensing coefficients to within 15 percent of the experimental values for R-12 and to within 20 percent of the experimental values for R-22.

### 6.2.6 Cavallini and Zecchin Correlation

Cavallini and Zecchin [26] developed an expression to predict local heat-transfer coefficients for forced-convection condensation inside tubes. Like many other correlations, this equation was derived using an analogy between momentum and heat transfer and is based on a model of the annular flow pattern.

For $11 < (\frac{\rho_\ell}{\rho_v}) < 314$ and $7000 < Re_{\ell s} < 53{,}000$,

$$h = 0.05 \left(\frac{k_\ell}{D}\right) Re_{eq}^{0.8} \, Pr_\ell^{0.33} \tag{6.17}$$

where

$$Re_{eq} = Re_{\ell s} + \left(\frac{\mu_v}{\mu_\ell}\right) \left(\frac{\rho_\ell}{\rho_v}\right)^{0.5} Re_{vs}. \tag{6.18}$$

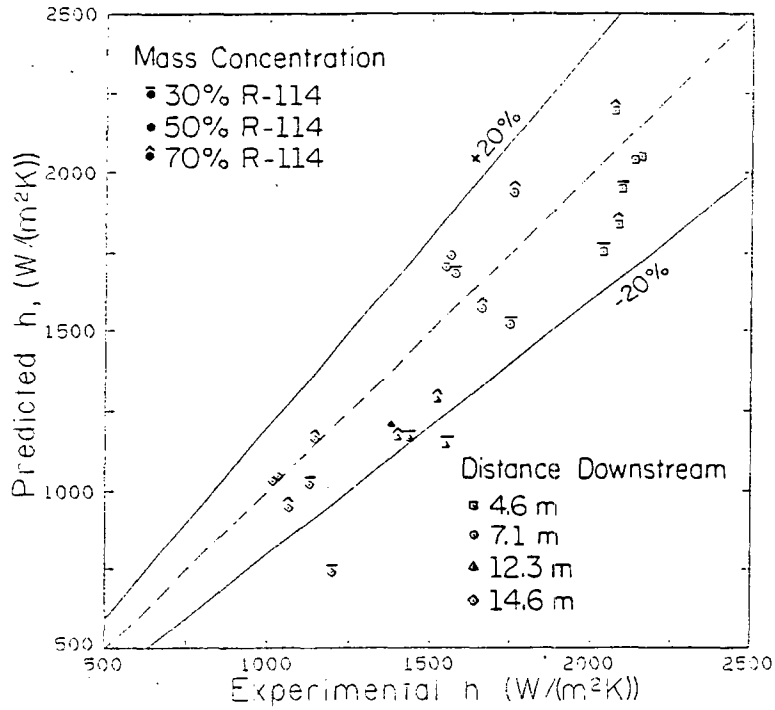


Figure 6.19. Tandon et al. correlation [15] applied to R-12/R-114 mixture tests of series B.

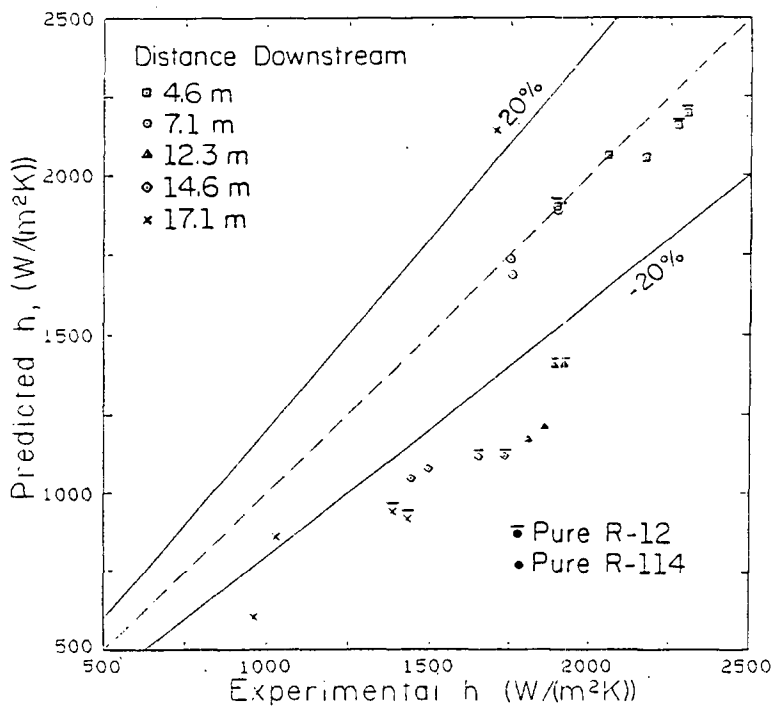


Figure 6.20. Tandon et al. correlation [15] applied to R-12 and R-114 tests of series B.

Because Eq. 6.17 is based on an annular flow pattern, it should be applicable to condenser locations 1, 2, and 3 for the tests in series A. However the equation did not agree well with our data at those three positions, but showed better agreement at locations 4 through 6.

Equation 6.17 was included in this study because it was well verified with pure halocarbon refrigerants [23]. The correlation was tested with experimental data from R-11, R-12, R-21, R-22, R-113, and R-114. The correlation showed a mean deviation varying between 8 to 47 percent.

## 6.3 Summary of Results

A total of eight condensing coefficient correlations were studied. Only five of these correlations fit the flow conditions of this work and yielded results. None of these correlations were formulated specifically for condensing refrigerant mixtures. Thus, the results of these expressions in predicting the refrigerant mixture coefficients will be noted. Also, comparisons will be made as to how well the correlations agreed with experimental data from others.

In general, the Akers and Rosson equations, Eqs. 6.1 and 6.2, were found to be fairly accurate, placing 89 percent of the predictions within 20 percent of the experimental values although in general they overpredicted the experimental results. The equations gave good results in predicting local heat-transfer coefficients for the series A mixture tests and marginal results for the series B mixture tests.

A majority of the predictions from the Azer et al. expression were in excess of the experimental values. Equation 6.4 was not effective, as it only placed 61 percent of the data points within 20 percent of the actual values. Despite its inadequacy, the correlation did an excellent job of predicting the heat-transfer coefficients for the series A mixture tests. As with the previous correlation, the accuracy of the predictions by Eq. 6.4 diminished when the equation was applied to the series B mixture tests. Also, there was a smaller range of deviation between the predicted and experimental heat-transfer coefficients found in this study compared with experimental results reported by others.

The Traviss et al. expression was found to be a good predictor of the condensing heat-transfer coefficients for this work. It placed 85 percent of its predictions within 20 percent of the experimentally determined values. Equation 6.6 was much more effective in predicting our data than the experimental data found by others. The correlation gave accurate predictions for the series A mixture tests but only marginal predictions for the series B mixture tests.

The Shah correlation showed a fair agreement, placing 74 percent of its predictions within 20 percent of the experimental values Equation 6.12 was found to underpredict the data from the mixture tests, with the accuracy of the predictions improving for the series B tests over the series A tests. When applied to our data, the expression performed with the same accuracy reported by Shah. Shah reported a mean deviation of approximately 15 percent when Eq. 6.12 was applied to his data. The expression yielded a mean deviation of 14.7 percent when applied to our data.

The Tandon et al. correlation, Eqs. 6.15 and 6.16, placed 85 percent of the data within 20 percent of the experimental values. The expressions placed 97 percent of their predictions within 20 percent of the experimental values for the mixture tests. The accuracy of the predictions obtained herein were approximately the same as that attained by Tandon et al. with their own experimental data.

## 6.4 Effect of Slip

All of the results from the various correlations presented thus far were calculated using properties that did not account for the existence of slip. Realizing that the vapor could be moving faster than the liquid in the experimental condenser, we wanted to find out how slip would affect the results from the correlations. The computer program used to calculate the results from the correlations was modified allowing varying amounts of slip, acknowledging the different fluid properties of the liquid and vapor.

The percent of slip is defined as the difference in average velocity between the vapor and the liquid divided by the liquid velocity with the entire quotient multiplied by 100. The computer program that calculated all of the correlation results was modified to calculate the vapor and liquid velocities given an arbitrary percent slip. The methodology used in the

calculation was to first determine the no-slip velocity. This quantity was used as a reference point from which the vapor and liquid velocities were determined.

Since only five of the correlations previously presented fit the flow conditions of this experimental work, only these correlations were considered in determining the effects of slip. The effect that slip has on the results of the correlations can be predicted by studying the mathematical formulations. Slip alters the velocity of the vapor and the liquid in the condenser, and these velocities enter into the calculations through the vapor and liquid Reynolds numbers.

Two of the correlations presented depend on the total mass flow rate. The correlations that depend on the combined liquid and vapor mass flows are the Azer et al. expression (Eq. 6.4) and the Shah expression (Eq. 6.12). Therefore, the introduction of slip will not affect the results rendered from these correlations.

The correlation proposed by Traviss et al. [22] is a complex function of the liquid Reynolds number $Re_\ell$. The local heat-transfer coefficient calculated by Eq. 6.6 is directly dependent on $Re_\ell$. Therefore a decrease in $Re_\ell$ will result in a decrease in the condensing coefficient. With the introduction of slip, the liquid refrigerant velocity is decreased and thus $Re_\ell$ is decreased. The introduction of slip will improve the predictions of Eq. 6.6 only if the previous predictions were in excess of the experimental values. Recalling that the Traviss equation is to be applied only in the annular flow regime, the effect of slip on the results from this correlation should only be considered at condenser locations 2 and 3. Reviewing Figs. 6.9 through 6.12, one can see that the introduction of slip at condenser location 2 will benefit only the series B mixture test data. At test location 3, the introduction of slip will improve all of the results except those from the single-refrigerant tests of series A.

Some calculations were made with slip introduced into the analysis. It was found that 10 percent slip at location 2 reduced the heat-transfer coefficients predicted by Eq. 6.6 from 4.3 to 7.4 percent; a 20 percent slip caused an 8.6 to 14.7 percent reduction in the predicted values. At location 3 the predicted value was reduced from 4.0 to 7.3 percent for 10 percent slip and from 8.1 percent to 13.5 for 20 percent slip.

The correlations proposed by Akers and Rosson [18] (Eqs. 6.1 and 6.2) and by Tandon et al. [15] (Eqs. 6.15 and 6.16) are all directly dependent on the vapor Reynolds number $Re_v$. Thus, the introduction of slip will increase the predicted heat-transfer coefficient from these expressions. If the predicted coefficients are less than the experimentally determined values, the inclusion of slip in the calculations will help.

The Akers and Rosson equations are said to be applicable in the annular and semistratified flow regimes; therefore, the effect of slip on the data should be considered at locations 2, 3, and 4. On viewing Figs. 6.1 through 6.4 one clearly sees that the Akers and Rosson expressions overpredicted a majority of the experimental data points; including slip into the calculations will cause the amount of overprediction to increase for these data points.

The only predictions given by Eqs. 6.1 and 6.2 that slip would improve would be those at test location 4 for the single-refrigerant tests of series A. At condenser locations 2 through 4, 10 percent slip had the effect of increasing the predicted condensing coefficients from 0.4 percent to 4.2 percent. The predicted heat-transfer coefficients were increased from 1.3 to 8.3 percent for 20 percent slip.

The correlations proposed by Tandon et al. are to be applied to annular and semiannular flow regimes. Thus, the effect of slip on the data from these expressions should be considered at condenser locations 2 through 4. Viewing Figs. 6.17 through 6.20, one sees that a majority of the data were underpredicted by Eqs. 6.15 and 6.16. Therefore the introduction of slip will decrease the underprediction for these values. For the condenser locations under consideration, 10 percent slip caused anywhere from 0.4 to 3.7 percent increase in the predicted heat-transfer coefficient; a 20 percent slip caused an increase in the predicted condensing coefficient of 1.1 to 7.4 percent.

One of the reasons for interest in the effect of slip is that the region of the condenser where mixtures suffered the greatest degradation was in the midsection of the condenser where the liquid and vapor flowed in a stratified manner with the vapor above and the liquid below. It would be in this section of the condenser where vapor slip would be most prominent, certainly more than where the vapor and liquid are turbulently mixed. In the case of mixtures a result of slip would be that vapor normally in contact with liquid of a given concentration is now further downstream. No analysis of the effect of this

shift was possible, but examining the effect of slip on the fluid properties would separate one of the potential influences.

## 6.5 Entrance Effects in the Condenser

All of the correlations presented thus far are to be applied to the condensation of saturated vapors. In most practical applications the vapor enters the condenser with some amount of superheat. The refrigerant tube temperature must be lower than the saturation temperature, so condensation occurs on the tube wall while the vapor core remains superheated. Although some condensation is occurring, the dominant mode of heat transfer is from the superheated vapor. The above situation was occurring at 2.4 m downstream from the condenser entrance (test location 1) during the tests. It is for this reason that the experimentally determined heat-transfer coefficients were much lower than those predicted by the correlations.

Shah [23] states that there is no verified technique available to predict the condensing coefficient under such nonequilibrium conditions. Shah references a study by Miropolskiy et al. [27] for a correlation that deals with this type of condenser entrance effect. Miropolskiy et al. focused on local heat-transfer coefficients for superheated steam inside cooled tubes. They noted that even if the tube temperature was below the saturation temperature of the fluid, $T_{SAT}$, condensation could not begin unless the vapor temperature was below a border temperature $T_B$ and the relative enthalpy Q was below a border value $Q_B$. Expressions for $T_B$ and $Q_B$ are given below.

$$T_B = T_{SAT} + \frac{q}{h_B} , \tag{6.19}$$

$$Q_B = 1 + \frac{q}{h_B} \frac{\overline{C}_p}{i_{\ell v}} . \tag{6.20}$$

The term $h_B$ is the local heat-transfer coefficient evaluated at $T_B$, and $h_B$ can be determined from any correlation suitable for superheated vapor. The term $\overline{C}_p$ is the mean vapor specific heat over the range $T_{SAT}$ to $T_B$, and q is the heat flux from the fluid.

When the temperature is above $T_B$ and $Q > Q_B$, heat transfer occurs solely by single-phase convection. However, for $T_{SAT} < T < T_B$ and $1 < Q < Q_B$. The

local heat-transfer coefficient, h, can be obtained from the following relationship:

$$\frac{h - h_B}{h_{(x=1)} - h_B} = \text{function of } \left(\frac{Q - 1}{Q_B - 1}\right) . \qquad (6.21)$$

This relationship is shown graphically in Fig. 6.21. Miropolskiy's study was done with superheated steam; and the curves on Fig. 6.21 were given in terms of absolute pressures. Shah [23] presented the curves in terms of reduced pressures in the hope that this figure may be applicable to other fluids.

Equation 6.21 was applied to the data obtained at 2.4 m from the condenser entrance (test location 1). It was stated previously that all of the correlations grossly overpredicted the condensing coefficient at this location. The correlation that yielded the best result was Eq. 6.12 from Shah which had an average overprediction of 141 percent. The results from Eq. 6.21 are presented in Fig. 6.22 which shows that Eq. (6.21) satisfactorily predicts h at this location. The results are a substantial improvement over those from the condensing correlations although, in general, the equation underpredicted the condensing coefficients. The predictions fell within a range of -43.2 percent to +17.7 percent with an average deviation of 22 percent. Equation 6.21 is much more accurate in the entrance region of the condenser than the condensing correlations.

We wanted to compare the performance of Eq. 6.21 to a correlation that predicts h based on single-phase convection heat transfer. Equation 6.14 was used to predict h for superheated refrigerant vapor. As expected, the equation underpredicted all of the data at 2.4 m downstream in the condenser. The accuracy of the predictions ranged from -24.3 percent to -70.7 percent with a mean deviation of 56 percent. From these results it is obvious that the single-phase heat transfer correlation is clearly inadequate for this situation and that the enhancement due to the limited amount of condensation must also be included.

In summary, when predicting the condensing coefficient in the entrance region of the condenser the correlation developed by Miropolskiy et al. [27] is clearly the best predictor. Equation 6.21 yielded fair results for refrigerants R-12 and R-114 with a functional relationship obtained from experimentation done with steam. Although in Fig. 6.21 the pressures were

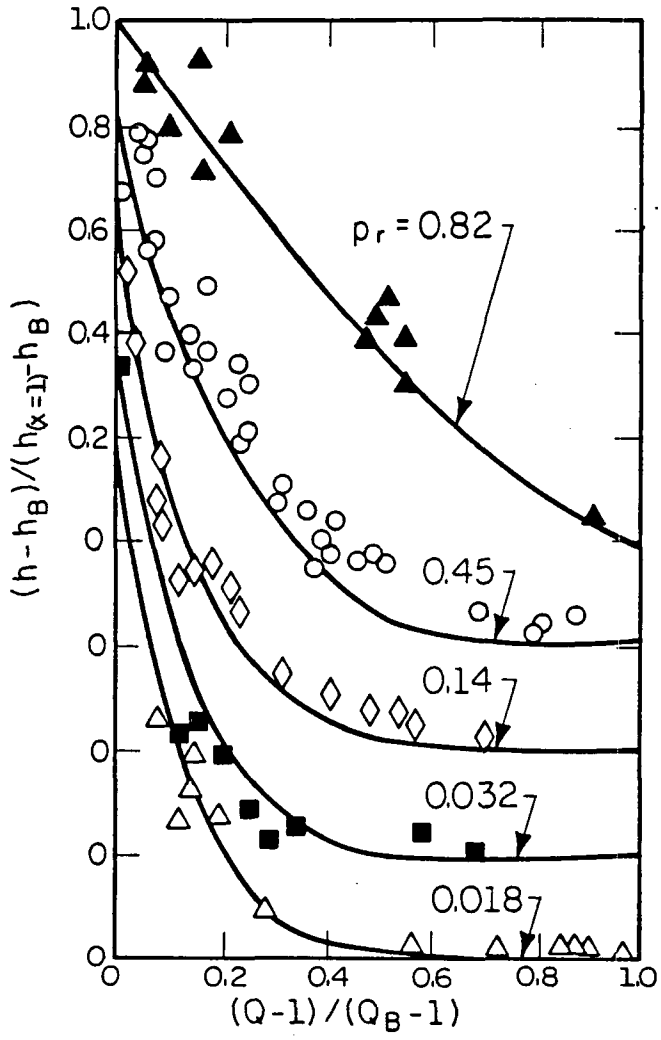


Figure 6.21. Graphic representation of Miropolskiy et al. correlation [27] with pressures reduced by Shah [23].

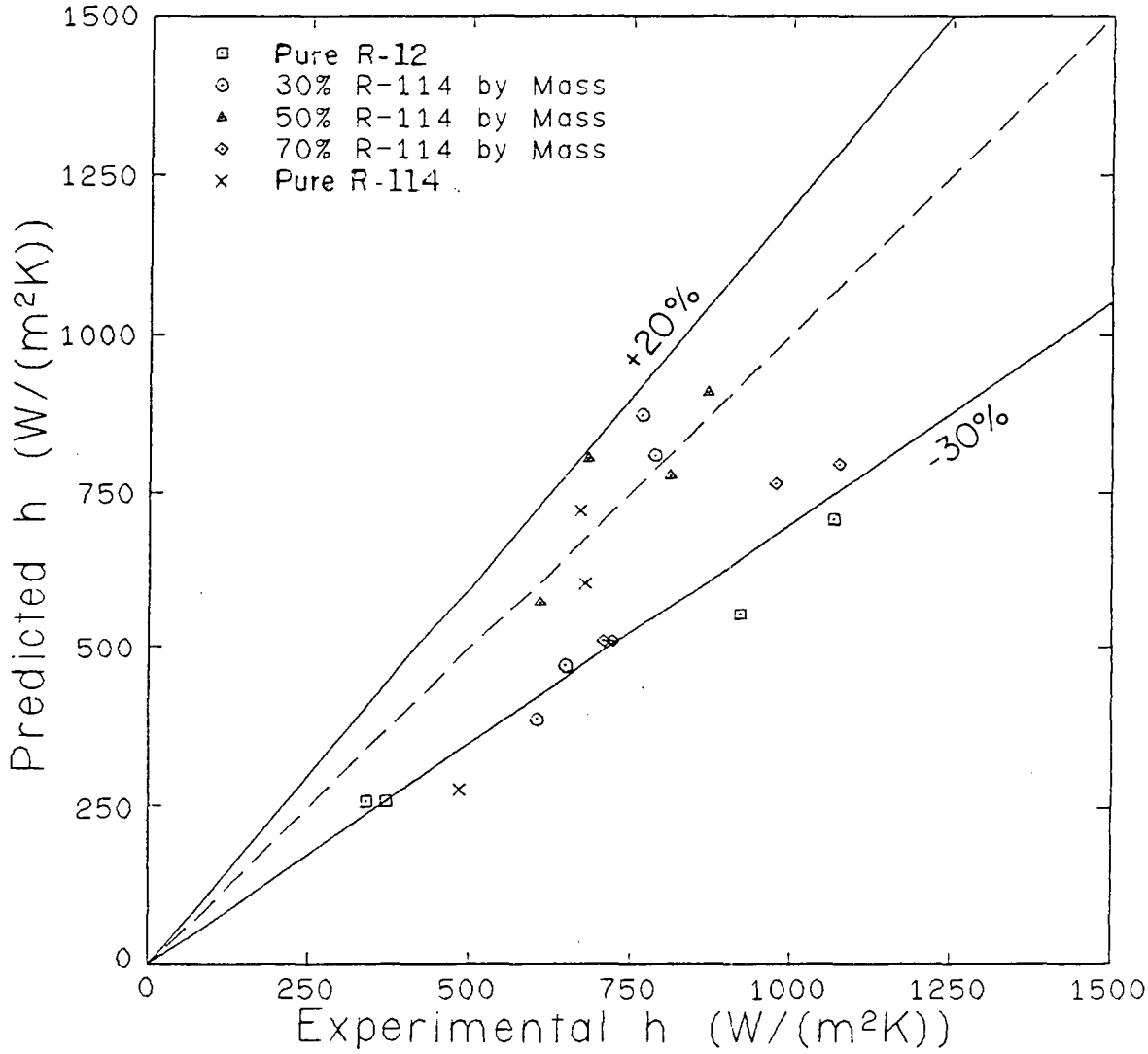


Figure 6.22. Miropolskiy et al. correlation [27] applied at 2.4 m downstream (test location 1) in the condenser.

reduced to extend the applicability of Eq. 6.21, we feel that curves developed specifically for R-12 and R-114 would have greatly improved the performance of the equations with this data.

# 7. SUMMARY AND CONCLUSIONS

## 7.1 Introduction

The two major parts of this study were experimental measurement of local heat-transfer coefficients for condensing refrigerant mixtures and a literature search for the selection of correlations to predict condensing coefficients. These correlations were employed to determine how well they could predict the experimentally-measured coefficients. A secondary part of this study dealt with the exploration of nonequilibrium phenomena occurring during the condensation of refrigerant mixtures.

## 7.2 Condensing Coefficient Results

### 7.2.1 Local Coefficients

The condensing coefficients were measured throughout the length of the condenser tube. The condensing coefficient profiles through the condenser for the different mass concentrations of R-114 exhibited many similarities. The lowest condensing coefficient occurred 2.4 m from the entrance of the condenser where the flow is annular. At this position the tube walls are wetted with a thin film of condensate and pools of liquid form in the bottom of the tube.

All but one of the profiles exhibited its highest coefficient 4.6 m from the entrance where the flow pattern is annular with a steady stream of liquid flowing in the bottom of the tube. Downstream from this point the coefficients for refrigerant mixtures differ slightly from the single-refrigerant values, with the mixtures showing a steady decline downstream of the maximum. For the single refrigerants the coefficients decrease after the maximum but maintain a nearly constant value from 7.1 to 12.3 m downstream. The flow pattern in this region of the condenser is wavy/stratified.

Like those of the refrigerant mixtures, the coefficients for the single refrigerants steadily decrease downstream of the 12.3 m point. Shortly downstream of the 12.3-m position, some slugs of liquid form and take up the entire cross-section of the tube. However, the flow remains predominantly stratified. At approximately 18 m downstream, the flow regime becomes slug flow.

### 7.2.2 Influence of Mixture Concentration on Condensing Coefficients

In the annular-flow regime of the first part of the condenser, the heat-transfer coefficients were found to remain fairly constant as the concentration of R-114 was varied in the R-12/R-114 mixture. At 2.4 m downstream (test location 1), the condensing coefficients from test series A showed a definite increase as the percent R-114 in the mixture was increased. The maximum coefficient occurred at a 50 percent R-114 concentration by mass and was approximately double the coefficient obtained from the pure R-12 test. This increase in the coefficient with mixture concentration at high vapor qualities has been noted by at least one other experimenter.

In the wavy/stratified and slug-flow regimes as the percent R-114 was increased in the mixture, the condensing coefficients fell. For the different condenser locations and the different series of tests, the minimum coefficients occurred at either 50 percent or 70 percent mass concentrations of R-114.

For the series A tests, the largest reduction attributable to the mixture in comparison to pure R-12 occurred 12.3 m downstream (condenser location 4) at a 50 percent R-114 concentration. The condensing coefficient for the 50 percent R-114 concentration is only 59 percent of the coefficient of pure R-12. The largest reduction in the series B tests (higher heat flux) occurred 14.6 m downstream (condenser location 5) at a 50 percent R-114 concentration. The condensing coefficient at the 50 percent R-114 concentration was 40 percent smaller than for pure R-12.

The two series of tests demonstrate similar maximum reductions in coefficients at the same R-114 concentrations but at different condenser locations. In the experimentation by Stoecker and McCarthy [11] using R-12/R-114 mixtures, condensing coefficients were shown to have their largest reductions of approximately 40 percent in the midrange of the condenser in the wavy/stratified flow regime and at an R-114 mass concentration of approximately 50 percent.

### 7.2.3 Effect of Heat Flux in Condenser

The series B tests with higher heat flux had an increased heat-transfer rate in the condenser compared with that of the series A tests. Increasing the heat flux in the condenser seems to have the effect of moving the flow

regimes downstream in the condenser. This assumption is demonstrated in the figures which depict the coefficient versus concentration at the various condenser locations. The series A Fig. 5.11 shows nearly uniform coefficients with respect to concentration in the annular flow regimes at test locations 1 and 2. The series B Fig. 5.19 shows constant coefficients at condenser locations 1, 2, and 3. This effect of increased heat flux would also explain the maximum reduction in the coefficient occurring further downstream in the series B tests than it did in the series A tests.

## 7.3 Condensing Coefficient Correlations

A total of eight correlations were studied, five of which fit the flow conditions of these experiments. All of the correlations were formulated for pure fluids and are to be used for a specific flow pattern or within a specified range of flow patterns.

The Traviss et al. correlation, Eq. 6.6, predicted the condensing coefficients for pure refrigerants R-12 and R-114 which agreed well with our experimental results in the annular, dispersed, wavy/stratified, and slug-flow regimes, even though it was developed for the annular and dispersed-flow regime. The equation placed 95 percent of the predicted h values within 20 percent of the experimental values for single refrigerants. All of the predictions were within 25 percent of the actual values.

It is recommended that the Tandon et al. correlations, Eqs. 6.15 and 6.16, be used to predict h for the R-12 and R-114 mixture tests. These equations were developed for the annular and the semiannular flow regimes; however, they proved to be effective at predicting h in all of the flow patterns, placing 97 percent of the mixture test data within 20 percent of the experimental values.

The test conditions used in our experiments demonstrated that entrance effects must be considered in predicting the coefficient. Heat transfer from the refrigerant in this region was due, in varying extents, to both condensation and single-phase convection. Although condensation was occurring, the condensation correlations were shown to be inaccurate in predicting h within this region. Likewise, the single-phase convection heat-transfer correlations also failed at predicting h within this region. A correlation developed by Miropolskiy et al. which was developed from data obtained from experimentation

with steam, predicted h quite closely within the entrance region. For the data from our experiments, the equation yielded a mean deviation of 22 percent. For vapor Reynolds Numbers varying from $15.7 \times 10^4$ to $21.8 \times 10^4$, the entrance region took up at least 12 percent but not more than 23 percent of the condenser length.

## 7.4 Nonequilibrium Phenomena

Tests were run using the transparent condenser with the intent of identifying nonequilibrium phenomena occurring during the condensation process. More specifically, an attempt was made to observe the existence of the nonequilibrium phenomenon known as slip. Temperature gradient measurements were made at various vertical locations along the tube diameter. These measurements gave inconclusive evidence that slip could be occurring within the flow. Likewise, concentration measurements were made at various vertical locations along the tube diameter. Again these measurements did not give definite proof of the existence of slip but did yield some results that could be caused by slip. Also, photographs were taken to locate the various flow regimes along the condenser. These photographs were used to correlate the copper condenser test data to the various flow patterns.

## 7.5 Conclusions

This study confirms that the local heat-transfer coefficients do decrease when a refrigerant mixture condenses in comparison to either constituent by itself. It was further established that the largest decrease occurs within the wavy flow regime. An explanation that has been proposed for the reduction is the counterdiffusion of the two constituents when a mixture condenses. Observation of the flow regimes in the section of the condenser where the reduction of coefficient is the greatest suggests that this would also be the region there the greatest amount of vapor-liquid slip occurs. Slip does not seem to contribute to the explanation, however, because its influence is to reduce the amount of counterdiffusion necessary. Instead, it appears that if the counterdiffusion explanation prevails, the low turbulence in the midsection of the condenser does little to cancel counterdiffusion there.

Because of performance in predicting the experimental heat-transfer coefficients, we recommend that the expression developed by Traviss et al., Eq. 6.6, be used for single refrigerants and that the correlation developed by

Tandon et al., Eqs. 6.15 and 6.16, be used for refrigerant mixtures. One can see major differences when comparing the two expressions.

Equations 6.15 and 6.16 show h to depend on the latent heat, liquid specific heat, temperature drop across the condensate film, and the vapor Reynolds number. None of these terms appear in Eq. 6.6. Instead, this equation depends on the liquid Reynolds number, quality, and ratios of the liquid to vapor viscosity and density. In addition to fluid properties, it seems that h for the condensation process should depend on the latent heat, temperature drop across the condensate film, quality, and the temperature difference between the saturation temperature and the the tube wall. None of the correlations employ all of these terms.

The above correlations were recommended because of their agreement with a limited number of data points. Before these expressions are totally accepted they should be subjected to flow conditions covering the full range of their applicability criterion. Accurate predictions under the above conditions would represent adequate verification of the equations.

# REFERENCES


1. P. S. Burr and G. G. Haselden, "A Non-Isothermal Mixed Refrigerant Cycle for Air Conditioning Duties," Proc., Inst. of Refrigeration, Vol. 71, 1974-75, pp. 18-23.

2. G. G. Haselden and L. Klimek, "An Experimental Study of the Use of Mixed Refrigerants for Non-isothermal Refrigeration," Proc., The Institute of Refrigeration, London, 1958.

3. P. Jakobs and H. Kruse, "The Use of Non-Azeotropic Refrigerant Mixtures in Heat Pumps for Energy Saving," Proc., Meeting of Commission B2, Int. Inst. of Refrigeration, Delft, 1978.

4. A. Lorenz and K. Meutzner, "On Application of Non-Azeotropic Two-Component Refrigerants in Domestic Refrigeration and Home Freezers," Proc., XIV Int. Congress of Refrigeration, Moscow, 1975.

5. A. Rojey, "Pompe A Chaleur Fonctionnant Avec Un Melange De Fluides."

6. S. N. Saluja "Use of Mixed Refrigerants in Vapour Compression Refrigeration Machines," Refrigeration and Air Conditioning, Vol. 81, Pts. I, II, and III, Nos. 958, 959, and 960, Jan., Feb., and Mar. 1978, pp. 27-34, 32-35, and 80-83.

7. H. K. Varma, C. P. Sharma, and M. P. Mishra, "Heat Transfer Coefficients During Forced Convection Evaporation of R-12 and R-22 Mixtures in Annular Flow Regime," Proc., XVth Int. Congress of Refrigeration, Vol. II, Venice, 1979.

8. C. P. Arora "Boiling Heat Transfer Data for Pure and Mixed Refrigerants," Proc., XII Int. Congress of Refrigeration, Madrid, 1967.

9. Y. G. Bokhanovskiy "Heat Transfer from Freon 12, Freon 22, and Their Mixtures in a Coiled-Tube Condenser," Heat Transfer-Soviet Res., 12(4); (July-August 1980).

10. E. Kornota and W. F. Stoecker, Flow Regimes of Refrigerant Mixtures Condensing Inside Tubes, ORNL/Sub/81-7762/4&01, University of Illinois for the Oak Ridge National Laboratory, 1985.

11. W. F. Stoecker and C. I. McCarthy, The Simulation and Performance of a Systems Using an R-12/R-114 Refrigerant Mixture, ORNL/Sub-81-7762/3&01, University of Illinois Report for Oak Ridge National Laboratory, May 1984.

12. F. M. White, Fluid Mechanics, McGraw-Hill Book Company, 1979.

13. American Society of Heating, Refrigeration, and Air Conditioning Engineers, Handbook of Fundamentals, 1981.

14. A. E. Bergles, J. G. Collier, J. M. Delhaye, G. F. Hewitt, and F. Mayinger, Two Phase Flow and Heat Transfer in the Power and Process Industries, McGraw-Hill Book Co., 1981.

15. T. N. Tandon, H. K. Varma, and C. P. Gupta, "An Experimental Investigation of Forced-Convection Condensation During Annular Flow Inside a Horizontal Tube," ASHRAE Trans., 91(1A) (1985).

16. R. C. Downing, "Refrigerant Equations," ASHRAE Trans., 80(2) (1974), 158-169.

17. L. C. Singal, C. P. Sharma, and H. K. Varma, "Experimental Heat Transfer Coefficient for Binary Refrigerant Mixtures of R-13 and R-12," ASHRAE Trans., 89(1), (1983).

18. W. W. Akers and H. F. Rosson, "Condensation Inside a Horizontal Tube," Chem. Eng. Prog. Symp. Ser., 56(30), 145-149 (1960).

19. W. W. Akers, H. A. Deans, and O. K. Crosser, "Condensing Heat Transfer Within Horizontal Tubes," Chem. Eng. Prog. Ser., 55(29), 171-176 (1959).

20. N. Z. Azer, L. V. Abis, and H. M. Soliman, "Local Heat Transfer Coefficients During Annular Flow Condensation," ASHRAE Trans., 78(2) 135-143 (1972).

21. S. Bae, J. S. Maulbetsch, and W. M. Rohsenow, "Refrigerant Forced-Convection Condensation Inside Horizontal Tubes," ASHRAE Trans., 77(2) 1972.

22. D. P. Traviss, W. M. Rohsenow, and A. B. Baron, "Forced-Convection Condensation Inside Tubes: A Heat Transfer Equation for Condenser Design," ASHRAE Trans., 79(1), 157-165 (1973).

23. M. M. Shah, "Heat Transfer During Film Condensation in Tubes and Annuli: A Review of the Literature," ASHRAE Trans., 87(1), 1981.

24. J. C. Chato, "Laminar Condensation Inside Horizontal and Inclined Tubes," ASHRAE Journal, 4(2), 52-60 (1962).

25. M. M. Shah, "A General Correlation for Heat Transfer During Film Condensation Inside Pipes," Int. J. Heat Mass Transfer, 22, 547-556 (April 1979).

26. A. Cavallini and R. Zecchin, "A Dimensionless Correlation for Heat Transfer in Forced Convection Condensation," Proc., Fifth Int. Heat Transfer Conference, 3, 309-313, (1974).

27. Z. L. Miropoloskiy, R. I. Shneerova, and L. M. Ternakova, "Heat Transfer at Superheated Steam Condensation Inside Tubes," Proc., Fifth Int. Heat Transfer Conf., Tokyo, Vol. 3, pp. 246-249, 1974.

# APPENDIX

## REFRIGERANT AND COOLING WATER TEMPERATURES ALONG WITH LOCAL HEAT-TRANSFER COEFFICIENTS

(Tests 2, 5, 7-14, 21-27, 29-31)

Table A.1 Refrigerant Temperatures Along Condenser

| Test No. | % R-114 by Mass | Refrigerant Temperatures Along Condenser (°C) by Distance Downstream Relative to Refrigerant Inlet | | | | | | | | |
|---|---|---|---|---|---|---|---|---|---|---|
| | | 0 m | 2.4 m | 4.6 m | 7.1 m | 9.7 m | 12.3 m | 14.6 m | 17.1 m | 19.8 m |
| 2 | 50 | 45.0 | 37.8 | 36.7 | 35.3 | 33.4 | 31.9 | 30.4 | 28.2 | 22.7 |
| 5 | 50 | 45.0 | 38.6 | 37.7 | 36.3 | 34.6 | 33.1 | 32.0 | 29.5 | 24.3 |
| 7 | 0 | 45.0 | 38.2 | 37.6 | 36.8 | 36.7 | 36.6 | 36.4 | 36.1 | 29.3 |
| 8 | 0 | 45.0 | 37.2 | 35.3 | 35.3 | 35.1 | 35.1 | 35.1 | 34.7 | 29.4 |
| 9 | 30 | 45.0 | 37.7 | 36.9 | 36.2 | 35.1 | 34.2 | 33.1 | 31.8 | 27.4 |
| 10 | 30 | 45.0 | 38.0 | 37.2 | 36.4 | 35.2 | 34.2 | 33.1 | 31.5 | 26.0 |
| 11 | 100 | 45.0 | 35.0 | 33.0 | 32.5 | 31.6 | 31.2 | 31.0 | 30.6 | 25.5 |
| 12 | 100 | 45.0 | 35.0 | 33.2 | 32.8 | 31.9 | 31.6 | 31.4 | 30.9 | 24.4 |
| 13 | 70 | 45.0 | 35.8 | 34.8 | 33.8 | 32.1 | 30.7 | 28.7 | 26.7 | 23.8 |
| 14 | 70 | 45.0 | 35.9 | 34.8 | 33.8 | 32.0 | 30.5 | 28.5 | 26.5 | 23.4 |
| 21 | 70 | 45.8 | 39.4 | 38.3 | 37.4 | 35.6 | 34.3 | 32.6 | 30.4 | 26.8 |
| 22 | 50 | 47.5 | 39.3 | 38.0 | 37.0 | 35.2 | 33.9 | 32.2 | 30.2 | 25.6 |
| 23 | 30 | 49.1 | 40.1 | 38.8 | 38.0 | 36.7 | 35.9 | 34.7 | 33.0 | 26.5 |
| 24 | 50 | 47.0 | 39.0 | 37.8 | 36.7 | 34.9 | 33.6 | 31.9 | 30.1 | 25.6 |
| 25 | 30 | 49.1 | 40.6 | 39.5 | 38.6 | 37.3 | 36.2 | 34.9 | 31.9 | 23.4 |
| 26 | 70 | 45.8 | 39.9 | 38.8 | 37.9 | 36.1 | 34.7 | 32.8 | 30.4 | 26.2 |
| 27 | 100 | 49.8 | 36.9 | 34.3 | 33.8 | 32.5 | 32.1 | 31.8 | 31.0 | 22.6 |
| 29 | 0 | 37.9 | 32.8 | 32.6 | 32.5 | 32.3 | 32.1 | 32.1 | 31.8 | 28.2 |
| 30 | 100 | 49.9 | 36.7 | 33.8 | 33.3 | 32.0 | 31.5 | 31.2 | 30.5 | 23.0 |
| 31 | 0 | 37.9 | 32.4 | 32.2 | 32.1 | 31.9 | 31.8 | 31.7 | 31.4 | 28.2 |

Table A.2 Condenser Cooling Water Temperatures Along Condenser

| Test No. | Condenser Water Flowrate kg/s | Condenser Cooling Water Temperatures Along Condenser (°C) by Distance Downstream Relative to Refrigerant Inlet | | | | | | | | |
|---|---|---|---|---|---|---|---|---|---|---|
| | | 0 m | 2.4 m | 4.6 m | 7.1 m | 9.7 m | 12.3 m | 14.6 m | 17.1 m | 19.8 m |
| 2 | 0.0489 | 33.7 | 32.7 | 30.8 | 27.7 | 25.0 | 22.7 | 20.3 | 18.6 | 16.5 |
| 5 | 0.0500 | 34.5 | 33.3 | 31.4 | 28.2 | 26.1 | 23.6 | 21.1 | 19.4 | 17.0 |
| 7 | 0.0481 | 35.3 | 34.7 | 34.0 | 32.3 | 30.7 | 28.0 | 25.2 | 22.8 | 17.6 |
| 8 | 0.0482 | 34.0 | 33.2 | 32.5 | 30.8 | 29.4 | 26.8 | 24.1 | 21.5 | 16.2 |
| 9 | 0.0438 | 34.6 | 33.8 | 32.5 | 29.8 | 27.8 | 25.1 | 22.4 | 20.3 | 15.8 |
| 10 | 0.0435 | 34.8 | 34.0 | 32.4 | 29.7 | 27.7 | 24.9 | 22.1 | 20.1 | 15.7 |
| 11 | 0.0551 | 30.8 | 30.0 | 28.8 | 26.8 | 25.4 | 23.2 | 21.0 | 18.9 | 15.3 |
| 12 | 0.0543 | 30.9 | 30.2 | 29.0 | 27.0 | 25.4 | 23.0 | 20.6 | 18.4 | 15.4 |
| 13 | 0.0515 | 31.4 | 30.4 | 28.4 | 25.4 | 23.3 | 21.1 | 18.8 | 17.3 | 15.2 |
| 14 | 0.0505 | 31.3 | 30.0 | 28.3 | 25.1 | 23.1 | 20.8 | 18.4 | 16.8 | 14.9 |
| 21 | 0.0522 | 35.4 | 33.8 | 32.1 | 28.7 | 26.4 | 23.6 | 20.7 | 18.4 | 15.4 |
| 22 | 0.0551 | 34.6 | 33.2 | 31.1 | 27.9 | 25.7 | 23.1 | 20.4 | 18.5 | 15.5 |
| 23 | 0.0512 | 36.2 | 34.7 | 33.0 | 30.1 | 27.9 | 24.9 | 21.9 | 19.3 | 15.3 |
| 24 | 0.0543 | 33.8 | 33.2 | 30.9 | 27.8 | 25.4 | 22.8 | 20.1 | 18.2 | 15.0 |
| 25 | 0.0505 | 36.4 | 35.1 | 33.1 | 29.9 | 27.4 | 24.1 | 20.8 | 18.2 | 15.3 |
| 26 | 0.0522 | 35.8 | 34.1 | 32.1 | 28.8 | 26.2 | 23.3 | 20.3 | 18.1 | 15.1 |
| 27 | 0.0656 | 31.4 | 30.0 | 28.4 | 26.2 | 24.3 | 21.9 | 19.4 | 16.9 | 15.0 |
| 29 | 0.0660 | 30.2 | 29.3 | 28.3 | 26.7 | 25.1 | 23.0 | 20.8 | 18.0 | 13.9 |
| 30 | 0.0654 | 31.1 | 29.7 | 27.9 | 25.8 | 24.0 | 21.6 | 19.2 | 16.7 | 14.5 |
| 31 | 0.0658 | 29.7 | 29.0 | 28.1 | 26.5 | 24.9 | 22.7 | 20.5 | 18.2 | 13.9 |

Table A.3 Local Heat-Transfer Coefficients Along Condenser

| Test No. | % R-114 by Mass | Local Heat-Transfer Coefficients Along Condenser ($W/m^2K$) by Distance Downstream Relative to Refrigerant Inlet | | | | | |
|---|---|---|---|---|---|---|---|
| | | 2.4 m | 4.6 m | 7.1 m | 12.3 m | 14.6 m | 17.1 m |
| 2 | 50 | 610 | 1846 | 1548 | 1121 | 860 | 685 |
| 5 | 50 | 811 | 1833 | 1540 | 1227 | 889 | 694 |
| 7 | 0 | 341 | 1288 | 1917 | 2033 | 1480 | 1226 |
| 8 | 0 | 372 | 1745 | 1946 | 1960 | 1495 | 1283 |
| 9 | 30 | 605 | 1884 | 1649 | 1426 | 1058 | 899 |
| 10 | 30 | 649 | 2035 | 1533 | 1418 | 1014 | 882 |
| 11 | 100 | 486 | 1988 | 1831 | 1875 | 1467 | 1178 |
| 12 | 100 | 485 | 1939 | 1792 | 1844 | 1413 | 1046 |
| 13 | 70 | 708 | 2053 | 1478 | 1158 | 910 | 599 |
| 14 | 70 | 722 | 1834 | 1469 | 1179 | 913 | 576 |
| 21 | 70 | 976 | 2069 | 1756 | 1521 | 1141 | 799 |
| 22 | 50 | 870 | 2152 | 1560 | 1377 | 1031 | 778 |
| 23 | 30 | 767 | 2035 | 1747 | 1548 | 1196 | 979 |
| 24 | 50 | 683 | 2131 | 1544 | 1375 | 1014 | 780 |
| 25 | 30 | 787 | 2092 | 1574 | 1435 | 1126 | 833 |
| 26 | 70 | 1075 | 2083 | 1658 | 1397 | 1062 | 732 |
| 27 | 100 | 671 | 2056 | 1756 | 1807 | 1439 | 962 |
| 29 | 0 | 1067 | 2272 | 1897 | 1887 | 1733 | 1431 |
| 30 | 100 | 679 | 2173 | 1751 | 1858 | 1493 | 1030 |
| 31 | 0 | 921 | 2302 | 1894 | 1920 | 1652 | 1385 |